Title
Photocurable Bioinks for the 3D Pharming of Pharmaceutical Tablets

Author
Acosta-Vélez, Giovanny Francisco

Publication Date
2017

Peer reviewed|Thesis/dissertation

UNIVERSITY OF CALIFORNIA

Los Angeles

Photocurable Bioinks for the 3D Pharming of Pharmaceutical Tablets

A dissertation submitted in partial satisfaction of the

requirements for the degree Doctor of Philosophy

in Chemical Engineering

by

Giovanny Francisco Acosta-Vélez

2017

ABSTRACT OF THE DISSERTATION

Photocurable Bioinks for the 3D Pharming of Pharmaceutical Tablets

by

Giovanny Francisco Acosta-Vélez

Doctor of Philosophy in Chemical Engineering

University of California, Los Angeles, 2017

Professor Yi Tang, Co-Chair

Professor Benjamin M. Wu, Co-Chair

New technologies for the fabrication of on-demand oral dosage forms are needed in order to provide personalized medicine accessible to patients at pharmacies and point-of-care locations. 3D Pharming, the direct printing of pharmaceutical tablets, is an attractive technology towards the manufacture of oral dosage forms with controlled dosages, drug release kinetics, and the potential to combine multiple drugs into a single tablet. Powder bed 3D printing and fused deposition modeling (FDM) have been the two most explored 3D printing technologies towards the manufacture of personalized medicine. However, these techniques experience limitations in terms of printing speed and operation at high temperatures causing potential drug degradation, respectively. To overcome these limitations, the objective of this dissertation was to design a 3D Pharming system based on the inkjet printing of photocurable bioinks, capable of dispensing hydrophilic and hydrophobic APIs, with quick printing speeds at room temperature. The procedure included the dispensing of drug loaded bioinks onto blank preform tablets, their

subsequent light induced polymerization, and the attachment of a preform cap to complete the oral dosage form.

This objective was achieved by 1) chemically manipulating hyaluronic acid to incorporate norbornene moieties into its backbone, resulting in a photoreactive biocompatible polymer to be used as the main component of a hydrophilic bioink; 2) designing a poly(ethylene glycol) based photocurable formulation for the dispensing of hydrophobic compounds; and 3) demonstrating the use of these bioinks towards the fabrication of combination therapies by creating a polypill including two drugs for the treatment of hypertension. The capacity of these bioinks for droplet formation was analyzed by calculating the inverse of the Ohnesorge number and the mechanical properties of the polymerized gels were assessed. Dissolution tests were performed on fabricated tablets containing the hydrophilic drug Ropinirole, Naproxen as a hydrophobic compound, and the combination of Lisinopril and Spironolactone within a polypill for the treatment of hypertension. Immediate and sustained release profiles were achieved for Ropinirole and Naproxen, respectively, demonstrating control over drug release kinetics. This work presents a new 3D Pharming technique with a special application towards drugs that achieve their pharmacological effect at low dosages.

The dissertation of Giovanny Francisco Acosta-Vélez is approved.

Yvonne Y. Chen

Harold G. Monbouquette

Yi Tang, Committee Co-Chair

Benjamin M. Wu, Committee Co-Chair

University of California, Los Angeles

2017

DEDICATION

Para los seres que me dieron la vida, Papá y Mamá
(To the beings that granted me life, Mom and Dad)

Y para Doña Iris
(And for Doña Iris)

TABLE OF CONTENTS

Abstract of the Dissertation ……..…….. ii

Committee Page ……..…… iv

Dedication …….. v

List of Figures ……..... x

List of Tables ……..…….. xvii

Acknowledgments ……..…….. xviii

Vita ……..…… xx

Chapter 1: Introduction to 3D Pharming – Direct Printing of Pharmaceutical Tablets ..……1

1.1 Abstract …..……..…….. 1

1.2 Introduction ……...……..……... 1

1.3 Powder Bed Inkjet 3D Printing …….…… 3

1.4 Fused Deposition Modeling (FDM) …….…… 8

1.5 Multiple Drugs Incorporation ……..…….. 11

1.6 Conclusion and Future Directions ……..…… 14

1.7 Dissertation Objective and Specific Aims ……..…….. 16

1.8 Figures …….. 18

1.9 References ……...… 27

Chapter 2: Photocurable Bioink for the Inkjet 3D Pharming of Hydrophilic Drugs ……..… 32

2.1 Abstract …… 32

2.2 Introduction ……..… 32

2.3 Materials and Methods …….. 34

2.3.1 Norbornene Functionalized Hyaluronic Acid (HANB) Synthesis

2.3.2 Photocurable Formula Preparation

2.3.3 Gelation and Mechanical Properties

2.3.4 Thiols Consumption

2.3.5 Preform Tablet Fabrication

2.3.6 Drug Dispensing and Release Kinetics

2.3.7 Hydrogel Drying

2.3.8 Statistical Analysis

2.4 Results and Discussion 38

2.4.1 HANB Synthesis and Gelation

2.4.2 Hydrogel Characterization and Droplet Formation

2.4.3 Preform Tablet Fabrication

2.4.4 Tablet Fabrication and Dissolution Test

2.5 Conclusion 42

2.6 Figures 43

2.7 Tables 53

2.8 References 54

Chapter 3: Photocurable Poly(ethylene glycol) as bioink for the inkjet 3D Pharming of Hydrophobic Drugs 57

3.1 Abstract 57

3.2 Introduction 57

3.3 Materials and Methods 60

3.3.1 Photocurable Formula Preparation

3.3.2 Gelation and Mechanical Properties

3.3.3 Scanning Electron Microscopy (SEM)

3.3.4 Preform Tablet Fabrication and Characterization

3.3.5 Drug Dispensing and Release Kinetics

3.3.6 2D Spatial Control

3.3.7 Statistical Analysis

3.4 Results and Discussion 65

3.4.1 Formulation Characterization

3.4.2 Droplet Formation

3.4.3 Preform Tablet Characterization

3.4.4 Tablet Dissolution Test

3.4.5 2D Spatial Control

3.5 Conclusion ……..…… 71

3.6 Figures …….. 73

3.7 Tables ……..... 88

3.8 References ……..…. 91

Chapter 4: Use of Photocurable Bioinks for the 3D Pharming of Combination Therapies ……. 96

4.1 Abstract ……. 96

4.2 Introduction ……..…… 96

4.3 Materials and Methods ……...…….. 98

4.3.1 Hydrophilic Photocurable Bioink Preparation

4.3.2 Hydrophobic Photocurable Bioink Preparation

4.3.3 Bioinks Gelation and Mechanical Properties

4.3.4 Scanning Electron Microscopy (SEM)

4.3.5 Preform Tablet Fabrication and Characterization

4.3.6 Drug Release Kinetics

4.3.7 Statistical Analysis

4.4 Results and Discussion …….. 102

4.4.1 Bioinks Characterization

4.4.2 Droplet Formation

4.4.3 Preform Tablet Characterization

4.4.4 Polypill Dissolution Test

4.5 Conclusion ……. 106

4.6 Figures …… 108

4.7 Tables …… 120

4.8 References …… 121

Chapter 5: Conclusion and Future Directions ……..…… 125

5.1 Future Directions ……..…… 126

5.2 Challenges for the Transition of 3D Pharming into Pharmacies ……..…… 127

5.3 References …… 130

LIST OF FIGURES

Figure 1.1: Powder bed 3D printing procedure schematic ……..……... 18

Figure 1.2: (A) Schematic of immediate-extended release tablet and (B) its corresponding drug release profile ……..…… 19

Figure 1.3: (A) Drug delivery device with material gradients. (B) Erosion process of the device after 0, 1, 3, 5, 7, and 10 h of dissolution. ……..…… 20

Figure 1.4: Schematic of fast disintegrating tablets with bound regions within the middle of the device …….. 21

Figure 1.5: Fused deposition modeling procedure schematic …..…….... 22

Figure 1.6: Cross-sectional view of fluorescein infused devices featuring different infill percentages under UV light …… 23

Figure 1.7: (A) Schematic of polymer precursor solution curing procedure and tablet manufacture. (B) Effect of polymer geometry on dissolution profiles …..…….. 24

Figure 1.8: Schematic of tablets containing multiple drugs. (A) Multilayer device and (B) DuoCaplet ……..…… 25

Figure 1.9: Schematic of the polypill design featuring 5 drugs within immediate and extended release compartments …… 26

Figure 2.1: (A) Norbornene functionalized hyaluronic acid (HANB) two-step synthesis pathway; (B) Bioink photopolymerization for drug loaded hydrogel formation through thiol-ene reaction ……..... 43

Figure 2.2: HANB hydrogel mechanical properties. (A) In-situ photorheology of hydrogel solution (W_{HANB} = 3%, r_{ratio} = 0.6, T_L = 2 min) indicating gelation kinetics; (B) G' of hydrogels (W_{HANB} = 3%, r_{ratio} = 0.6) exposed to different visible light exposure times; (C) G' of hydrogels (T_L = 2 min, r_{ratio} = 0.6) with varying W_{HANB}; (D) G' of hydrogels (W_{HANB} = 3%, T_L = 2 min) with varying r_{ratio}; (E) G' of hydrogels (W_{HANB} = 3%, r_{ratio} = 0.6, T_L = 2 min) with increasing Ropinirole HCL concentrations; (F)

Results of Ellman's reagent test on thiol concentration over time (W_{HANB} = 3%, r_{ratio} = 0.6, T_L = 2 min). All the bioink formulations contained 80 mg/mL of Ropinirole HCL, with the exception of (E). Asterisks denote statistical significance (** denotes $p < 0.01$; *** denotes $p < 0.001$). …….. 44

Figure 2.3: Bioink droplet formation picture sequence ……... 46

Figure 2.4: Mechanical properties of blank preform tablets. (A) Hardness (HV) and (B) tensile strength (MPa) of microcrystalline cellulose preform tablets; (C) Fabricated preform tablets …….. 47

Figure 2.5: Ropinirole HCL release profile ……..…… 48

Figure 2.6: Hydrogel water content removal. (A) Hydrogels exposed to 50 °C for varying times; (B) Percent of weight loss in the hydrogel due to water removal with increasing drying times …… 49

Figure 2.S1: ^{1}H NMR shifts of norbornene groups (D_2O): Z (methyl protons in hyaluronic acid, 3H); A (α protons in the ADH group, 4H); B (β protons in the ADH group, 4H); C (*endo* vinyl protons, 2H); D (bridgehead protons, 2H); E (norbornene α protons, 2H) …….. 50

Figure 2.S2: Custom preform tablet punches and die for direct powder compression ……... 51

Figure 2.S3: Statistics on tablet water removal percentage over drying time. A One-way ANOVA test with a Dunnett's post-test analysis was done, with column (180min) taken as control (* denotes statistical significance; P < 0.0001). Results show no statistical difference after 60 minutes of drying at 50 °C ……..…. 52

Figure 3.1: Polymerized PEGDA gels with different W_{PEGDA} values. The bioinks were exposed to a T_L of 1.5 min. It can be observed that the gels have a higher opacity as the W_{PEGDA} decreases, due to a higher concentration of PEG200 …….. 73

Figure 3.2: Mechanical properties of polymerized hydrophobic gels. (A) Effect of different W_{PEGDA} and T_L values on polymerized gels. (B) Effect of increased temperatures

on the viscosity of formulations with different W_{PEGDA} values. (C) Gelation time of bioinks containing different W_{PEGDA} values. The formulations were exposed to visible light after 30 s of G' data collection 74

Figure 3.3: Tensile strength of Naproxen and Ibuprofen loaded gels with a W_{PEGDA} of 100% and a T_L of 45 s. (A) Tensile strength of Naproxen tablets with diverse drug concentrations. 40 mg/mL was the maximum solubility achieved for this API in this bioink formulation. (B) Tensile strength of Ibuprofen tablets with diverse drug concentrations. 180 mg/mL was the maximum solubility achieved for this API. (C) Tensile strength comparison between gels loaded with Naproxen and Ibuprofen at a concentration of 40 mg/mL. The difference observed shows that the mechanical properties of these gels can be impacted by both, the concentration of the drug utilized and the compound chosen as model drug. Asterisks denote statistical significance (* denotes p < 0.1; ** denotes p < 0.01; *** denotes p < 0.001) 75

Figure 3.4: SEM images of polymerized bioinks with W_{PEGDA} of 100% and 20%, exposed to a T_L of 45 s. The images show an increased porosity for the gel with a W_{PEGDA} of 20%. This characteristic explains the increased opacity observed on gels with low PEGDA concentrations 76

Figure 3.5: Droplet formation sequence for PEGDA bioink with a W_{PEGDA} of 100% and loaded with Naproxen at a concentration of 40 mg/mL. This formulation had a Z value of 4.47, falling within the printable range (4-14) 77

Figure 3.6: Images of uncoated/coated preform tablets and SEM images of their surface. (A) Microcrystalline cellulose uncoated preform tablet made by powder compression. (B) Microarchitecture of the uncoated well center section. (C) Microarchitecture of the well edge (walls of the well in the preform tablet). A high porosity is observed in this area, causing a leak of bioink in uncoated preform tablets. (D)

Microcrystalline cellulose E-100 coated preform tablet. (E) Well center of the preform tablet coated with E-100. (F) Edges of the preform tablet coated with E-100, where a significant decrease in porosity is observed 78

Figure 3.7: Dissolution test of preform tablets loaded with Naproxen at a concentration of 40 mg/mL. (A) Percent of drug release over time. The impact of different W_{PEGDA} and T_L values over drug release is observed, with higher W_{PEGDA} and T_L values resulting in slower drug release kinetics. (B) Statistical analysis on percent of drug release after 24 h of dissolution time. (* denotes $p < 0.1$; *** denotes $p < 0.001$) 79

Figure 3.8: 2D spatial control of the bioinks through the inkjet deposition process. (A) Formation of a circular shape through the dispensing procedure. (B) Control of 2D spatial distribution for the formation of a square 80

Figure 3.S1: Images of Ibuprofen loaded gels (180 mg/mL) with varying W_{PEGDA} values and a T_L of 3 min. An increased opacity is observed as the W_{PEGDA} is decreased, as seen in Figure 1 81

Figure 3.S2: Effect of increased temperatures on the viscosity of Ibuprofen loaded formulations (180 mg/mL) with different W_{PEGDA} values 82

Figure 3.S3: Gelation time of Ibuprofen loaded bioinks (180 mg/mL) containing different W_{PEGDA} values. The formulations were exposed to visible light after 30 s of G' data collection 83

Figure 3.S4: SEM images of polymerized bioinks with W_{PEGDA} values of 100%, 80, and 20%, exposed to a T_L of 3 min. The images show an increased porosity in gels with decreased W_{PEGDA} values. This characteristic explains the increased opacity observed on gels with low PEGDA concentrations in Figure S1 84

Figure 3.S5: Droplet formation sequence for PEGDA bioink with a W_{PEGDA} of 100% and loaded with Ibuprofen at a concentration of 180 mg/mL 85

Figure 3.S6: Preform tablet schematics. (A) Preform tablet dimensions. (B) Preform tablet 3D model. (C) Preform tablet fabricated by powder compression …….. 86

Figure 3.S7: Mechanical properties of different areas within the preform tablet. (A) Image demonstrating the two areas tested for tensile strength within the tablet, to assess differences in mechanical properties. (B) Tensile strength values of different sections in the preform tablet …….. 87

Figure 4.1: The upper row shows images of the polymerized hyaluronic acid based bioink, loaded with Lisinopril at a concentration of 40 mg/mL. This bioink has a W_{HANB} value of 3% and a T_L of 2 min. The bottom images show polymerized PEGDA gels with a W_{PEGDA} value of 30%, a W_{EtOH} value of 20%, and a T_L of 1.0 min. It can be observed that the hydrophobic gel has a high opacity due to a high concentration of PEG200 (50%) …….. 108

Figure 4.2: Tensile strength of Lisinopril and Spironolactone gels. (A) Tensile strength of Lisinopril tablets with diverse drug concentrations. 40 mg/mL was the maximum solubility achieved for this API in this bioink formulation. No statistic difference was observed between samples with varying Lisinopril concentrations. (B) Tensile strength of Spironolactone tablets with diverse drug concentrations. 100 mg/mL was the maximum solubility achieved for this API. No statistical difference was observed between samples with varying concentrations …… 109

Figure 4.3: Cross-sectional SEM images of polymerized bioinks loaded with Lisinopril and Spironolactone. (A) Lyophilized Lisinopril loaded hydrogel (40 mg/mL) with a W_{HANB} of 3% and an r_{ratio} of 0.6. This bioink was exposed to a T_L of 2 min. (B) Polymerized hydrophobic ink loaded with Spironolactone (20 mg/mL). This formulation contained a W_{PEGDA} of 20% and a T_L of 1 min …….. 110

Figure 4.4: Droplet formation sequence for hyaluronic acid based bioink with a W_{PEGDA} of 3%, an r_{ratio} of 0.6, and loaded with Lisinopril at a concentration of 40 mg/mL. This formulation had a Z value of 6.99, falling within the printable range (4-14) ….. 111

Figure 4.5: Droplet formation sequence for PEGDA based bioink with a W_{PEGDA} of 30%, and loaded with Spironolactone at a concentration of 20 mg/mL. This formulation had a Z value of 10.52, falling within the printable range (4-14) …… 112

Figure 4.6: Multiple compartments fabricated preform tablet. (A) Side view of the 3 pieces constituting the preform tablet. From left to right, top cap, top compartment, and bottom compartment. These pieces were manufactured by powder bed 3D printing using as binder DI water with 5% ethanol and 0.25% Tween 80. The powder utilized for their construction was calcium sulfate. Each of the two wells have a 250 µL capacity. (B) Front view of the preform tablet fabricated. (C) Comparison between the assembled version of the preform tablet and commercially available gel capsules …….... 113

Figure 4.7: SEM imaging of the untreated and coated preform tablet surfaces. (A) Surface of untreated preform tablet. (B) Bottom compartment infused with a 10% E-100 in acetone solution. (C) Top compartment infused with a 15% PEG (35 kDa) in acetone solution. (D) Inner section of the top compartment preform tablet, brushed with a 20% E-100 in acetone solution ……. 114

Figure 4.8: Multiple compartments preform tablet loaded with hydrophilic (bottom) and hydrophobic (top) bioinks …….. 115

Figure 4.9: Dissolution test of polypill. A sustained release profile was achieved for both APIs. Around 90% of the Lisinopril loaded was release in a period of 24 h, releasing most of the drug within the first 8 h. Above 60% of the Spironolactone loaded was released in a period of 24 h …… 116

Figure 4.S1: Gelation kinetics obtained through in-situ photorhelogy of the hydrophilic bioink. The gelation kinetics were assessed through in-situ photorheology in a rheometer, at a constant strain of 1% and an angular frequency of 10 rad/sec. In this test, the storage modulus (G') of the bioinks was measured for 30 secs without light exposure. Immediately after this time, a visible light source was turned on and the G' was measured for another 270 s. Results show that the formulation achieves a G' higher than 100 Pa in 8.54 s …….. 117

Figure 4.S2: Tensile Strength of PEGDA based (W_{PEGDA} = 100%) gels loaded with varying concentrations of Spironolactone. These gels were exposed to light for a period of 3 min. We can see that light exposure time has a direct effect on tensile strength, since significant differences were observed under these conditions, diverging from results shown in Figure 2B …… 118

Figure 4.S3: Exposed gels after 24 h of dissolution time. It can be observed that most of the preform tablet is dissolved after the dissolution process …… 119

LIST OF TABLES

Table 2.1 Swelling ratio and parameters for *Z* value analysis of bioink 53

Table 3.1 Mesh size of polymerized gels with different W_{PEGDA} values and a T_L of 45 s ... 88

Table 3.2 Droplet formation capacity of Naproxen loaded bioinks 89

Table 3.S1 Mesh size of polymerized gels with different W_{PEGDA} values and a T_L of 3 min .. 90

Table 4.1 Physical properties and Z value of formulated bioinks 120

ACKNOWLEDGEMENTS

Gratitude. That word summarizes the sentiment and gratefulness I have towards my advisor Professor Benjamin M. Wu. This dissertation would not have been possible without your support and guidance. Thank you for the opportunity to work in your research group and for trusting my abilities going into a new industry collaboration. I would also like to thank Prof. Yvonne Y. Chen, Prof. Harold G. Monbouquette, and Prof. Yi Tang for their support throughout this interesting journey.

Research is a lot easier with the support of dedicated and talented scientists. I would like to thank Dr. Chase S. Linsley for his continuous help throughout these years. Thank you for listening to all my ideas and for always been available when I knocked your door. I would also like to thank Timothy Zhu for brainstorming and troubleshooting problems with me on a daily basis. It was a pleasure working and celebrating each little victory with you. Many thanks to Yunchang Lee and Dr. Yulong Zhang for your valuable help in this project.

As the years went by, I had the privilege to know special individuals that became my friends and extended family, being so far from my country. Thank you, Nikki, Jon, Elias, Lam, Talar, Shiva, Nicole, Chabeli, Nitzaira, José, Jorge, Julian, Roxana, and Pablo for maintaining my sanity and all the fun times together.

Chemical engineering was the discipline I chose to learn as the foundation of my professional career. Through this discipline many years ago, I met a person that during these years served as some sort of pressure relief valve and who is also my best friend. Felix, thanks for listening. I made it. Good stuff.

In our existence, professional advice is important to be successful. But more important is to have guidance through the combination of daily experiences that, in a condensed form, we define as the word “life”. Doña Iris, thank you for all the advice given during the years you and I co-existed in this planet. Thank you for teaching me ways of thought that are not learned in academia and are only acquired as we experience life and all its complexities. I will always remember our conversations and your words for the rest of my days.

A*mor*, Katie, thank you for being there each and every day. Thank you for listening to the chronicles of my scientific development and encouraging me to write them. Thank you for being with me in the successful times and in the less fun ones. Your company made this adventure an easier one to walk through.

Support from my family has been vital throughout this journey. Mom and Dad, thank you for your constant emotional support and love. Thanks Marco for making me laugh and for being an awesome brother. *Los amo*.

Chapter One is a version of [Acosta-Vélez, G. F. & Wu, B. M. 3D Pharming: Direct Printing of Personalized Pharmaceutical Tablets Abstract Powder Bed Inkjet 3D Printing. *Polym. Sceiences* **1,** 1–10 (2016).]

Chapter Two is a version of [Acosta-Vélez, G. F., Linsley, C. S., Craig, M. C. & Wu, B. M. Photocurable Bioink for the Inkjet 3D Pharming of Hydrophilic Drugs. *Bioengineering* **4,** 1–11 (2017).]

VITA

Education

University of Puerto Rico - Mayagüez, Mayagüez, PR — Aug. 2006 – May. 2011
Chemical Engineering
Bachelor of Science

Teaching Experience

Teaching Associate — Oct. 2014 – Dec. 2014
Henry Samueli School of Engineering and Applied Sciences
University of California, Los Angeles

Teaching Assistant — Oct. 2012 – Dec. 2013
Henry Samueli School of Engineering and Applied Sciences
University of California, Los Angeles

Work Experience

Global Technical Operations Engineer — June 2010 – July 2010
Merck Sharp and Dohme, Barceloneta, P.R.

Process Engineer — Jan. 2009 – July 2009
Eli Lilly and Company, Carolina, P.R.

Publications

Journal Publications

Acosta-Vélez, G. F., Linsley, C. S., Craig, M. C. & Wu, B. M. Photocurable Bioink for the Inkjet 3D Pharming of Hydrophilic Drugs. *Bioengineering* 4, 1–11 (2017).

Acosta-Vélez, G. F. & Wu, B. M. 3D Pharming: Direct Printing of Personalized Pharmaceutical Tablets Abstract Powder Bed Inkjet 3D Printing. *Polym. Sceiences* 1, 1–10 (2016).

Griffin, D. R., Borrajo, J., Soon, A., Acosta-Vélez, G. F. *et al.* Hybrid photopatterned enzymatic reaction (HyPER) for in situ cell manipulation. *ChemBioChem* 15, 233–242 (2014).

Publications in Preparation

Acosta-Vélez, G. F., Zhu, T.Z., Linsley, C. S. & Wu, B. M. Photocurable Poly(ethylene glycol) as Bioink for the Inkjet 3D Pharming of Hydrophobic Drugs.

Acosta-Vélez, G. F., Linsley, C. S., Zhu, T.Z. & Wu, B. M. Use of Photocurable Bioinks for the 3D Pharming of Combination Therapies.

Proceedings

Acosta-Vélez, G. F., Zhu, T.Z., Linsley, C. S. & Wu, B. M., “Photocurable Bioink for the Inkjet 3D Pharming of Hydrophilic Drugs” Poster presentation at 2016 GSK Postdoctoral Symposium, Philadelphia, PA.

Acosta-Vélez, G.F., Griffin, D.R., Segura, T., “Hybrid photoactive-enzymatic platform for the patterning of biomolecules and in-situ cell manipulation” Poster presentation at 2014 UCLA Tech Forum, Los Angeles, CA.

Acosta-Vélez, G.F., Griffin, D.R., Segura, T., “Hybrid photoactive-enzymatic platform for the patterning of biomolecules within hydrogels” Poster presentation at 2013 Vasculata Conference, San Diego, CA.

CHAPTER ONE: INTRODUCTION TO 3D PHARMING - DIRECT PRINTING OF PERSONALIZED PHARMACEUTICAL TABLETS

1.1 ABSTRACT

Personalized medicine aims to tailor drug combination and dosage manufacturing to the specific needs of a patient by taking into consideration its genetic profile, phenotypic response, and pathophysiology. New technologies are needed to enable the rapid manufacturing of custom pharmaceutical tablets in a scalable manner, while meeting quality assurance regulatory standards. 3D Pharming, the use of 3D Printing to directly fabricate personalized pharmaceutical tablets, is under intense development by many investigators due to its unprecedented control for: 1) stability of multiple drugs within a pill; 2) precise dose of each drug; and 3) release kinetics of each component by incorporating designed structures that can modulate dissolution and diffusion profiles. Additionally, it has the potential to scale in order to meet the economics and quality that the pharmaceutical industry demands. This article reviews the manufacture of pharmaceutical tablets through powder bed inkjet 3D printing and fused deposition modeling, the two 3D printing techniques with the greatest progress towards personalized pharmaceutical tablets. The engineering of pills through these two methods, featuring varied dissolution profiles, chemical complexions, dosages, and multiple drugs incorporation, is thoroughly discussed.

1.2 INTRODUCTION

Currently, the ten top-grossing drugs in the United States effectively benefit only 4 to 25 percent of the patients that take them [1]. For instance, some drugs have been proven to have higher efficiencies in people with certain genetic variations, while others have been proven harmful to particular ethnic groups [2,3]. More specifically, a person diagnosed with cancer back in 2004 might have received a treatment only effective on ten percent of the population and caused significant side effects. Advances in the field of Pharmacogenomics, the study of how the genetic makeup of a person affects their particular drug response, are providing more precise information about the dosage and choice of drug that would best benefit a specific individual

based on their genetic makeup [4,5]. In contrast nowadays, a biopsy tissue of that person could be genetically screened, predicting which treatment would more reliably treat the pathological condition [6].

Personalized medicine aims to provide patients with treatments tailored to their pathophysiology. This is done by coupling a patient's pharmacogenomics with information about their diet, environment, lifestyle, microbiome, and epigenetics [7]. This new approach for prescription drugs requires technology capable of producing tablets with a variety of dosage strengths, in order to satisfy the specific medical needs of each individual. Currently, pharmaceutical companies manufacture tablets with universal predetermined dosage amounts [8]. This method requires large facilities with high production costs, trained personnel for its operation, and involves a variety of processing steps [9]. To make personalized medicine a reality, a paradigm shift in the way oral drug forms are currently manufactured is required. The new strategy should have the ability to reproducibly generate a wide range of dosages and have a short manufacturing time. These features would allow tablet manufacture technology to adapt to the rapid changeover of formulations experienced by scientists within R&D and clinical trial studies, accelerating drug development. Additionally, it should be economically viable, have minimal space and operational training requirements, comply with standards of regulation agencies, and able to be digitally controlled by healthcare staff [10]. 3D printing was first demonstrated in 1996 as a promising candidate to replace conventional tableting techniques [11]. In 2015, the U.S. Food and Drug Administration agency (FDA) granted the approval of Spritam® (levetiracetam), the first 3D printed tablet for the treatment of epileptic seizures [12]. This landmark event marks a milestone in 3D Pharming and motivates further development of this technology towards the fabrication of customized tablets and improved personalized medicine. 3D Pharming promises to enable rapid point-of-care formulations with patient-specific dosages [13]. Furthermore, 3D Pharming provides control over drug release kinetics through methods that precisely manipulate the spatial distribution of multiple drugs within a pill, as well as their diffusion

gradients [14]. This potential reduction in the number of tablets prescribed, combined with their improved efficacy, could result in enhanced patient compliance [15]. Finally, the economic benefits of this technology include reduced manufacturing and inventory wastes and the potential to grow to an industrialized scale [16].

The term 3D Pharming encompasses the various 3D printing and 2D material deposition technologies that are used to create personalized dosage forms. This review paper will focus on recent advances in 3D Pharming efforts between 1996 and February 2016. During this period, powder bed inkjet printing and fused deposition modeling (FDM) were 3D printing platforms commonly used, since these material deposition techniques allow for the fabrication of structures with 2D and 3D spatial gradients. In contrast, platforms that build structures through energy deposition, such as stereolithography, cannot produce point- to-point variations in composition of matter without combining with secondary 2D material deposition techniques. A special focus is given to the advantages and limitations of these two techniques, as well as to the different materials utilized among them for immediate and sustained drug delivery applications. Efforts towards the inclusion of multiple drugs and the synthesis of polypills are reviewed. Finally, the challenges ahead and future work required to make 3D Pharming a reality are evaluated.

1.3 POWDER BED INKJET 3D PRINTING

Inkjet printing technology is based on two main droplet formation techniques: continuous jet (CJ) printing and drop on demand (DOD) printing. CJ printing relies on a pressurized flow to produce a continuous stream of charged droplets. After being released through a nozzle, these droplets are directed by electrostatic plates into the substrate intended for their deposition, or deviated into a waste recirculation line when not needed for the printing process [17]. DOD printing has a more precise and less wasteful execution, producing droplets that are dispensed only when required by the process, with volumes as low as 1-300 pL [18,19] and frequencies of up to 10,000 Hz. [20]. DOD printheads are primarily actuated by thermal and piezoelectric trigger mechanisms. Thermal printheads have embedded resistors that produce heat upon the induction of an electrical

current. This heat creates a bubble within the volatile material being printed that mobilizes a small volume out of the nozzle, resulting in droplet formation. Thermal inkjet printing requires the use of high vapor pressure solvents and produces high temperatures that, although short lived, can result in the degradation of heat-liable bioactive compounds. These factors limit the use of thermal printheads for pharmaceutical applications [21]. In contrast, piezoelectric printheads incorporate piezoelectric materials that expand and contract when induced to an electrical current. These physical deflections generate the pressure required to mobilize liquid out of the nozzle in the form of droplets [22]. The capacity of operating at room temperature with less volatile and more biocompatible liquids makes the piezoelectric printing technology more suitable for the development of drug delivery devices [14,23].

Powder bed 3D printing, a technology originated at MIT, makes use of an inkjet printhead to deposit a layer of binder solution onto a powder bed containing the material desired for object construction [24,25]. The object is defined through the use of computer-aided design (CAD) software and digitally sliced in detailed pieces of information that delineate each one of the layers to be printed through the process. After each layer deposition, a piston that supports the powder bed is lowered allowing a subsequent layer of powder to be spread and selectively bound, as depicted in **Figure 1** [26]. This process is repeated several times, stacking layers of solidified material until a predetermined 3D geometry is produced. Excess powder not bound is then removed exposing the final product, which can go through further processing to tune its final mechanical and physical properties [27]. This technology allows for direct control over both, the macro and microstructure of objects, enabling the creation of complex biochemical devices. Incorporating patient specific anatomical data into the process have made possible the creation of implants, prosthetics, diagnostic platforms, and drug delivery systems [28]. Based on the literature research done, Wu et al. conducted the first experiments involving 3D Pharming by printing multi-drug delivery devices in 1996 [11]. In this study, the release profiles of methylene blue and alizarin yellow dyes were controlled by manipulating the three -dimensional position of

dyes within the device, its microstructure, and chemical composition. A square grid pattern of 5 cells by 5 cells composed of polyethylene oxide (PEO) was printed and dyes were localized in predefined patterns within the squares. A polycaprolactone (PCL) sheet was printed at the top and bottom of this grid to seal it and prevent dye diffusion upon resorption, yielding a two-dimensional diffusion profile limited to the plane of the device. In vitro release studies showed a multiphasic release profile of the dyes incorporated.

Kastra et al. demonstrated that the drug release mechanisms of these newly conceived devices could be controlled by the chemical properties of the binder utilized and its final concentration within the pill [29]. Eudragit E-100, a cationic methacrylic ester copolymer soluble under acidic conditions below pH 5, was used as a binder to fabricate cellulose tablets with an erosion dominated drug release mechanism. Tablets with diffusion controlled release profiles were made by utilizing Eudragit RLPO as binder. Eudragit RLPO is a permeable and insoluble ammonio-methacrylic acid copolymer and its properties have no dependence on pH. Dissolution studies of these tablets in simulated intestinal fluid demonstrated an increase in drug release time with an increased binder content within the tablet printed. The hardness and friability of the designed drug delivery devices were comparable to commercially available compressed tablets. Moreover, using fluorescein as a model drug, it was shown that this technology can precisely control the dosage of drugs by achieving loads in the pico moles range.

Taking advantage of the control that binders offer over drug release mechanisms, Rowe et al. made use of diverse binders to fabricate tablets with complex drug release profiles [30]. A device with an immediate-extended release profile of the molecule chlorpheniramine was fabricated by using E-100 as a binder for half of the pill and E-RLPO for the second half, as shown in **Figure 2A**. The immediate release section delivered the full load of chlorpheniramine maleate within the first 30 min of the dissolution process. The extended release part maintained a sustained release for a period of 6 h (**Fig. 2B**). A tablet with a pulse release profile of diclofenac was designed to trigger drug release in both gastric and intestinal fluid by using various binders

sensitive to pH values characteristic of these areas. E-100 was used to print a section of the pill sensitive to the low pH found in gastric fluid, whereas Eudragit L-100, an anionic methacrylic ester copolymer sensitive to solutions with pH values above 6, was used to achieve drug release in intestinal fluid. Additionally, breakaway tablets were fabricated to extend the distribution of drugs with low pharmacokinetic transport rates throughout the gastrointestinal wall.

Wang et al. fabricated cubic drug delivery devices with a near- zero controlled release profile containing pseudoephedrine hydrochloride [31]. The device was composed of hydroxypropyl methylcellulose (HPMC) and Kollidon SR as main materials. The cubic shell portion of the device was printed by utilizing a 15% triethyl citrate solution in ethanol as binder. An inner cubic core was printed with an aqueous binder containing 50% by weight of pseudoephedrine hydrochloride. The system's drug release mechanism was dominated by diffusion of the drug located at the inner core through the shell layer and out into the dissolution medium. Control of the release profile was shown by the tuning of the HPMC to Kollidon SR ratio, achieving formulations with drug release profile times of 8, 12, and 16 h as the concentration of HPMC increased, respectively. This near-zero release profile proved to be independent of pH changes in the dissolution medium, paddle stirring rate, or the inclusion of a sinker. To increase the drug load within the tablets, Yu et al. fabricated tablets by pre-mixing the active acetaminophen with the main excipients located in the powder bed, rather than incorporating the drug through the binder [32]. Tablets with acetaminophen concentrations as high as 68% by weight were produced. Furthermore, a zero-order release profile was achieved by printing insoluble layers at the top and bottom of the cylindrical device, resulting in a two-dimensional release profile. Moreover, the devices included a radial gradient of the release- retardation material ethyl cellulose. This gradient decreased towards the inner part of the tablet, while the void space was gradually increased (**Fig. 3A**). The combination of these factors allowed for a higher drug diffusion as the tablet eroded, causing a constant release rate throughout the dissolution process. **Figure 3B** shows the erosion process of the device after 0, 1, 3, 5, 7, and 10 h of dissolution. The incorporation of central holes

in compressed tablets has been used to promote zero-order release profiles by maintaining a constant surface area during the simultaneous erosion of its inner aperture and outer layer [33,34]. More recently, Yu et al. fabricated doughnut-shaped acetaminophen tablets and obtained zero-order drug release profiles by printing insoluble and impermeable top and bottom layers, resulting in a 2-dimensional drug release limited to the plane of the device [35]. Other design parameters, such as inner aperture radius, annular thickness, height, and number of binder passes per layer were manipulated. Results showed that the total drug release time increased with decreasing inner radiuses and increasing number of binder passes.

Powder bed 3D printing has also been applied towards the fabrication of fast disintegrating/dissolving tablets (FDTs). Yu et al. produced FDTs with average disintegration times of 23.4 s [36]. This was achieved by printing tablets with compact top, bottom, and lateral layers, while leaving loose powder in the middle section of the pill resulting in an area of high porosity and permeability (**Fig. 4**). Binder was dispensed in selected areas of the middle section of the pill to increase its mechanical stability. In vitro dissolution tests showed that 98.5% of the active acetaminophen was released within 2 min. The FDTs had an acceptable harness value of 63.4 ± 5.4 N/cm2. However, friability studies demonstrated an unsatisfactory mass loss of 3.55 ± 1.16%. This was corrected in a further study by incrementing the number of binder passes through the printing process and not printing selected areas in the middle section of the tablet, resulting in a net weight loss of 0.92 ± 0.14% [37]. Net weight loss values below 1% are considered acceptable based on regulations by the United States Pharmacopeia (USP).

In 2015, the FDA approved the first FDT manufactured through powder bed 3D printing [12]. The company Aprecia designed a tablet containing the active levetiracetam, a drug for the treatment of epilepsy, with a dissolution time of about 15 s in saliva or 10mL of water [38]. This advancement highlights the potential within this technology for the development of specialized drug forms with features not achievable through compression or other conventional tablet fabrication methods. Nonetheless, prior to its implementation as a definite replacement of current

tableting techniques, this technology would require improvements in several areas such as the combination of multiple drugs at high dosages, printing time, and the production of porous, hollow, and more complex architectures for the further regulation of drug release profiles.

1.4 FUSED DEPOSITION MODELING (FDM)

Fused deposition modeling (FDM) was patented in 1989 by Scott Crump, co-founder of Stratasys Ltd, and developed as an alternative to the inherent limitations of powder bed 3D printing [16,39]. This technique involves the melting, extrusion, and layer by layer deposition of materials that after solidification result in objects with predetermined structures (**Fig. 5**) [40]. To control the pore size and the configuration of the object, variables such as raster angle and thickness, space between rasters, and the extrusion tip diameter can be manipulated. The appropriate heat transfer characteristics and rheological properties are the most critical material qualities evaluated for FDM use. Molten metals, self-hardening waxes, and thermoplastic materials such as nylon, acrylonitrile butadiene styrene, and polyvinyl chloride have been utilized successfully [16,28].

Among the advantages of FDM are its lower costs, the ability to print multiple polymers in a single structure, and the capacity to create hollow and porous objects with good mechanical strengths [28]. These characteristics enable FDM as a suitable technique for the manufacturing of personalized tablets and their subsequent discharge at dispense/point-of-care locations. Challenges of this process include the limited amount of thermoplastic materials with appropriate rheological properties and the possible degradation of incorporated drugs, caused by the exposure of active ingredients to high temperatures. These factors combine to severely limit the choice of extrusion materials for tablet printing. The concept of extruding a material containing an active drug for 3D Pharming was first used by Khaled et al. in 2014 [41]. The authors printed bi - layer tablets loaded with the active guaifenesin, an expectorant used to reduce chest congestion. The fabricated tablets contained an immediate release compartment composed of HPMC 2910 as binder, in combination with microcrystalline cellulose and sodium starch glycolate as

disintegrants. The other half of the pill featured a sustained release section constituted of HPMC 2208 and poly(acrylic acid) as hydrophilic matrix. These materials were processed separately and combined with the active, resulting in the synthesis of two viscous pastes that were used as feedstock for the printing process. A dissolution analysis of the tablets was performed where the pills were exposed to an acidic medium representative of the stomach for a period of 2 h, followed by exposure to a 0.2 M trisodium phosphate dodecahydrate solution with a pH of 6.8, representative of the small intestine. The authors reported complete depletion of the drug in the immediate release compartment within the first 30 min of dissolution, while maintaining a sustained release for a period of 12 h. It was demonstrated that the drug release rate at the sustained release section could be controlled by tuning the concentration of HPMC 2208 in the paste, showing a decrease in release rate as the HPMC 2208 was increased. Release profiles were similar to commercially available guaifenesin tablets.

Even though Khaled et al. demonstrated the extrusion of excipients containing actives for the printing of pharmaceutical tablets, their procedure was carried at room temperature and the materials were not melted prior to extrusion, both intrinsic characteristics of FMD. FDM per se was first applied for 3D Pharming when Goyanes et al. printed fluorescein-loaded polyvinyl alcohol (PVA) filaments in 2014 [42]. The authors loaded fluorescein by swelling the polymer filaments in a fluorescent-ethanol solution. The amount of fluorescein incorporated into the filaments was 0.29% w/w, mainly located at the surface of the filaments due to a slow diffusion of the drug into the polymer. Tablets with different infill percentages (**Fig. 6**) were printed by extruding the drug loaded filaments at a temperature of 220°C. Dissolution tests carried out in a bicarbonate buffer at pH 6.8 demonstrated that the drug release rate could be tuned by changing the infill percentage of the tablets, with lower percentages resulting in faster release rates.

The team later demonstrated the importance of adequate drug selection by the incorporation of two isomeric molecules [43]. The aminosalicylates 5-aminosalicylic acid (5-ASA) and 4-aminosalicylic acid (4-ASA) were incorporated into separate PVA filaments resulting in

tablets with drug loads of 0.063 ± 0.001% w/w and 0.236 ± 0.004% w/w, respectively. Even though these molecules are isomers, 5-ASA had a faster release rate than 4-ASA. Moreover, differential scanning calorimetry (DSC) analysis of the 4 -ASA tablet after printing showed a drug degradation of 50%, stating the limitation of the technique regarding thermally labile molecules.

Skowyra et al. used FDM to print ellipse-shaped tablets loaded with the steroid prednisolone and demonstrated the weight and dosage accuracy that can be achieved through the FMD technique [10]. PVA filaments were immersed in a methanol solution containing prednisolone, achieving a drug load of 1.9% w/w. The mass of the pills was manipulated by tuning the volume of the tablets. Tablets with weights of 2, 3, 4, 5, 7.5, and 10 mg were printed at an extrusion temperature of 230°C with a dosage accuracy range of 88.7-107%. Thermal analysis by DSC and x-ray powder diffraction (XRPD) confirmed that the drug loaded existed in the amorphous form within the tablets.

An important aspect considered during the design of pharmaceutical tablets is its shape and its effect on drug release profiles. To evaluate this aspect, tablets with several geometries including cube, pyramid, cylinder, sphere, and torus, were printed and their drug release profiles were analyzed [44]. In an effort to increase the drug content within PVA filaments, the drug paracetamol was incorporated by hot melt extrusion (HME), a technique in which multiple materials are extruded at high temperatures to obtain a homogeneous mixture with uniform shape [45–47]. The drug load achieved in the tablets printed was 3.78% w/w. During dissolution studies, tablets with different geometries and equivalent surface areas resulted in drug release rates in the following order; pyramid > torus > cube > sphere and cylinder. This result indicated that drug release rate is dependent on the surface area/volume ratio of the tablet, with higher ratios producing faster release rates. In this case, the pyramid design had the highest surface area/volume ratio (1.169) while the sphere had the lowest (0.634).

HME has also been utilized to create drug loaded filaments made of methacrylic polymers. Pietrzac et al. incorporated the drug theophylline into Eudragit RL, Eudragit RS, and Eudragit E,

and 3D printed tablets with a drug loading of 50% and dose accuracy between 91 and 95 percent [9]. It was demonstrated that the mass of the tablet and its printed volume followed a linear relationship. Moreover, increasing the printing resolution of the process did not affect the final mass loaded into the tablet, but resulted in higher printing times. Goyanes et al. expanded the application of FDM by incorporating fluid bed coating techniques into the pills manufactured, in an effort to develop pH controlled drug release profiles [48]. The drug budesonide, commonly used to treat inflammatory bowel disease (IBD), was embedded into PVA through HME resulting in filaments with a drug load of 4.14 ± 0.273%. Tablets containing 9 mg of budesonide were 3D printed and coated with an Eudragit L100 based solution. Drug release studies demonstrated that budesonide release began at the mid- small intestine and maintained a sustained release up to the distal intestine and colon. FMD has also been utilized to fabricate hollow capsular devices for drug incorporation. Melocchi et al. created hydroxypropyl cellulose filaments and demonstrated the feasibility of FMD for this purpose by comparing the product obtained to capsules manufactured by injection molding [49]. Capsules made through both methods were loaded with 80 mg of acetaminophen and dissolution tests showed similar drug release profiles. This technique features advantages over the powder bed 3D printing technology such as the ability to produce more complex structures, print multiple materials in a single tablet, and a lower cost of equipment. Yet, more efforts towards the reduction of drug degradation due to heat exposure and the development of more materials suitable for FDM are required.

1.5 MULTIPLE DRUGS INCORPORATION

Since the first publication on this topic [11], one of the goals of 3D Pharming has been to deliver patient-specific combinations of multiple drugs into a single tablet, customized to the needs of the patient in terms of drug choice and dosage. This advancement would reduce the number of pills consumed by patients on a daily basis and potentially enhance patient compliance [15]. 3D Pharming has been applied within several studies in order to incorporate multiple drugs into one tablet, while controlling their individual release rates, profiles, and release mechanisms.

These are critical parameters to take into consideration during the design of a drug delivery device such as pharmaceutical tablets, as they define the location and the time where the drug release occurs within the gastrointestinal (GI) track, as well as the concentration of drug secreted through a defined period of time. Sun et al. demonstrated a novel technique to create customized drug release profiles within a tablet, producing profiles with a constant rate of release, pulsed rate, increased rate, and decreased rate release [50]. In their study, an impermeable polylactic acid (PLA) tablet was 3D printed, leaving an opening at the top of it to allow for drug diffusion, as observed in **Figure 7A**. To fill the tablet, a pre-polymer solution was casted in polydimethylsiloxane (PDMS) molds with different shapes and cured by exposing the solution to UV light for a period of 10 min. The precursor solution was composed of 4-pentenoic anhydride, pentaerythritol tetrakis (3-mercaptopropionate) (PETMP), and/or ethylene glycol dithiol (EGDT; 3,5 -dioxa-1,8- dithioocatne) as crosslinker, using 1-hydroxycyclohexyl phenyl ketone as photoinitiator. After polymerization, the drug loaded material was located inside the tablet and the void spaces were filled by drug-free pre-polymer solution and exposed to UV light, culminating the tablet fabrication. Orange G and Brilliant Blue G were utilized as model drugs. **Figure 7B** shows how the release profiles of the two dyes are directly dependent on the shape of the polymerized solution introduced. The study showed a novel technique for the release of multiple drugs within a tablet with diverse customized release profiles. Moreover, the release rate could be further modified by manipulating the ratio between PETMP and the crosslinker EGDT, with lower crosslinking ratios resulting in faster drug release rates.

In a different study, Goyanes et al. used FDM to manufacture tablets containing the molecules paracetamol and caffeine [51]. The filaments used for the printing process were made by mixing each drug per separate with PVA and applying HME. Filaments with two different drug concentrations were made for each molecule, achieving drug loads of 4.3% and 8.2% for paracetamol and 4.7% and 9.5% for caffeine. In order to obtain diverse drug release profiles, tablets with two different designs were 3D printed. The first design featured 1 mm alternate layers

of caffeine and paracetamol, as shown in **Figure 8A**. The second design, named DuoCaplets (9.0 mm length x 3.34 mm diameter), consisted of a capsule shaped core containing one drug in the inside of the tablet and an outer layer where the opposite drug was located (**Fig. 8B**). Release studies were performed in a bicarbonate buffer at different pH values to simulate various sections of the GI track. Results demonstrated a simultaneous release of both drugs within the model featuring alternate layers, whereas the DuoCaplets model showed release of the drug located at the outer layer followed by the drug located at the inner side of the capsule. It was also demonstrated that the release rate of the drugs increased with an increased drug concentration within the filaments extruded.

Besides achieving control of the release profile of multiple drugs through adjustments on the tablet's design, other studies have incorporated diverse drug release mechanisms to regulate this parameter. Khaled et al. designed a polypill containing the drugs captopril, nifedipine, and glipizidine, a combination of drugs used to treat diabetics suffering from hypertension [52]. These drugs were released through two different mechanisms: diffusion and osmosis. The drug captopril was incorporated within an osmotic pump designed by incorporating sodium chloride as an osmogen in the mixture of excipients extruded, which resulted in a porous shell upon dissolution of the sodium chloride. The drugs nifedipine and glipizide were incorporated within HPMC, a material that swells upon exposure to a liquid medium and promotes a sustained release of the drugs encapsulated. Release studies demonstrated that the drug captopril showed a zero order drug release profile, induced by the osmotic pump designed. The drugs nifedipine and glipizidine followed a Korsmeyer-Peppas or first order release kinetics that varied with the active/excipient ratio utilized. These pills were printed by extruding pastes of excipients and actives at room temperature, a technique developed by Khaled et al. previously discussed in the Fused Deposition Modeling section [41].

The team subsequently printed a polypill containing 5 drugs: pravastatin, atenolol, ramipril, aspirin, and hydrochlorothiazide [53]. Developed to treat and prevent a multitude of cardiovascular

diseases and high blood pressure, the drugs were incorporated and segregated through different compartments in a single tablet (**Fig. 9**). The drugs aspirin and hydrochlorothiazide were located within immediate release compartments containing sodium starch glycolate as disintegrant, which induced the release of 100% of the drug within the first 30 min of dissolution. The drugs pravastatin, atenolol, and ramipril were located into compartments containing HMPC, designated to have a sustained release that continued for a period of 720 min. This study represents the maximum number of drugs incorporated into a single 3D printed tablet to date.

1.6 CONCLUSION AND FUTURE DIRECTIONS

The literature is replete with exciting demonstrations of 3D Pharming that can enable personalized medicine by producing patient specific formulations with speed and precision. Additionally, the required equipment is capable of being installed and operated in diverse settings, including traditional pharmacies as well as point of care locations such as hospitals and residential care facilities. Besides being highly scalable and cost effective, the precise quantity of drugs and excipients deposited during pill fabrication can be tracked, offering unprecedented access to quality assurance. Most excitingly, the patient specific formulations and dosages can be adjusted according to phenotypic evidence of intended results and undesirable side effects. This information can be loaded into the patient's individual database.

Additional efforts are required to increase the speed of production and satisfy the high demand for tablets loaded with multiple drugs at tailored dosages. Besides powder printing and FDM, other technologies that deposit matter through physiological and drug-compatible manners are being developed. PolyJet printing, a technology that dispenses photocurable polymer solutions into a tray, would reduce the manufacturing time of oral drug forms by maximizing the speed capabilities inherent of inkjet printing. More importantly, the engineering of biocompatible materials that maximize drug stability for the application of such technology would provide a novel alternative towards 3D Pharming. Different excipient materials are needed to print

hydrophilic/hydrophobic drugs with varying degrees of solubility. In addition, these excipients must be compatible with each other and with the deposition technology.

Beyond the scientific and engineering challenges, there are also regulatory obstacles that need to be addressed for the implementation of this technology. Advantages of depositing drugs drop-by-drop include precise control over dosage, high spatial resolution to create compositional gradients, and ability to monitor with video camera for quality assurance. A common limitation for both CJ and DOD printheads for 3D Pharming is that many drugs are poorly soluble in most biocompatible printable fluids, and they may need to be deposited in dispersions or particulate forms. Practical quality assurance monitoring subsystems that allow real-time and high resolution determination of drug dosing will be needed to ensure patient safety and efficacy.

An analysis of the economic feasibility of this paradigm shift within the pharmaceutical industry is needed regarding equipment expenditures, drug production, and adjustment of current regulations to overview novel protocols and pharmaceutical apparatuses. Currently, a tablet containing a variety of drugs would be considered by the FDA as a new combination drug formulation, requiring extensive clinical trials to assess its effectiveness and guarantee patient safety. Additionally, each location operating a 3D printer for the production and discharge of pharmaceutical prescriptions would require certification as a GMP facility. Efforts from regulating agencies in concert with the scientific community are required to develop regulations that ensure the safety of patients while promoting scientific advancement.

The choice of drug combination and dose that suits a patient's physiology will come from a combination of clinical phenotypic findings, pharmacogenomics data, and optimization search algorithms. Studies have demonstrated that primary care physicians do not feel confident regarding their ability to analyze data derived from genetic tests [54]. Reforms to medical curriculums, development of specialist training for medical geneticists, and implementation of personalized medicine certifications for on-going physicians are measures required to satisfy the demand of professionals in this new emerging field [55]. Furthermore, efforts to develop the

infrastructure required to store the biomedical data acquired and guidelines defining how this information is used to drive the identification and qualification of diverse biomarkers are necessary [56]. Since optimization search algorithms tend to improve with increasing data, guidelines will be needed to balance performance versus sharing of big data.

3D Pharming brings us a step closer to personalized medicine. The numerous cutting edge technologies described in this review are being developed to overcome basic limitations. This powerful transformation must be carefully controlled to protect society and individual privacy, while maximizing safety and efficacy.

1.7 DISSERTATION OBJECTIVES AND SPECIFIC AIMS

Advancements in technology are needed to overcome the current limitations experienced with Powder Bed 3D Printing and Fused Deposition Modeling (printing speed and high temperatures, respectively). Inkjet printing allows for the deposition of drug loaded formulations in high quantities (using multiple nozzles) and short periods of time, decreasing significantly the printing time. Moreover, this deposition technique operates at room temperature, preventing the degradation of drugs susceptible to degradation at high temperatures. Therefore, the objective was to develop a system for the manufacture of pharmaceutical tablets by dispensing photocurable drug-loaded formulations into blank preform tablets (vessel to the drug-loaded solution) through inkjet printing. This objective was accomplished by completing the following specific aims:

1. Design of a photocurable bioink for the inkjet 3D Pharming of **hydrophilic** drugs, demonstrate its droplet formation capability and further dispensing into blank preform tablets, and perform dissolution test to assess the drug release profile out of the designed oral dosage form.
2. Design of a photocurable bioink for the inkjet 3D Pharming of **hydrophobic** drugs, demonstrate its droplet formation capability and further dispensing into blank preform

tablets, and perform dissolution test to assess the drug release profile out of the designed oral dosage form.

3. Demonstrate the use of this technique towards the combination of multiple APIs into a single tablet by creating a polypill carrying a **combination therapy**, using hydrophilic and hydrophobic pharmaceutical compounds.

1.8 FIGURES

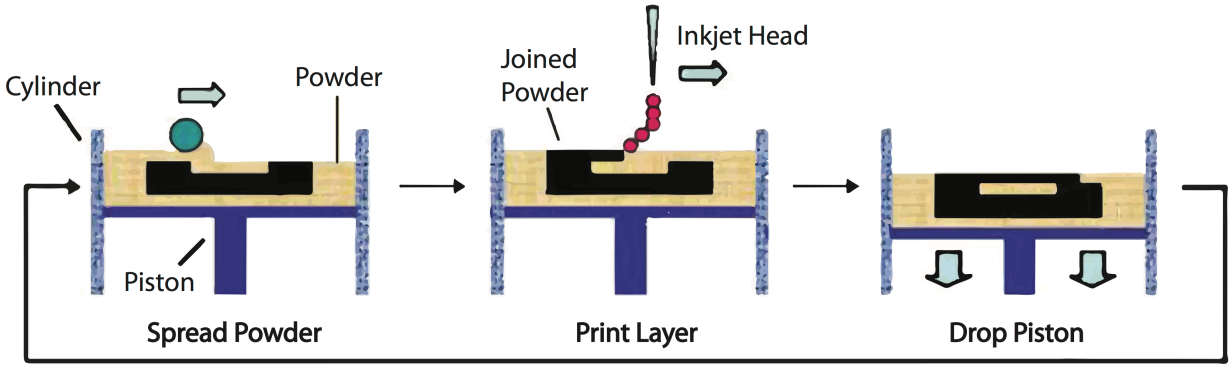

Figure 1. Powder bed 3D printing procedure schematic. Reproduced with permission from [26].

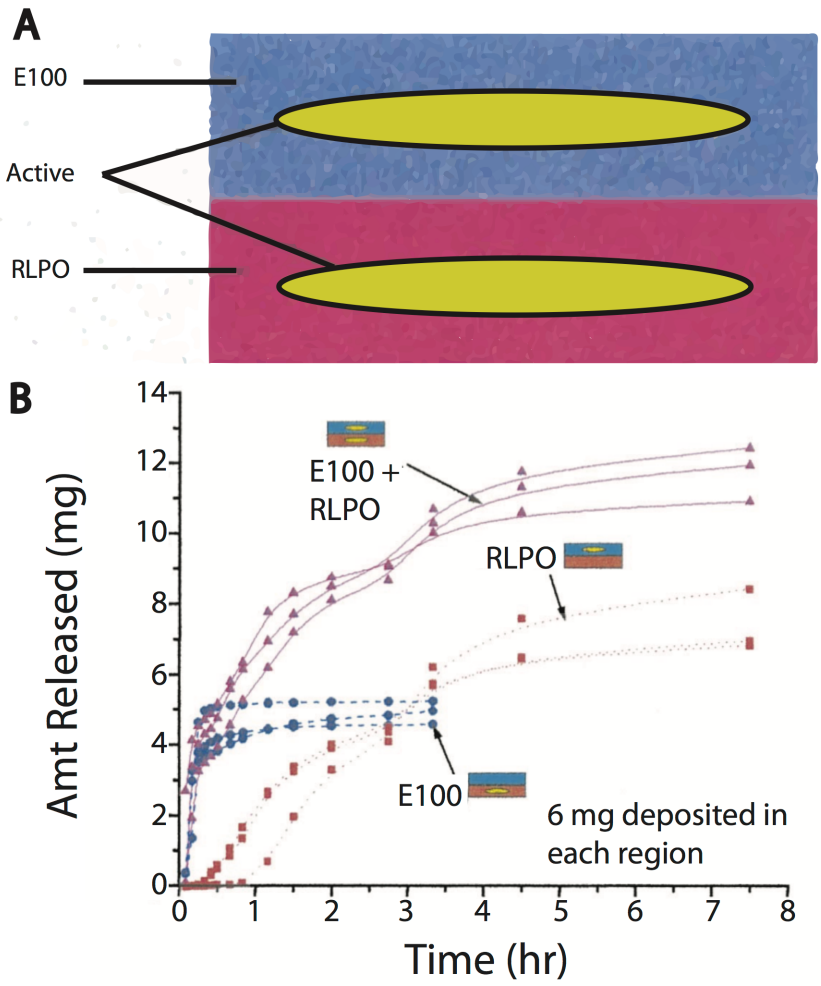

Figure 2. (A) Schematic of immediate-extended release tablet and (B) its corresponding drug release profile. Reproduced with permission from [30].

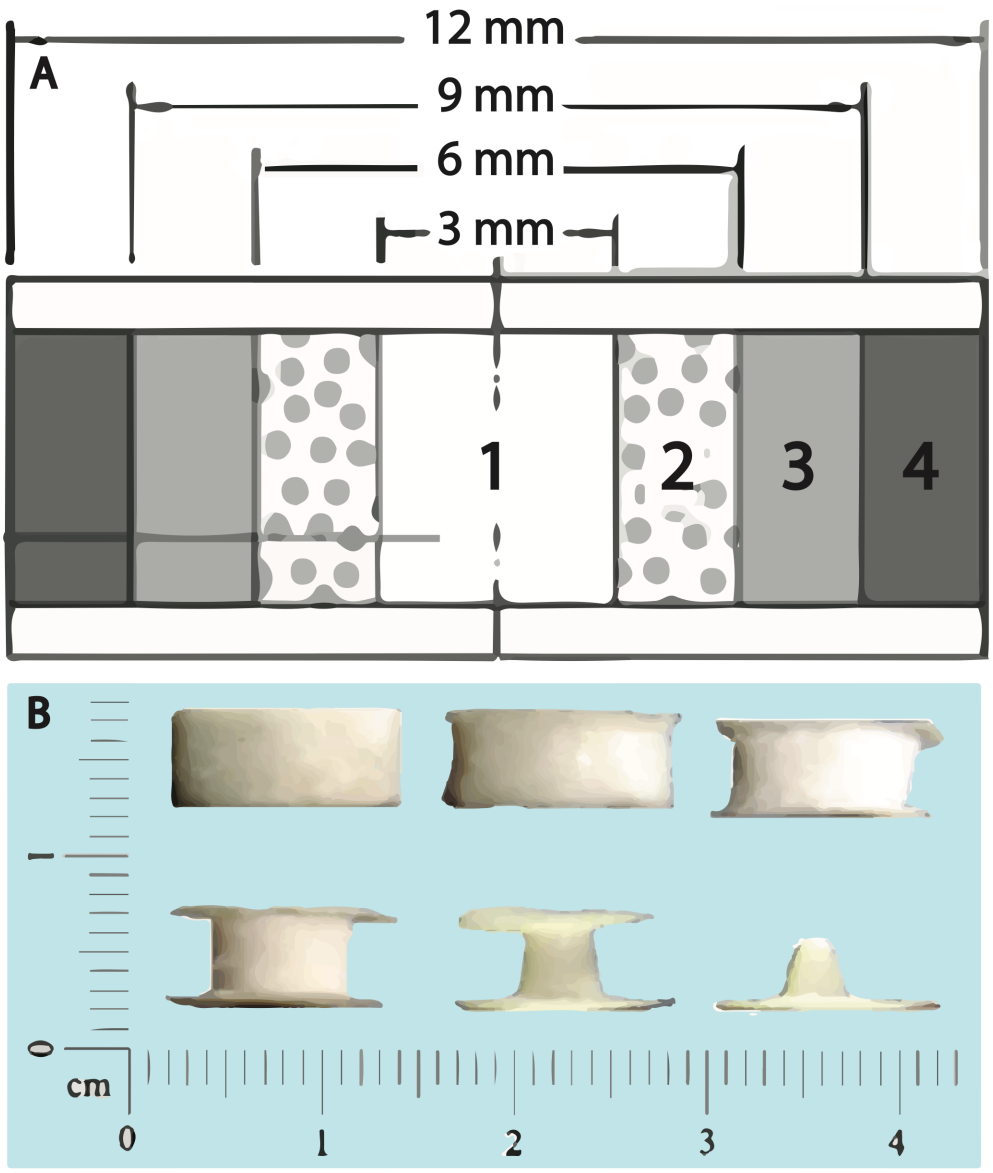

Figure 3. (A) Drug delivery device with material gradients. (B) Erosion process of the device after 0, 1, 3, 5, 7, and 10 h of dissolution. Reproduced with permission from [32].

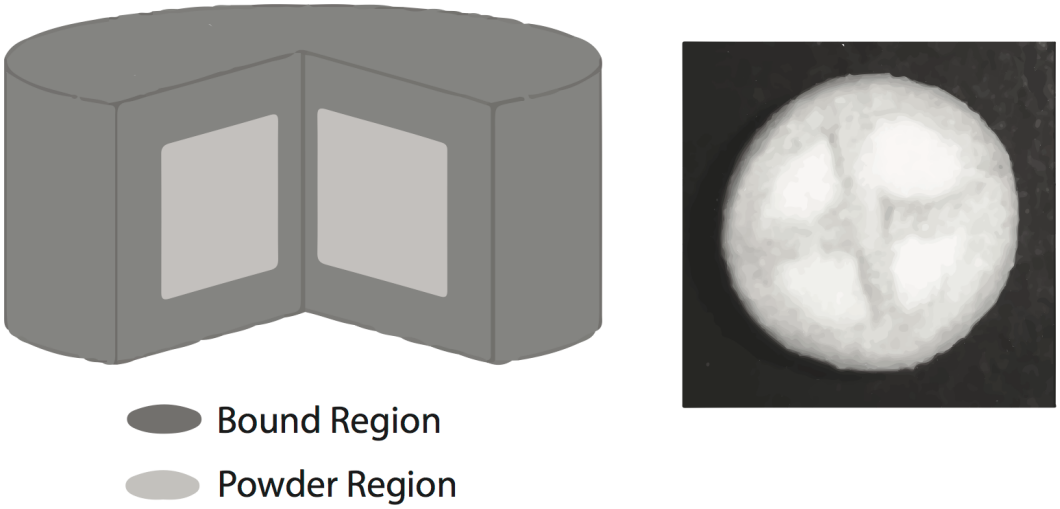

Figure 4. Schematic of fast disintegrating tablets with bound regions within the middle of the device. Reproduced with permission from [36].

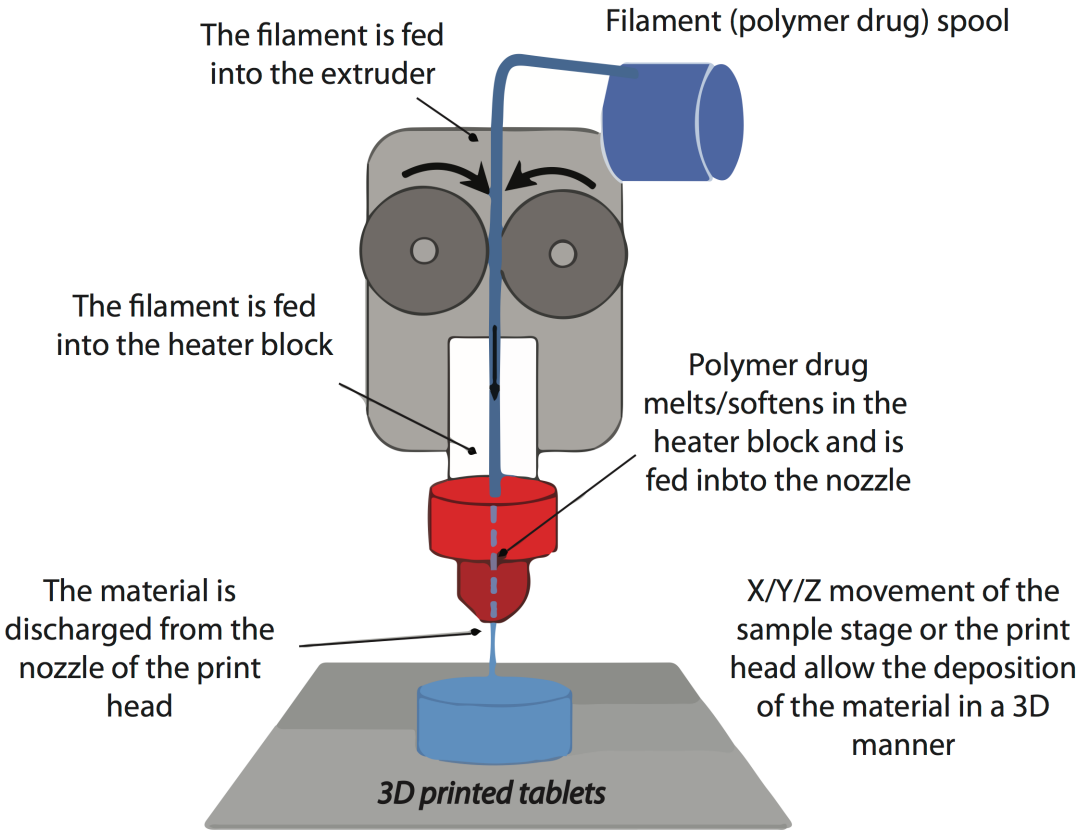

Figure 5. Fused deposition modeling procedure schematic. Reproduced with permission from [40].

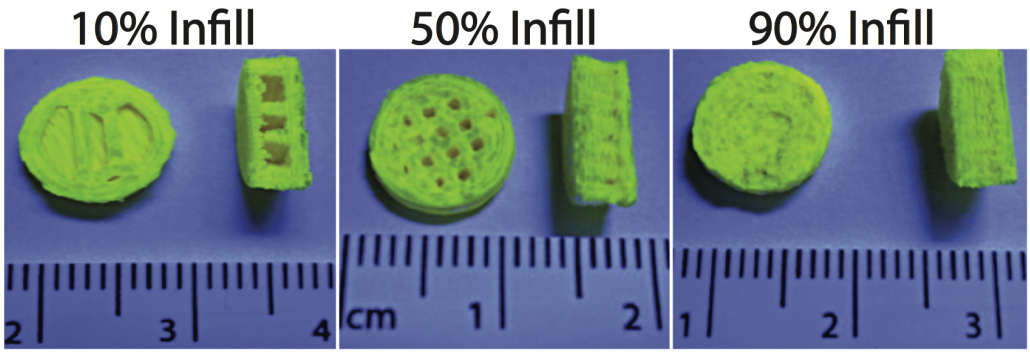

Figure 6. Cross-sectional view of fluorescein infused devices featuring different infill percentages under UV light. Reproduced with permission from [42].

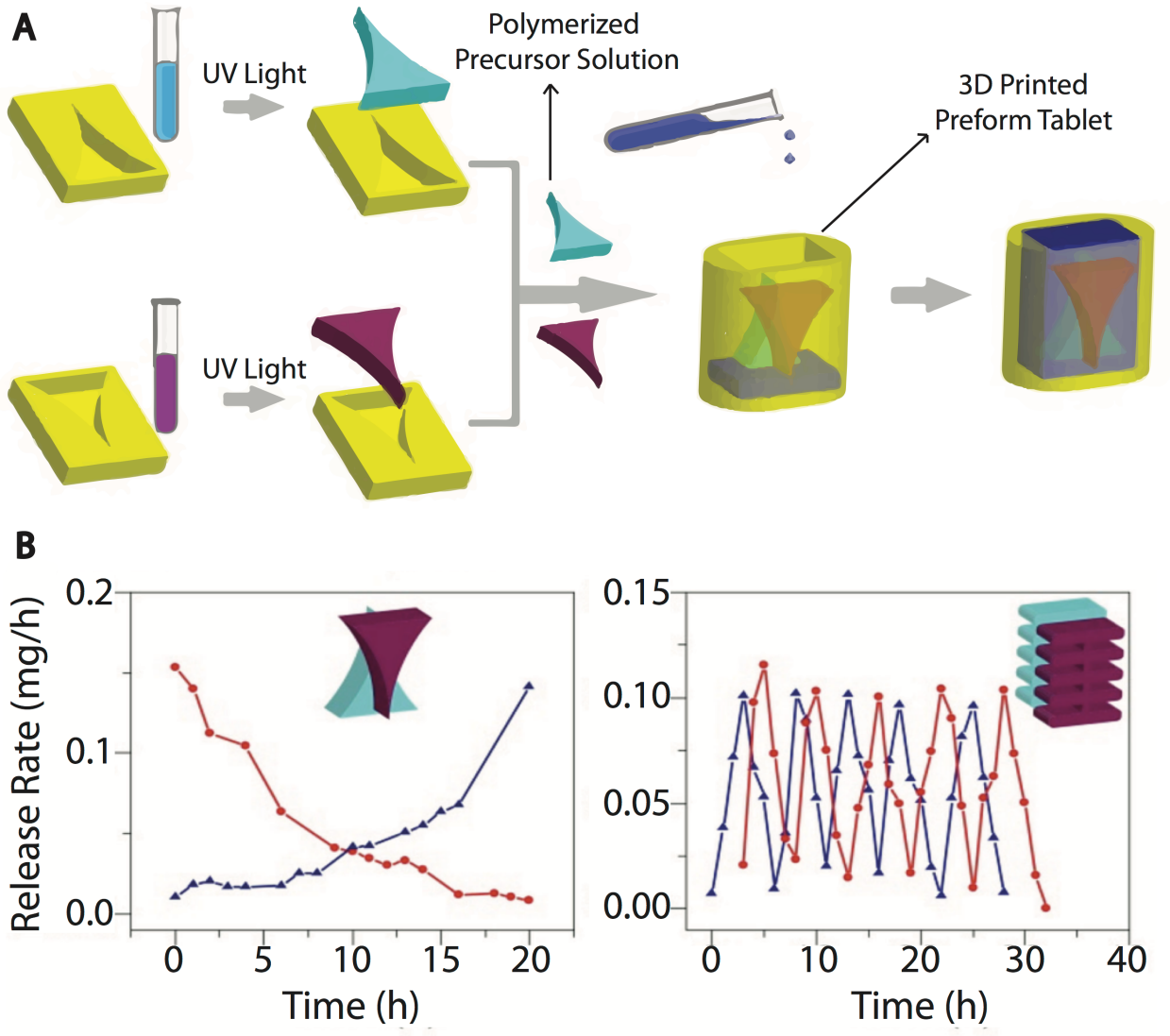

Figure 7. (A) Schematic of polymer precursor solution curing procedure and tablet manufacture. (B) Effect of polymer geometry on dissolution profiles. Reproduced with permission from [50].

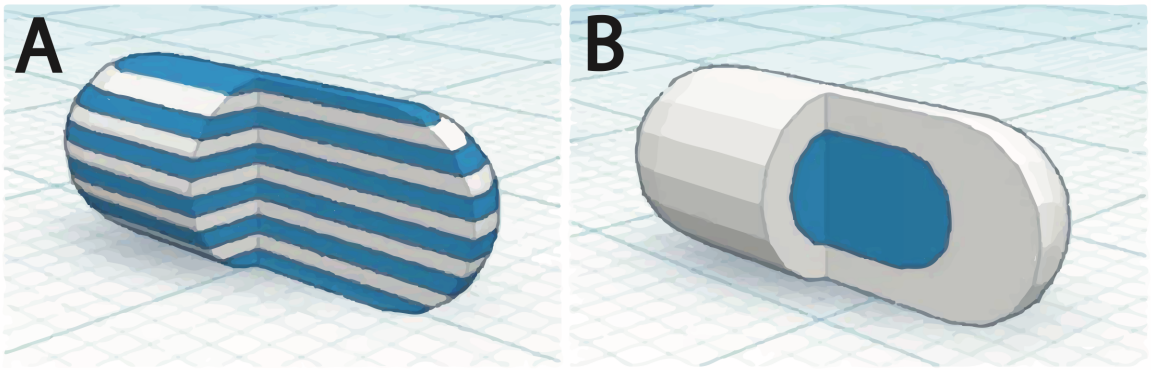

Figure 8. Schematic of tablets containing multiple drugs. (A) Multilayer device and (B) DuoCaplet. Reproduced with permission from [51].

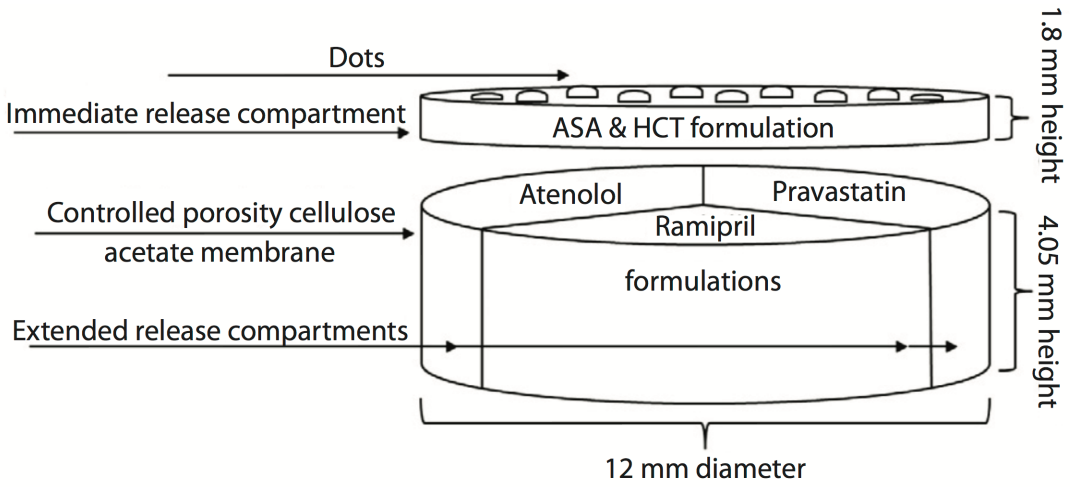

Figure 9. Schematic of the polypill design featuring 5 drugs within immediate and extended release compartments. Reproduced with permission from [53].

1.9 REFERENCES

1. Schork, N. J. Personalized medicine: Time for one-person trials. *Nature* **520,** 609–611 (2015).
2. Karapetis, C. S. K-ras Mutations and Benefit from Cetuximab in Advanced Colorectal Cancer. *N. Engl. J. Med.* **359,** 1757–1765 (2008).
3. Ting, S. & Schug, S. The pharmacogenomics of pain management: prospects for personalized medicine. *J. Pain Res.* **9,** 49–56 (2016).
4. Chadwick, R. Ethical issues in personalized medicine. *Drug Discov. Today Ther. Strateg.* **10,** e171–e174 (2013).
5. Burke, W., Brown Trinidad, S. & Press, N. A. Essential elements of personalized medicine. *Urol. Oncol.* **32,** 193–197 (2014).
6. Mirnezami, R., Nicholson, J. & Darzi, A. Preparing for Precision Medicine. *N. Engl. J. Med.* **366,** 489–491 (2012).
7. Beebe, K. & Kennedy, A. D. Sharpening Precision Medicine by a Thorough Interrogation of Metabolic Individuality. *Comput. Struct. Biotechnol. J.* **14,** 97–105 (2016).
8. Tutton, R. Personalizing medicine: Futures present and past. *Soc. Sci. Med.* **75,** 1721–1728 (2012).
9. Pietrzak, K., Isreb, A. & Alhnan, M. A. A flexible-dose dispenser for immediate and extended release 3D printed tablets. *Eur. J. Pharm. Biopharm.* **96,** 380–387 (2015).
10. Skowyra, J., Pietrzak, K. & Alhnan, M. a. Fabrication of extended-release patient-tailored prednisolone tablets via fused deposition modelling (FDM) 3D printing. *Eur. J. Pharm. Sci.* **68,** 11–17 (2015).
11. Wu, B. M. *et al.* Solid free-form fabrication of drug delivery devices. *J. Control. Release* **40,** 77–87 (1996).
12. Aprecia_Pharmaceuticals, FDA approves the first 3D printed drug product (2015).
13. Choonara, Y. E., du Toit, L. C., Kumar, P., Kondiah, P. P. D. & Pillay, V. 3D-printing and

the effect on medical costs: a new era? *Expert Rev. Pharmacoecon. Outcomes Res.* **16,** 23–32 (2016).

14. Yu, D. G., Zhu, L.-M., Brandford-White, C. J. & Yang, X. L. Three-Dimensional Printing in Pharmaceutics: Promises and Problems. *J. Pharm. Sci.* **97,** 3666–3690 (2008).
15. Sleight, P., Pouleur, H. & Zannad, F. Benefits, challenges, and registerability of the polypill. *Eur. Heart J.* **27,** 1651–1656 (2006).
16. Prasad, L. K. & Smyth, H. 3D Printing technologies for drug delivery: a review. *Drug Dev. Ind. Pharm.* **9045,** 1–13 (2015).
17. Derby, B. Inkjet Printing of Functional and Structural Materials: Fluid Property Requirements, Feature Stability, and Resolution. *Annu. Rev. Mater. Res.* **40,** 395–414 (2010).
18. Sekitani, T., Noguchi, Y., Zschieschang, U., Klauk, H. & Someya, T. Organic transistors manufactured using inkjet technology with subfemtoliter accuracy. *Proc. Natl. Acad. Sci. U. S. A.* **105,** 4976–80 (2008).
19. Singh, M., Haverinen, H. M., Dhagat, P. & Jabbour, G. E. Inkjet printing-process and its applications. *Adv. Mater.* **22,** 673–685 (2010).
20. Demirci, U. & Montesano, G. Single cell epitaxy by acoustic picolitre droplets. *Lab Chip* **7,** 1139–45 (2007).
21. Alomari, M., Mohamed, F. H., Basit, A. W. & Gaisford, S. Personalised dosing: Printing a dose of one's own medicine. *Int. J. Pharm.* **494,** 568–577 (2015).
22. Tekin, E., Smith, P. J. & Schubert, U. S. Inkjet printing as a deposition and patterning tool for polymers and inorganic particles. *Soft Matter* **4,** 703–713 (2008).
23. Sumerel, J. *et al.* Piezoelectric ink jet processing of materials for medical and biological applications. *Biotechnol. J.* **1,** 976–987 (2006).
24. Cima, M. J. *et al.* Computer-derived microstructures by 3D Printing : Bio and Structural Materials. *Solid Free. Fabr. Symp.* 181–190 (1994).

25. Griffith, L. G. *et al.* In vitro organogenesis of liver tissue. *Ann. N. Y. Acad. Sci.* **831,** 382–397 (1997).

26. Lu, Y. & Chen, S. C. Micro and nano-fabrication of biodegradable polymers for drug delivery. *Adv. Drug Deliv. Rev.* **56,** 1621–1633 (2004).

27. Chia, H. N. & Wu, B. M. Improved resolution of 3D printed scaffolds by shrinking. *J. Biomed. Mater. Res. - Part B Appl. Biomater.* **103,** 1415–1423 (2015).

28. Chia, H. N. & Wu, B. M. Recent advances in 3D printing of biomaterials. *J. Biol. Eng.* **9,** 1–14 (2015).

29. Katstra, W. E. *et al.* Oral dosage forms fabricated by Three Dimensional Printing. *J. Control. Release* **66,** 1–9 (2000).

30. Rowe, C. W. *et al.* Multimechanism oral dosage forms fabricated by three dimensional printing. *J. Control. Release* **66,** 11–17 (2000).

31. Wang, C.-C. *et al.* Development of Near Zero-Order Release Dosage Forms Using Three-Dimensional Printing (3-DP^{TM}) Technology. *Drug Dev. Ind. Pharm.* **32,** 367–376 (2006).

32. Yu, D. G. *et al.* Tablets With Material Gradients Fabricated by Three-Dimensional Printing. *J. Pharm. Sci.* **96,** 2446--4456 (2007).

33. Cheng, K., Zhu, J., Song, X., Sun, L. & Zhang, J. Studies of hydroxypropyl methylcellulose donut-shaped tablets. *Drug Dev. Ind. Pharm.* **25,** 1067–71 (1999).

34. Sundy, E. & Paul Danckwerts, M. A novel compression-coated doughnut-shaped tablet design for zero-order sustained release. *Eur. J. Pharm. Sci.* **22,** 477–485 (2004).

35. Yu, D. G. *et al.* Novel drug delivery devices for providing linear release profiles fabricated by 3DP. *Int. J. Pharm.* **370,** 160–166 (2009).

36. Yu, D.-G. *et al.* Novel oral fast-disintegrating drug delivery devices with predefined inner structure fabricated by Three-Dimensional Printing. *J. Pharm. Pharmacol.* **61,** 323–329 (2009).

37. Yu, D.-G. *et al.* A novel fast disintegrating tablet fabricated by three-dimensional printing. *Drug Dev. Ind. Pharm.* **35,** 1530–1536 (2009).

38. Jacob J, Coyle N, West TG, Rapid disperse dosage form containing levetiracetam. (2014).

39. Van Noort, R. The future of dental devices is digital. *Dent. Mater.* **28,** 3–12 (2012).

40. Qi, S. & Craig, D. Recent developments in micro- and nanofabrication techniques for the preparation of amorphous pharmaceutical dosage forms. *Adv. Drug Deliv. Rev.* (2016). doi:10.1016/j.addr.2016.01.003

41. Khaled, S. a., Burley, J. C., Alexander, M. R. & Roberts, C. J. Desktop 3D printing of controlled release pharmaceutical bilayer tablets. *Int. J. Pharm.* **461,** 105–111 (2014).

42. Goyanes, A., Buanz, A. B. M., Basit, A. W. & Gaisford, S. Fused-filament 3D printing (3DP) for fabrication of tablets. *Int. J. Pharm.* **476,** 88–92 (2014).

43. Goyanes, A., Buanz, A. B. M., Hatton, G. B., Gaisford, S. & Basit, A. W. 3D printing of modified-release aminosalicylate (4-ASA and 5-ASA) tablets. *Eur. J. Pharm. Biopharm.* **89,** 157–162 (2015).

44. Goyanes, A., Robles Martinez, P., Buanz, A., Basit, A. W. & Gaisford, S. Effect of geometry on drug release from 3D printed tablets. *Int. J. Pharm.* (2015). doi:10.1016/j.ijpharm.2015.04.069

45. Breitenbach, J. Melt extrusion: from process to drug delivery technology. *Eur. J. Pharm. Biopharm.* **54,** 107–117 (2002).

46. Lang, B., McGinity, J. W. & Williams, R. O. Hot-melt extrusion - basic principles and pharmaceutical applications. *Drug Dev. Ind. Pharm.* **40,** 1133–1155 (2014).

47. Thiry, J., Krier, F. & Evrard, B. A review of pharmaceutical extrusion: Critical process parameters and scaling-up. *Int. J. Pharm.* **479,** 227–240 (2015).

48. Goyanes, A. *et al.* Fabrication of controlled-release budesonide tablets via desktop (FDM) 3D printing. *Int. J. Pharm.* (2015). doi:10.1016/j.ijpharm.2015.10.039

49. Melocchi, A. *et al.* 3D printing by fused deposition modeling (FDM) of a swellable/erodible capsular device for oral pulsatile release of drugs. *J. Drug Deliv. Sci. Technol.* **30,** 360–367 (2015).

50. Sun, Y. & Soh, S. Printing Tablets with Fully Customizable Release Profiles for Personalized Medicine. *Adv. Mater.* 1–7 (2015). doi:10.1002/adma.201504122

51. Goyanes, A. *et al.* 3D printing of medicines: Engineering novel oral devices with unique design and drug release characteristics. *Mol. Pharm.* 4077–4084 (2015). doi:10.1021/acs.molpharmaceut.5b00510

52. Khaled, S. a., Burley, J. C., Alexander, M. R., Yang, J. & Roberts, C. J. 3D printing of tablets containing multiple drugs with defined release profiles. *Int. J. Pharm.* (2015). doi:10.1016/j.ijpharm.2015.07.067

53. Khaled, S. A., Burley, J. C., Alexander, M. R., Yang, J. & Roberts, C. J. 3D printing of five-in-one dose combination polypill with defined immediate and sustained release profiles. *J. Control. Release* **217,** 308–314 (2015).

54. Powell, K. P. *et al.* Primary care physicians' awareness, experience and opinions of direct-to-consumer genetic testing. *J. Genet. Couns.* **21,** 113–126 (2012).

55. Mcgrath, S. & Ghersi, D. Building towards precision medicine : empowering medical professionals for the next revolution. *BMC Med. Genomics* 1–6 (2016). doi:10.1186/s12920-016-0183-8

56. Elefsinioti, A. *et al.* Key factors for successful data integration in biomarker research. *Nat. Rev. Drug Discov.* (2016). doi:10.1038/nrd.2016.74

CHAPTER TWO: PHOTOCURABLE BIOINK FOR THE INKJET 3D PHARMING OF HYDROPHILIC DRUGS

2.1 ABSTRACT

Novel strategies are required to manufacture customized oral solid dosage forms for personalized medicine applications. 3D Pharming, the direct printing of pharmaceutical tablets, is an attractive strategy, since it allows for the rapid production of solid dosage forms containing custom drug dosages. This study reports on the design and characterization of a biocompatible photocurable pharmaceutical polymer for inkjet 3D printing that is suitable for hydrophilic active pharmaceutical ingredients (API). Specifically, hyaluronic acid was functionalized with norbornene moieties that, in the presence of poly(ethylene) glycol dithiol, Eosin Y as a photoinitiator, and a visible light source, undergoes a rapid step-growth polymerization reaction through thiol-ene chemistry. The engineered bioink was loaded with Ropinirole HCL, dispensed through a piezoelectric nozzle onto a blank preform tablet, and polymerized. Drug release analysis of the tablet resulted in 60% release within 15 min of tablet dissolution. The study confirms the potential of inkjet printing for the rapid production of tablets through the deposition of a photocurable bioink designed for hydrophilic APIs.

2.2 INTRODUCTION

Pharmaceutical dosages are set in the early clinical trial phase and are defined by the amount of active pharmaceutical ingredient (API) with a therapeutic effect in the most number of patients [1]. This “one size fits all” approach fails to account for physiological differences and genomic diversity among the patient population [2]. Consequently, the top 10 highest grossing medications only have a positive therapeutic effect in 4–25 percent of the patients that take them [3]. Personalized medicine aims to provide patients with API dosages tailored to their genomic and pathophysiological profile for improved clinical outcomes. However, changes in the manufacturing of pharmaceuticals tablets are needed to achieve such control over API dosages. Specifically, technology that: (1) can operate at drug dispensing locations, such as pharmacies

and hospitals; (2) is economically viable; (3) dispenses precise drug dosages; and (4) has a short production time is required. 3D printing is one such technology. 3D Pharming—the direct printing of pharmaceutical tablets [4]—offers a viable alternative to fabricate personalized dosage forms over traditional tablet manufacturing techniques, such as direct powder compression where the best case is that a tablet can be split into smaller sections as a way to individualize dosages. Indeed, previous studies have used 3D printing technologies to control a drug's location within a tablet, the drug release kinetics, and to load multiple APIs within a single tablet [5–8].

The aim of this study was to engineer a photocurable bioink suitable for the inkjet printing of pharmaceutical tablets loaded with a hydrophilic API. Inkjet printing for 3D Pharming is advantageous for a number of reasons, including its precise dosage control, high spatial resolution, and the ability to monitor droplet dispensing using high-speed cameras for quality assurance [9–11]. Additionally, inkjet printing offers fast printing speeds and the ability to print at room temperature for the preservation of temperature labile APIs, which is an advantage over 3D printing techniques previously used for 3D Pharming, such as powder bed printing and fused deposition modeling (FDM), respectively.

Hyaluronic acid (HA), a glycosaminoglycan typically found in connective, neural, and epithelial tissue [12,13], was functionalized with norbornene moieties and used as the main backbone of the photocurable hydrogel precursor solution. This photocurable polymer solution was dispensed into blank preform tablets, made by direct powder compression, and subsequently exposed to visible light to induce rapid polymerization. Finally, the rapid release of the hydrophilic API from the resulting tablet was characterized. The high specificity of the thiol-norbornene reaction preserves the stability of the API loaded in the formulation throughout the gelation process, given the absence of thiols and reactive carbon-carbon double bonds (enes) within the model hydrophilic drug [14–16]. For this study, Ropinirole, a non-ergoline dopamine agonist for the treatment of Parkinson's disease and restless legs syndrome [17], was utilized as model drug due to its high hydrophilicity.

2.3 MATERIALS AND METHODS

2.3.1 Norbornene Functionalized Hyaluronic Acid (HANB) Synthesis

Hyaluronic acid (HA) was functionalized with norbornene moieties in a two-step synthesis. Briefly, hyaluronic acid (60 kDa·MW) (Genzyme Corporation, Cambridge, MA, USA) (2 g, 5.27 mmol) was dissolved in 400 mL of DI water. Adipic acid dihydrazide (ADH) (18.37 g, 105.45 mmol) was added to the HA solution and the pH was adjusted to 4.75 with hydrochloric acid. 1-ethyl-3-(dimethylaminopropyl) carbodiimide hydrochloride (EDC) (4.05 g, 21.09 mmol) was added to the reaction while maintaining the pH at 4.75. Once the pH stabilized at 4.75, the reaction was allowed to run overnight. The solution was dialyzed for 3 days against DI water (Fisherbrand regenerated cellulose, MWCO 12,000–14,000 Da, Houston, TX, USA). The HA functionalized with hydrazide groups (HA-ADH) was lyophilized and stored at −20 °C until further use. HA-ADH was dissolved in 400 mL of DI water and the pH was adjusted to 7.0. Cis-5-norbornene-*endo*-2,3-dicarboxylic anhydride (Sigma-Aldrich, St. Louis, MO, USA) (4.33 g, 26.36 mmol) was dissolved in 100 mL of dimethylformamide, added dropwise into the HA-ADH solution while maintaining the pH at 7.0 and reacted overnight. The norbornene functionalized HA (HANB) was dialyzed against DI water for 3 days, filtered, lyophilized, and stored at −20 °C. The resulting HANB was characterized by proton nuclear magnetic resonance spectroscopy (^{1}H NMR) on a Bruker AV300 broad band FT NMR Spectrometer (Billerica, MA, USA). ^{1}H NMR shifts of norbornene groups (D_2O): δ 6.20 (*endo* vinyl protons, 2H), δ 3.46 (bridgehead protons, 2H), δ 3.61 (norbornene α protons, 2H) (**Fig. S1**). All chemicals were purchased from Sigma-Aldrich unless otherwise stated.

2.3.2 Photocurable Formula Preparation

HANB was dissolved in phosphate-buffered saline (PBS) and mixed with variable amounts of Poly(ethylene) glycol dithiol (1500 Da, PEGDT). Eosin-Y was added at a concentration of 0.1 mM and Poly(ethylene) glycol (MW 200, PEG200) constituted 10% of the solution. The hydrophilic drug Ropinirole HCL (obtained as a gift from GlaxoSmithKline, Philadelphia, PA, USA) was loaded into the solution at a concentration of 80 mg/mL. The weight percent of HANB in solution (W_{HANB}),

the ratio of PEGDT thiol groups to norbornenes (r_{ratio}), and the light exposure time (T_L) were manipulated to achieve the desired hydrogel mechanical properties. All the reagents were purchased from Sigma-Aldrich unless otherwise stated.

2.3.3 Gelation and Mechanical Properties

To prepare gels for mechanical testing, 40 µL of solution was pipetted between two Sigmacote functionalized glass slides and exposed to visible light (Volpi, V-lux 1000) at an intensity of 120 mW/cm^2, resulting in hydrogels with a cylindrical shape. To assess the effect of light exposure time on hydrogel mechanical properties, gels with W_{HANB} = 3% and r_{ratio} = 0.6 were exposed to visible light for 5, 10, 30, 60, 120, and 180 s. Hydrogels with r_{ratio} = 0.6, T_L = 2 min, and W_{HANB} = 2%, 3%, and 4% were fabricated to analyze the effect of HANB weight percent. Finally, hydrogels with W_{HANB} = 3%, T_L = 2 min, and r_{ratio} = 0.2, 0.4, 0.6, and 0.8 were made to analyze the effect of crosslinking ratio. The storage modulus (G') of the hydrogels was measured in a rheometer (Discovery HR-2, TA Instruments, New Castle, DE, USA) with an 8 mm parallel plate (Peltier plate Steel) geometry at a constant strain of 1%. The final formulation for further characterization and drug dispensing had the following parameters: W_{HANB} = 3%, r_{ratio} = 0.6, and T_L = 2 min. In-situ photorheology was performed to analyze the gelation kinetics of the hydrogel.

The inverse of the Onhesorge number (Z) was calculated to assess the printability and droplet formation capability of the formula **Equation 1** [18], where $\boldsymbol{a}$ is the diameter of the printing orifice, $\boldsymbol{\rho}$ is the density, $\boldsymbol{\gamma}$ is the surface tension, and $\boldsymbol{\eta}$ is the viscosity of the formulation.

$$\boldsymbol{Z} = \frac{(\boldsymbol{a\rho\gamma})^{\mathbf{1/2}}}{\boldsymbol{\eta}} \quad (1)$$

Viscosity was measured with a rheometer in a 40 mm 2.016° cone plate geometry with shear rate ranging from 10 to 100 Hz. The density of the formula was obtained by weighing an amount of solution and dividing the mass over its predetermined volume. The surface tension was calculated with a tensiometer (Cole-Parmer, Kimble Chase 14818 Tensiometer, Vernon Hills, IL,

USA). **Equation 2** [19] was used to determine $\boldsymbol{\gamma}$, where $\boldsymbol{h}$ is the distance between menisci, $\boldsymbol{r}$ is the radius of the capillary, $\boldsymbol{\rho}$ is the density of the formulation, and $\boldsymbol{g}$ is the acceleration due to gravity.

$$\boldsymbol{\gamma = \frac{1}{2} hr\rho g} \quad (2)$$

To measure the swelling ratio of the polymerized formula, hydrogels were left in PBS overnight, weighed, and subsequently lyophilized to obtain their dry weight. The mass swelling ratio ($\boldsymbol{Q_M}$) was calculated by taking the ratio between the mass of the swollen hydrogel ($\boldsymbol{M_S}$) and the dry mass of the lyophilized gel ($\boldsymbol{M_D}$) in **Equation 3** [20].

$$\boldsymbol{Q_M = \frac{M_S}{M_D}} \quad (3)$$

2.3.4 Thiols Consumption

To assess the photopolymerization reaction kinetics, Ellman's reagent analysis was performed on hydrogels fabricated with T_L = 5, 10, 30, 60, 120, and 180 s. The unreacted thiol concentration in the hydrogels over light exposure time was calculated.

2.3.5 Preform Tablet Fabrication

The drug-containing bioinks were directly printed into tablet preforms that were fabricated by direct compression technique using microcrystalline cellulose (Avicel(R) PH-103; FMC Corporation; Philadelphia, PA, USA) as the binder, and croscarmellose sodium (VIVASOL(R); JRS Pharma, Patterson, NY, USA) was added as a superdisintegrant (5% (*w*/*w*)). The preform tablets are shown in **Figure S2A**, and are comprised of two fitting parts—a 100 µL well and a cap—with a locational interference fit. A customized press design was used to make the preform tablets and was machined by Proto Labs, Inc. (Maple Plain, MN, USA). Briefly, Standard B-Type upper punches were modified to produce the positive features of the cap and the well. The lower punch was designed to sit flush on a hydraulic press stage and had a tip with a 0.04-inch radius of curvature and a 0.02-inch blended landing. A standard 0.945 die with a 3/16-inch-deep TSM

standard taper and an increased die bore dimension of 0.003 inch at the face of the die was used in the manufacturing of the tablets (**Fig. S2B**). The preform tablets (150 mg caps; 300 mg wells) were compressed at different compression pressures (1–10 kN), with a dwell time of 30 s. To prevent dissolution of the preform tablet during the printing of the drug-containing bioink, the well was brush-coated with Eudagrit(R) E100 (Evonik, Essen, Germany) (polymethacrylate copolymer) dissolved in acetone at 20% (*w*/*w*) E100. The tablet hardness was measured using Buehler Vicker Hardness indenter 1600-6305 (Buehler, Lake Bluff, IL, USA) with Vickers indentations from 200 to 500 g load.

2.3.6 Drug Dispensing and Release Kinetics

The formula was filtered through a 0.22 μm filter (Fisherbrand) and dispensed into preform tablets (71.25 μL for 5.7 mg of Ropinirole HCL) by using a piezoelectric dispenser with an 80 μm diameter nozzle (MJ-ABP-01-080, MicroFab Technologies, Plano, TX, USA). A dispensing system (MD-E-3000, Microdrop Technologies, Norderstedt, Segeberg, Germany) was used to drive the piezoelectric nozzle, set at 45 V, with a pulse width of 16 μs and a frequency of 2000 Hz. Droplet formation and continuous monitoring of the process was done with an analog camera (JAI CV-S3300), lens (Edmund Optics, Barrington, NJ, USA), and an LED light controlled by the Microdrop driver. After dispensing the formula into preform tablets, the solution was exposed to light for 2 min at 120 mW/cm^2 to induce polymerization and the tablets were capped. In vitro drug release was measured by placing the tablets inside Uni-cassettes (Tissue-Tek) and submerging them in 200 mL of dissolution medium (2.9 g/L of sodium citrate dihydrate and 3.3 g/L of anhydrous citric acid in water at a pH of 4.0). The dissolution test was conducted at 37 °C and stirred at 60 rpm. 1 mL aliquots were taken after 5, 10, 15, 30, 60, and 120 min of dissolution. The volume removed was replaced with fresh dissolution medium to keep the total volume constant. The aliquots were centrifuged, filtered, and the Ropinirole HCL content was measured by HPLC analysis (Prominence Modular HPLC, Shimadzu, Nakagyō-ku, Kyoto, Japan).

2.3.7 Hydrogel Drying

To improve the stability of the API loaded within the hydrogel for prolonged storage, water must be removed from the gel to avoid possible degradation of the therapeutic compounds. The time required to remove the water content of the hydrogels was calculated by exposing hydrogels to 50 °C for up to 3 h and monitoring the weight of the gels over time.

2.3.8 Statistical Analysis

Statistical analysis was performed with GraphPad Prism software (GraphPad Software, Inc., San Diego, CA, USA). Statistical significance was assessed using single factor ANOVA test with a Tukey post-test and 95% confidence interval. A Dunnett's post-test analysis was performed on **Figure S3** to assess statistical significance.

2.4 RESULTS AND DISCUSSION

2.4.1 HANB Synthesis and Gelation

Previously, Gramlich et al. modified HA with norbornene groups by converting it to its tetrabutylammonium salt and further reacting it with 5-norbornene-2-carboxylic acid in the presence of di-tert-butyl dicarbonate, achieving a degree of modification of 20% [21]. In this study, HANB was synthesized in a two-step process (**Fig. 1A**). First, the carboxyl groups in HA were conjugated with ADH by using the carbodiimide EDC as coupling agent. Subsequently, Cis-5-norbornene-*endo*-2,3-dicarboxylic anhydride was reacted to the incorporated hydrazide groups. ^{1}H NMR analysis revealed that 50% of the HA monomers were functionalized with norbornene groups. This high degree of modification allows for hydrogel formation with low concentration solutions of HANB, which are required to keep the viscosity of the bioink within the printable region for inkjet printers (<20 mPa·s) [22]. HANB was mixed with PEGDT, Eosin Y (photonitiator), and Ropinirole HCL (model hydrophilic drug). The abundant norbornene groups in the HA backbone react with PEGDT in the presence of visible light (120 mW/cm^2), forming multiple crosslinks through a light induced step-growth polymerization reaction (**Fig. 1B**). Visible light represents a safer light source than UV light to be used for the operation of printing equipment and to maintain the stability of certain UV light labile APIs [23].

2.4.2 Hydrogel Characterization and Droplet Formation

In situ photorheology was carried out to assess the gelation kinetics of the bioink. Hydrogel precursor solution was placed in a rheometer and exposed to light after 30 s of G' monitoring. The bioink experienced fast gelation, achieving a soft hydrogel in less than 5 s of light exposure (**Fig. 2A**). Moreover, the G' of hydrogels with T_L = 5, 10, 30, 60, 120, and 180 s was measured and a statistical difference was observed between gels cured for up to 3 min of light exposure time (**Fig. 2B**). The effect of HANB weight percent and crosslinking ratio over the storage modulus of the gels was analyzed (**Fig. 2C,D**). Results demonstrate that HANB weight percent has a stronger effect on storage modulus when compared to crosslinking ratio, with a W_{HANB} = 4% achieving G' values over 12,000 Pascals. However, increasing HANB weight percent within the bioink represents a direct increase in the viscosity of the solution, whereas the addition of PEGDT for the increase of crosslinking ratio has a lower effect on viscosity, allowing for increases in hydrogel strength without detrimentally affecting the bioink's droplet formation capacity. The effect of API concentration on G' was assessed by making hydrogels with Ropinirole HCL at concentrations of 0, 40, and 80 mg/mL (**Fig. 2E**). A statistical difference was found between the 80 mg/mL hydrogels and the less concentrated conditions, where higher API concentrations resulted in lower G' values. These results indicate that the mechanical properties of the hydrogel remain stable at low dosages, indicating higher consistency over mechanical stability when loading potent drugs that achieve their therapeutic effect at low quantities.

The swelling ratio of the hydrogel was measured by taking the ratio of the hydrogel swollen state mass over the dry mass. A swelling ratio of 21.14 was obtained, denoting the water absorption ability of the hyaluronic acid matrix (Table 1).

An Ellman's reagent test was performed on hydrogels with T_L = 5, 10, 30, 60, 120, and 180 s, in order to quantify the thiol conjugation within the bioink as the step growth reaction occurs. A drastic decrease in thiol concentration was observed within 30 s of light exposure with over 90% of the thiols being conjugated, validating the fast reaction kinetics of the bioink (**Fig. 2F**).

A critical characteristic of the bioink design is the ability for droplet formation and inkjet printability. To quantify this, the inverse of the Ohnesorge number (*Z*) was determined, which relates the viscosity, surface tension, and density parameters of a substance [18]. Materials with *Z* values within the range $4 \leq Z \leq 14$ are considered printable fluids, where values above 14 exhibit the formation of satellite droplets and values below 4 present strong viscous forces. Table 1 shows the values for the density, surface tension, viscosity, and nozzle diameter of the piezoelectric nozzle used to dispense the bioink. These values resulted in a *Z* value of 7.82, which falls in the category of printable fluids.

The droplet formation was further tested in an 80 µm piezoelectric nozzle, with driver settings at 45 V, a pulse width of 15 µs, and a frequency of 2000 Hz. Under these parameters, consistent droplet formation and dispensing was achieved (**Fig. 3**), with a continuous printing time of at least 1 h and an idle time of 1 min between prints.

2.4.3 Preform Tablet Fabrication

The hardness (**Fig. 4A**) and tensile strength (**Fig. 4B**) of custom preform tablets made of microcrystalline cellulose using direct powder compression increased with compression force, and at least 5 kN compression force was required to produce tablets with adequate mechanical strength and handling properties (**Fig. 4C**). To facilitate the rapid disintegration of the preform tablet, croscarmellose sodium was added to the preform tablet at 5% (*w*/*w*) [[24]]. Addition of the super disintegrant to the preform tablet did not greatly impact the mechanical properties of the tablet (10 kN compression force; HV = 9; Tensile Strength = 88 MPa). The advantages of using microcrystalline cellulose as the diluent include its good compressibility, as well as compactibility due to its plastic deformation and strong hydrogen bonding among hydroxyl groups [25]. This was particularly important for the successful formation of the positive features of the preform tablet. Furthermore, it is broadly compatible with APIs and physiologically inert [26]. However, microcrystalline cellulose also acts as a disintegrant and the printing of hydrophilic bioinks directly into the preform tablet causes swelling and the tablet to break apart. As such, a thin hydrophobic

coating (Eudagrit(R) E100) was added to the preform tablet to maintain the integrity of the preform tablet while the bioink was being printed. A 20% (*w*/*w*) Eudagrit(R) E100 solution in acetone was required to prevent tablet swelling during the printing time. However, a reduction in printing time achieved by increasing the number of inkjet nozzles dispensing bioink loaded with API would reduce the contact time between the water-based bioink and the preform tablet. Accordingly, lower concentrations of polymer coating could be used to line the preform tablet well.

2.4.4 Tablet Fabrication and Dissolution Test

The tablet formation scheme designed in this study allows for the manufacture of dosage controlled tablets at fast manufacturing times. A Ropinirole HCL dose of 5.7 mg was dispensed into a blank preform tablet with an accuracy of 92.87% ± 4.08%. Drug release data (**Fig. 5**) shows that 60% of the Ropinirole HCL was released within the first 15 min of dissolution and over 80% was released in 30 min. The preform tablet was designed to undergo rapid dissolution under acidic aqueous mediums. This preform tablet property and the high permeability of the hydrogel result in quick drug release kinetics applicable to API requiring such release profiles for fast therapeutic effects.

To extend drug stability and tablet shelf life, the tablet would require removal of the water content. Drying tests of the hydrogels show that the water can be removed from the hydrogel in 1.5 h at a temperature of 50 °C (**Fig. 6, Fig. S3**).

The photocurable bioink developed here could potentially be used for PolyJet 3D printing [27,28], where the liquid is dispensed under constant light exposure to create solid materials with diverse shapes and mechanical properties. Improvements on the mechanical strength of pharmaceutical hydrophilic photocurable bioinks would allow for their application in polyjet technology, and eliminate the need for blank preform tablets. Additionally, future work using multiple nozzles simultaneously would further improve the printing speed of pharmaceutical tablets over other 3D Pharming techniques, such as powder bed 3D printing and fused deposition modeling. The combination of fast printing speeds with rapid polymerization upon short exposures

to light results in the rapid production of pharmaceutical tablets for immediate consumption. This would be exceptionally advantageous for APIs with a short shelf life. Finally, more research is required in the development of hydrophilic bioinks capable of incorporating large drug dosages.

2.5 CONCLUSION

This study reports the synthesis of a norbornene modified hyaluronic acid photocurable bioink for the inkjet dispensing of hydrophilic API and subsequent manufacture of pharmaceutical tablets. The bioink was engineered to undergo polymerization through a thiol-ene reaction upon exposure to visible light. The mechanical tunability of the bioink was demonstrated by manipulating the HANB weight percent, crosslinking ratio, and light exposure time. The drug loaded bioink was dispensed through an inkjet piezoelectric nozzle into blank preform tablets made by direct powder compression, specifically designed to undergo rapid dissolution when exposed to acidic aqueous mediums. Drug release studies revealed a 60% Ropinirole HCL release within the first 15 min of tablet dissolution. This work demonstrates the utility of inkjet printing for the 3D Pharming of hydrophilic APIs.

2.6 FIGURES

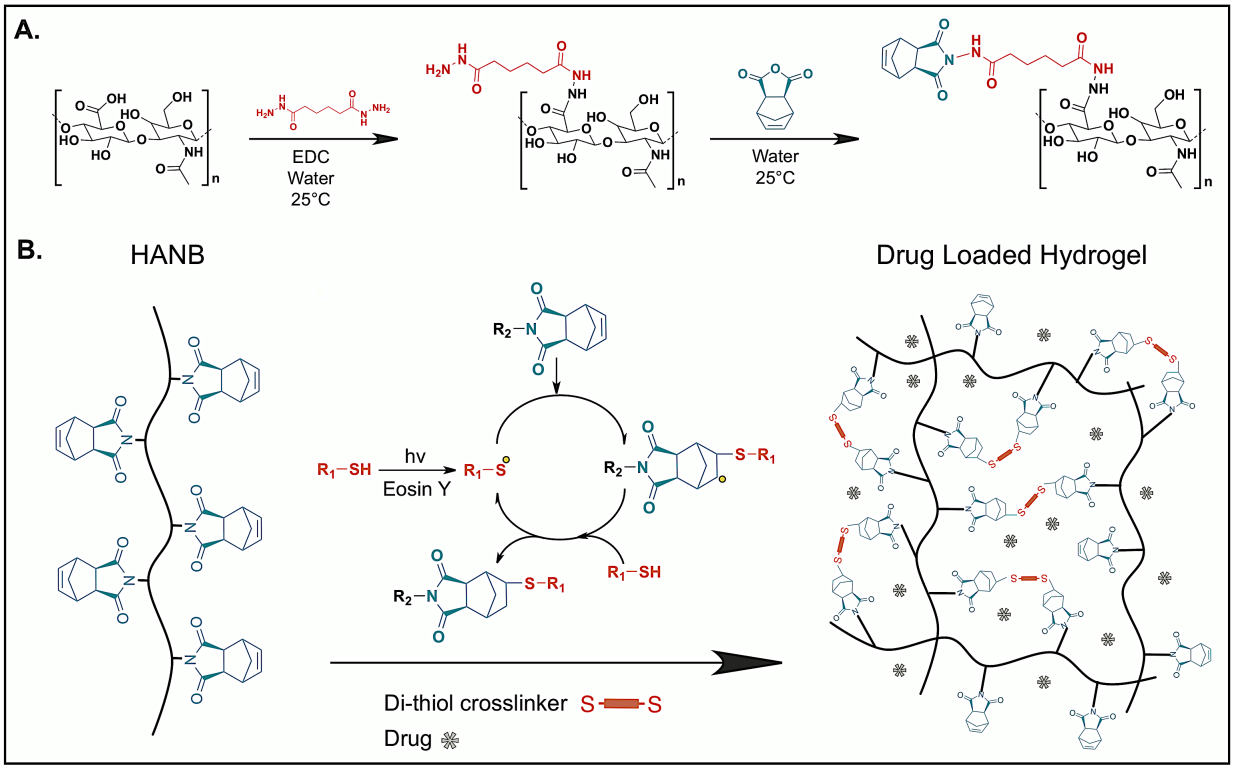

Figure 1. (A) Norbornene functionalized hyaluronic acid (HANB) two-step synthesis pathway; (B) Bioink photopolymerization for drug loaded hydrogel formation through thiol-ene reaction.

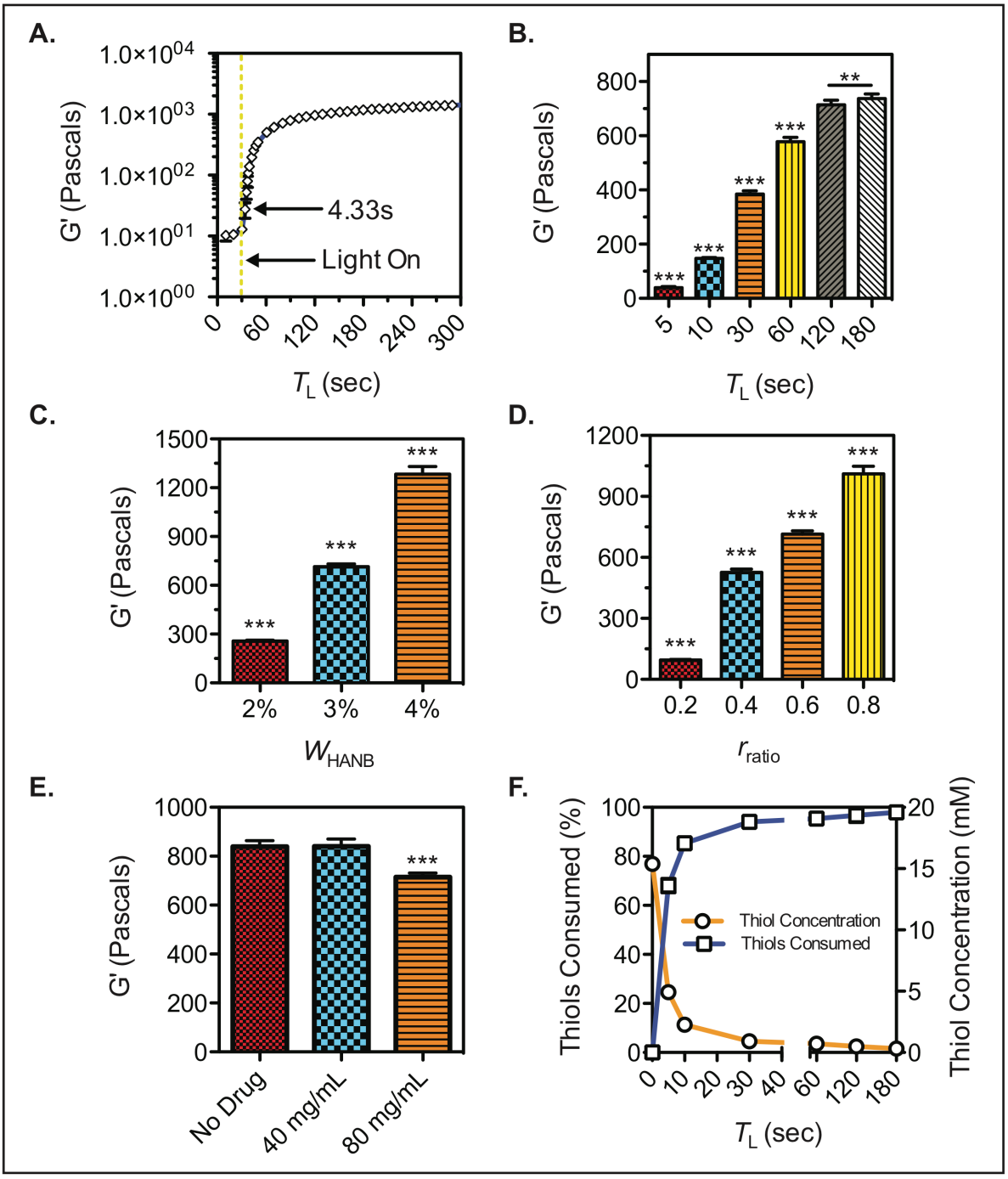

Figure 2. HANB hydrogel mechanical properties. (**A**) In-situ photorheology of hydrogel solution (W_{HANB} = 3%, r_{ratio} = 0.6, T_L = 2 min) indicating gelation kinetics; (**B**) G' of hydrogels (W_{HANB} = 3%, r_{ratio} = 0.6) exposed to different visible light exposure times; (**C**) G' of hydrogels (T_L = 2 min, r_{ratio} = 0.6) with varying W_{HANB}; (**D**) G' of hydrogels (W_{HANB} = 3%, T_L = 2 min) with varying r_{ratio}; (**E**) G' of

hydrogels (W_{HANB} = 3%, r_{ratio} = 0.6, T_L = 2 min) with increasing Ropinirole HCL concentrations; (**F**) Results of Ellman's reagent test on thiol concentration over time (W_{HANB} = 3%, r_{ratio} = 0.6, T_L = 2 min). All the bioink formulations contained 80 mg/mL of Ropinirole HCL, with the exception of (**E**). Asterisks denote statistical significance (** denotes $p < 0.01$; *** denotes $p < 0.001$).

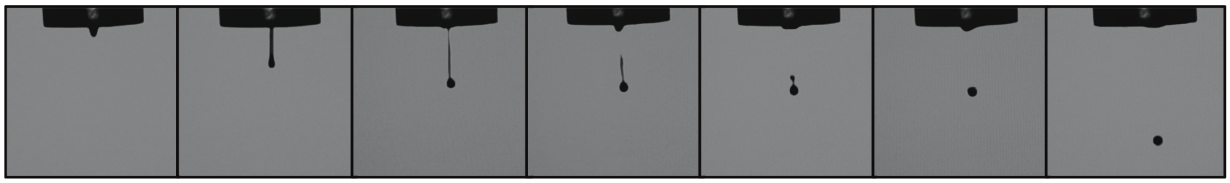

Figure 3. Bioink droplet formation picture sequence.

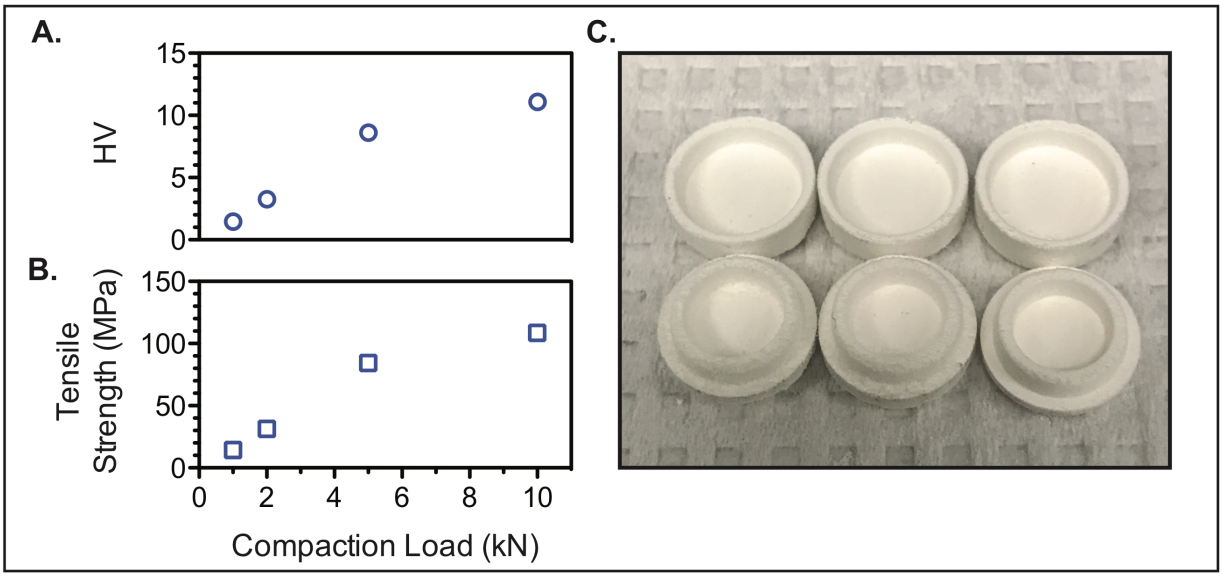

Figure 4. Mechanical properties of blank preform tablets. (**A**) Hardness (HV) and (**B**) tensile strength (MPa) of microcrystalline cellulose preform tablets; (**C**) Fabricated preform tablets.

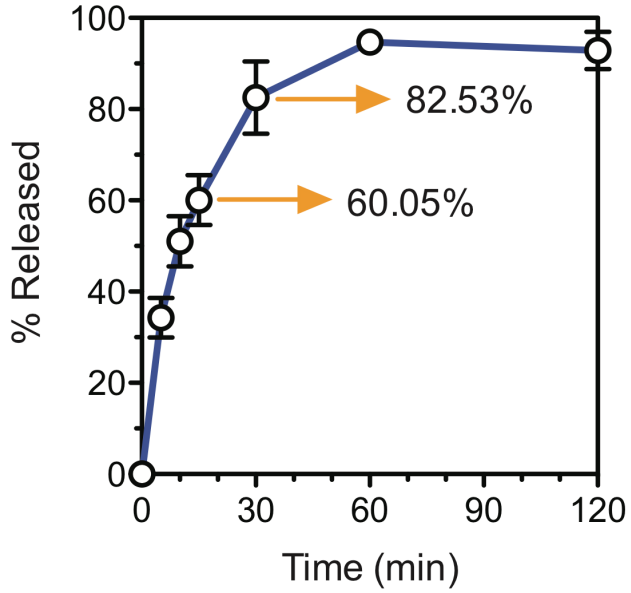

Figure 5. Ropinirole HCL release profile.

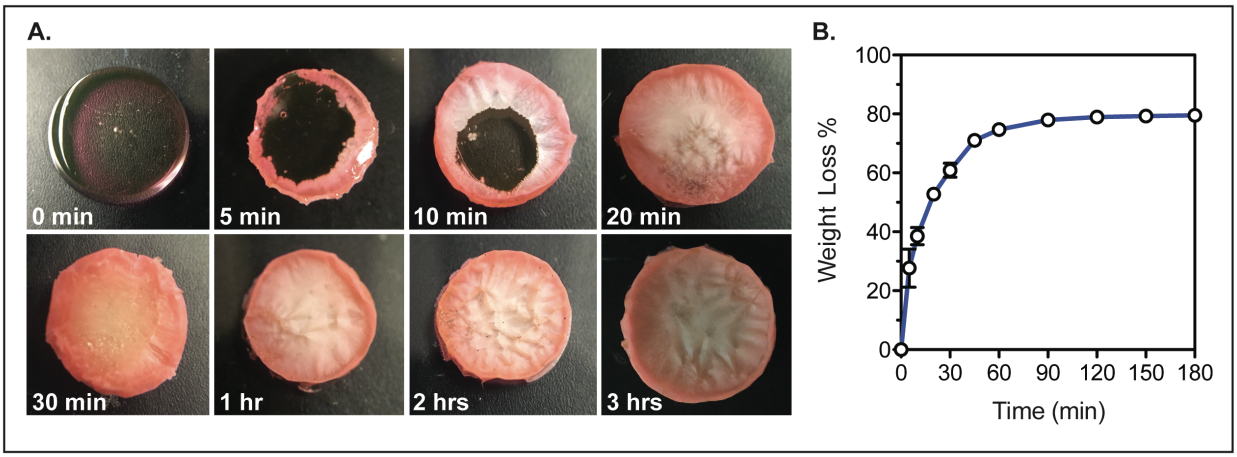

Figure 6. Hydrogel water content removal. (**A**) Hydrogels exposed to 50 °C for varying times; (**B**) Percent of weight loss in the hydrogel due to water removal with increasing drying times.

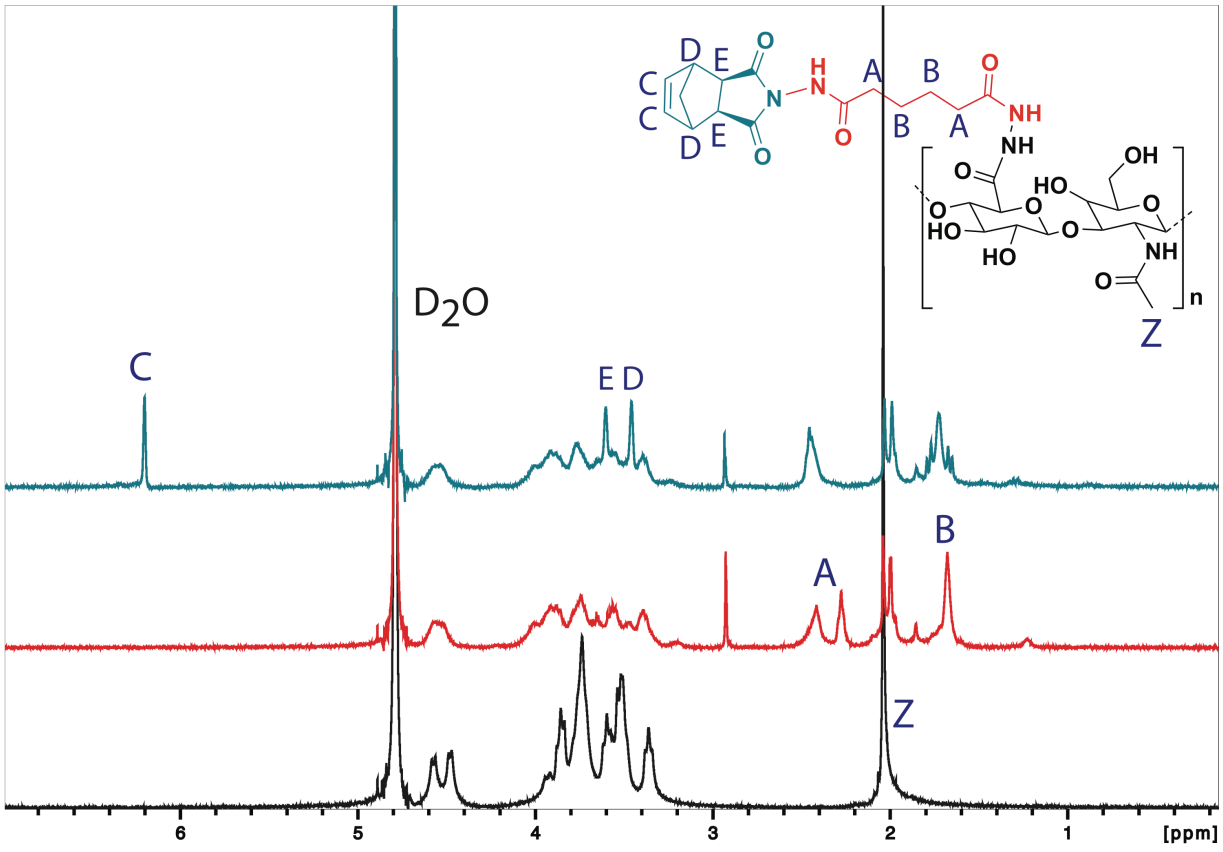

Figure S1. ^{1}H NMR shifts of norbornene groups (D_2O): **Z** (methyl protons in hyaluronic acid, 3H); **A** (α protons in the ADH group, 4H); **B** (β protons in the ADH group, 4H); **C** (*endo* vinyl protons, 2H); **D** (bridgehead protons, 2H); **E** (norbornene α protons, 2H).

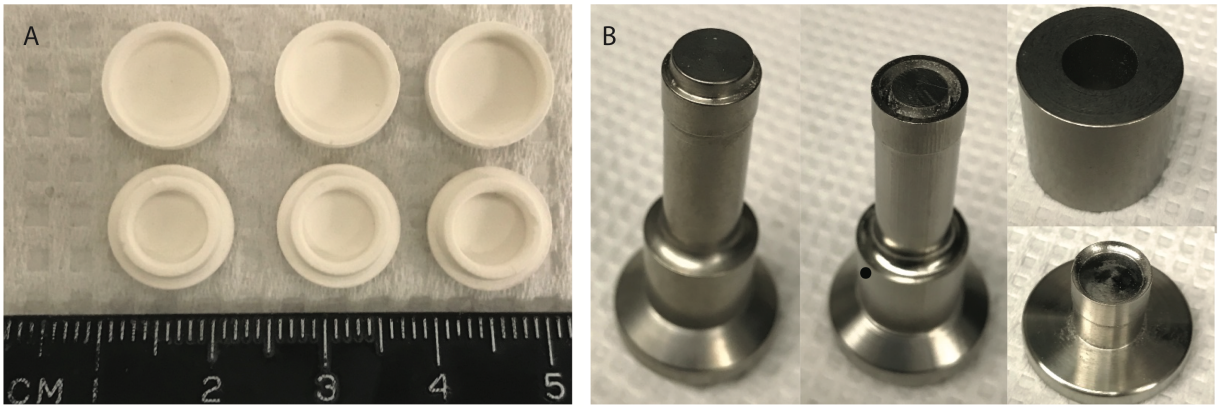

Figure S2. Custom preform tablet punches and die for direct powder compression.

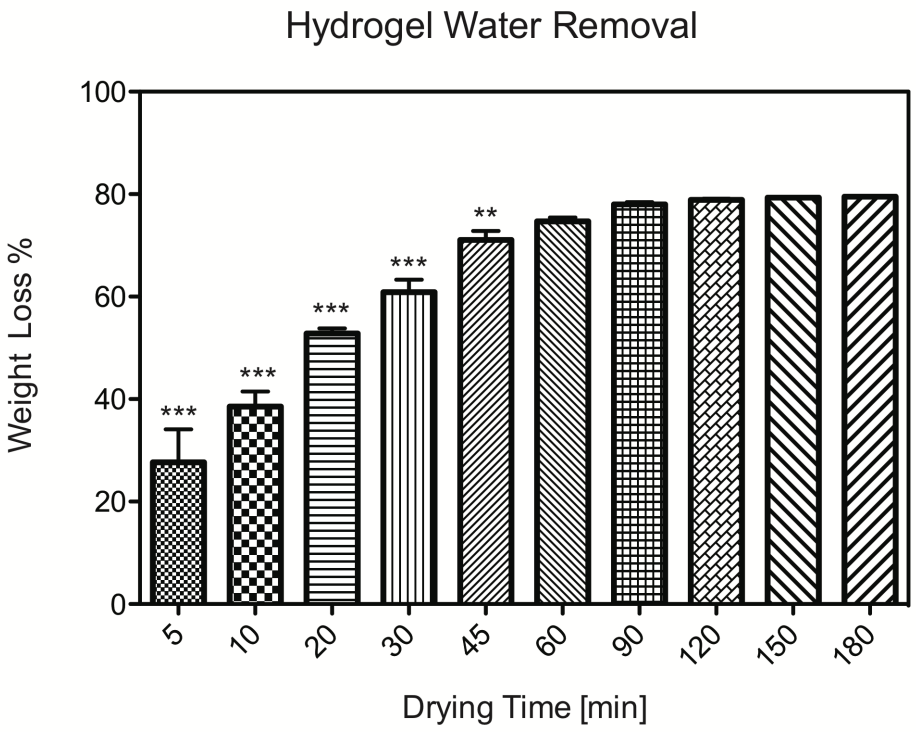

Figure S3. Statistics on tablet water removal percentage over drying time. A One-way ANOVA test with a Dunnett's post-test analysis was done, with column (180min) taken as control (* denotes statistical significance; $P < 0.0001$). Results show no statistical difference after 60 minutes of drying at 50 °C.

2.7 TABLES

Table 1. Swelling ratio and parameters for *Z* value analysis of bioink.

Nozzle Diameter (mm)	Density (kg/m^3)	Surface Tension (mN/m)	Viscosity (mPa·s)	*Z*	Swelling Ratio
0.08	1042	51.47	8.38	7.82	21.14

2.8 REFERENCES

1. Cohen, J. S. Dose Discrepancies Between the Physicians' Desk Reference and the Medical Literature, and Their Possible Role in the High Incidence of Dose-Related Adverse Drug Events. *Arch Intern Med.* **161,** 957–964 (2001).
2. Florence, A. T. & Lee, V. H. L. Personalised medicines: More tailored drugs, more tailored delivery. *Int. J. Pharm.* **415,** 29–33 (2011).
3. Schork, N. J. Personalized medicine: Time for one-person trials. *Nature* **520,** 609–611 (2015).
4. Acosta-Vélez, G. F. & Wu, B. M. 3D Pharming : Direct Printing of Personalized Pharmaceutical Tablets Abstract Powder Bed Inkjet 3D Printing. *Polym. Sceiences* **1,** 1–10 (2016).
5. Wu, B. M. *et al.* Solid free-form fabrication of drug delivery devices. *J. Control. Release* **40,** 77–87 (1996).
6. Sun, Y. & Soh, S. Printing Tablets with Fully Customizable Release Profiles for Personalized Medicine. *Adv. Mater.* 1–7 (2015). doi:10.1002/adma.201504122
7. Goyanes, A. *et al.* 3D printing of medicines: Engineering novel oral devices with unique design and drug release characteristics. *Mol. Pharm.* 4077–4084 (2015). doi:10.1021/acs.molpharmaceut.5b00510
8. Khaled, S. A., Burley, J. C., Alexander, M. R., Yang, J. & Roberts, C. J. 3D printing of five-in-one dose combination polypill with defined immediate and sustained release profiles. *J. Control. Release* **217,** 308–314 (2015).
9. Daly, R., Harrington, T. S., Martin, G. D. & Hutchings, I. M. Inkjet printing for pharmaceutics – A review of research and manufacturing. *Int. J. Pharm.* **494,** 554–567 (2015).
10. Verkouteren, R. M. & Verkouteren, J. R. Inkjet metrology: High-accuracy mass measurements of microdroplets produced by a drop-on-demand dispenser. *Anal. Chem.*

81, 8577–8584 (2009).

11. Alomari, M., Mohamed, F. H., Basit, A. W. & Gaisford, S. Personalised dosing: Printing a dose of one's own medicine. *Int. J. Pharm.* **494,** 568–577 (2015).
12. Fraser, J. R., Laurent, T. C. & Laurent, U. B. Hyaluronan: its nature, distribution, functions and turnover. *J. Intern. Med.* **242,** 27–33 (1997).
13. Allison, D. D. & Grande-Allen, K. J. Review. Hyaluronan: A Powerful Tissue Engineering Tool. *Tissue Eng. Part A* **12,** 2131–2140 (2006).
14. Hoyle, C. E. & Bowman, C. N. Thiol-Ene Click Chemistry. *Angew. Chemie Int. Ed.* **49,** 1540–1573 (2010).
15. Wong, C.-H. & Zimmerman, S. C. Orthogonality in organic, polymer, and supramolecular chemistry: from Merrifield to click chemistry. *Chem. Commun.* **49,** 1679–1695 (2013).
16. Shih, H., Mirmira, R. G. & Lin, C.-C. Visible light-initiated interfacial thiol-norbornene photopolymerization for forming an islet surface conformal coating. *J. Mater. Chem. B* **3,** 170–175 (2015).
17. Tompson, D. J. & Vearer, D. Steady-state pharmacokinetic properties of a 24-hour prolonged-release formulation of ropinirole: Results of two randomized studies in patients with Parkinson's disease. *Clin. Ther.* **29,** 2654–2666 (2007).
18. Jang, D. *et al.* Influence of Fluid Physical Properties on Ink-Jet Printability. *Langmuir* **25,** 2629–2635 (2009).
19. Cole-Parmer Instrument Company. Available online: https://pim-resources.coleparmer.com/instruction manual/surface-tension-apparatus-instruction-manual.pdf (accessed on 12 January 2017).
20. Zustiak, S. P. & Leach, J. B. Hydrolytically Degradable Poly (Ethylene Glycol) Hydrogel Scaffolds with Tunable Degradation and Mechanical Properties. *Biomacromolecules* **11,** 1348–1357 (2010).
21. Gramlich, W. M., Kim, I. L. & Burdick, J. a. Synthesis and orthogonal photopatterning of

hyaluronic acid hydrogels with thiol-norbornene chemistry. *Biomaterials* **34,** 9803–9811 (2013).

22. Gudapati, H., Dey, M. & Ozbolat, I. A comprehensive review on droplet-based bioprinting: Past, present and future. *Biomaterials* **102,** 20–42 (2016).

23. Pilaniya, K.; Chandrawanshi, H.K.; Pilaniya, U.; Manchandani, P.; Jain, P.; Singh, N. Recent trends in the impurity profile of pharmaceuticals. *J. Adv. Pharm. Technol. Res.* **1**, 302–310 (2010).

24. Rowe, R.C.; Sheskey, P.J.; Paul, J. Weller, P.J. Handbook of Pharmaceutical Excipients, 6th ed.; Pharmaceutical, Press: London, UK, 206-208 (2009).

25. Bi, Y.X.; Sunada, H.; Yonezawa, Y.; Danjo, K. Evaluation of rapidly disintegrating tablets prepared by a direct compression method. *Drug Dev. Ind. Pharm.* **25**, 571–581 (1999).

26. Thoorens, G.; Krier, F.; Leclercq, B.; Carlin, B.; Evrard, B. Microcrystalline cellulose, a direct compression binder in a quality by design environment—A review. *Int. J. Pharm.*, **473**, 64–72 (2014).

27. Ibrahim, D.; Broilo, T.L.; Heitz, C.; Oliveira, G.D.E.; Oliveira, H.W.D.E.; Maris, S.; Nobre, W.; Silva, D.N. Dimensional error of selective laser sintering, three-dimensional printing and PolyJet models in the reproduction of mandibular anatomy. *J. Cranio-Maxillofac. Surg.*, **37**, 167–173 (2009).

28. Ionita, C.N.; Mokin, M.; Varble, N.; Bednarek, D.R.; Xiang, J.; Snyder, K.V.; Siddiqui, A.H.; Levy, E.I.; Meng, H.; Stroke, T. Challenges and limitations of patient-specific vascular phantom fabrication using 3D Polyjet printing. *Proc. SPIE Int. Soc. Opt. Eng.*, **9038**, 90380M (2014).

CHAPTER THREE: PHOTOCURABLE POLY(ETHYLENE GLYCOL) AS BIOINK FOR THE INKJET 3D PHARMING OF HYDROPHOBIC DRUGS

3.1 ABSTRACT

Conventional powder bed 3D printing and fused deposition modeling are the two most common additive manufacturing techniques used to create pharmaceutical tablets. However, these technologies are limited by slow printing times and high operating temperatures, respectively. Conversely, inkjet printing can dispense large volumes of material in short periods of time at room temperature. Unfortunately, there are a limited number of materials that are both printable and biocompatible. Therefore, the aim of this work was to engineer photocurable bioinks that have rapid gelation times upon visible light exposure and can carry hydrophobic active pharmaceutical ingredients. The bioink formulations included poly(ethylene glycol) diacrylate as the crosslinkable monomer, Eosin Y as the photoinitiator, and methoxide-poly(ethylene glycol)-amine as the coinitiator. Additionally, poly(ethylene glycol) (200 Da) was added as a plasticizer to modulate the drug release profiles from the gelled bioink, and Naproxen was used as the model drug due to its high hydrophobicity. These formulations were dispensed into blank preform tablets made via direct compression using a piezoelectric nozzle, photopolymerized, and a preform cap was attached to complete the pharmaceutical dosage form. Results indicate that the drug release kinetics of these tablets can be controlled by manipulating the percent of poly(ethylene glycol) diacrylate in the formulation and the light exposure time used to cure the bioinks. Thus, these bioinks represent a new technique towards the controlled dosage of hydrophobic drugs within pharmaceutical tablets.

3.2 INTRODUCTION

Currently, drug dosages are determined through clinical trials, where the dosage with the best therapeutic outcome for most of the population is approved [1,2]. This approach fails to account for variations in drug metabolism and response from patient to patient. Studies have shown that a patient's genetic makeup impacts a drug's efficacy [3–5]. Alternatively, the goal of personalized

medicine is to provide patients with tailored treatments based on the genomic, epigenomic, and other data on the individual's pathophysiology [6]. In addition to further developments in genomics and computational biology, novel technologies and strategies are required for the manufacturing and dispensing of customized dosage forms necessary to help make personalized medicine a reality. 3D Pharming, the use of 3D printing to directly fabricate personalized pharmaceutical tablets [7], is an attractive strategy for manufacturing personalized oral dosage forms. Specifically, this technology allows for the custom design of pharmaceutical tablets containing personalized drug dosages – determined by the application of genomic science – for optimal drug efficacy, reduced side effects, and overall improved patient satisfaction.

The first paper to use 3D printing for drug delivery, published in 1996, used a powder bed 3D printer to fabricate multi-drug delivery devices with controlled release profiles [8]. This technology deposit droplets of binder solution onto a powder bed including the desired compound for object fabrication [9]. Since then, powder bed 3D printing has been used to create tablets with multiple drugs and release profiles by controlling the binder's pH sensitivity [10], its location and concentration throughout the pill [11,12], and by adjusting the geometry of the construct [13]. Nearly 20 years later, in 2015, the FDA approved the first 3D printed pharmaceutical tablet: Spritam® (levetiracetam) from Aprecia, fabricated through powder bed 3D printing [14]. Yet, this technology has limitations regarding the loading of high dosages, lengthy printing times, and the design of complex structures for enhanced control of drug release profiles. Recently, fused deposition modeling (FDM) emerged as another option for 3D Pharming, where a drug loaded polymer filament is melted into a semi-liquid state, extruded though a heated nozzle, and deposited onto a platform for object construction [15]. This technology allows for higher resolution constructs with diverse geometries, including the design of hollow structures, and the incorporation of multiple polymers [16]. However, the reduced amount of thermoplastic materials compatible with the technology limits the materials available for 3D pharming. In addition, the high temperatures of the process can cause degradation of thermolabile active pharmaceutical

ingredients (API). Another recent option for 3D Pharming is stereolithography, which consist of an energy deposition technique where light is exposed on a layer by layer manner onto a photocurable resin for the formation of a 3D object [17]. This technique allows for object with higher resolution (20μm) [18] and is compatible with thermally labile APIs, since it does not requires high operating temperature. However, the large volume of formulation required for tablet manufacturing incapacitates the technology for mass production of pharmaceutical pills.

The ideal 3D pharming technology should incorporate the following characteristics: 1) Maintain the stability of the active ingredient, 2) Achieve fast printing times, 3) Be able to operate in drug dispensing locations and healthcare provider's offices, 4) Allow for the printing of hydrophilic and hydrophobic compounds, 5) Be able to print small and large dosages with great resolution, 6) Allow for its operation in a GMP setting, 7) Be cost-effective, 8) Allow for control of drug release profiles, 9) Allow for the combination of multiple compounds in a single tablet, and 10) Have controls for quality assurance. Inkjet printing allows for drug load resolution in the picomolar range [19], high spatial resolution that allows for drug gradients and printing of multiple drugs within a pill, while improving 3D pharming quality controls by monitoring the process of droplet formation and deposition through video cameras. Moreover, it allows for faster printing times when compared to other technologies and the equipment has lower costs [20]. The use of this technique towards 3D Pharming is limited by the small amount of biocompatible photocurable materials currently available that satisfy the physical properties needed for inkjet printing. Recent work demonstrated the synthesis and use of a hyaluronic acid based photocurable bioink for the inkjet 3D Pharming of hydrophilic drugs [21]. This paper introduces a poly(ethylene glycol) photocurable bioink for the inkjet 3D Pharming of hydrophobic drugs, which constitute over 40% of the new chemical entities developed within the pharmaceutical industry [22]. The low water solubility of these compounds is one of the major hurdles encountered when creating dosage forms, forcing these APIs to be manufactured through powder compressed tablets or gel capsules whose dosage is difficult to tune towards the patient.

Taking advantage of the hydrophobicity of low molecular weight poly(ethylene glycol) diacrylate (PEGDA), we utilized PEGDA (250 Da) as the crosslinking agent of our photocurable formulation along with PEG (200 Da). Other components utilized were Eosin Y, a biocompatible photoinitiator with maximum absorbance in the visible light range [23,24], and m-PEG amine (350 Da) as co-initiator to the free radical polymerization. Typical photocurable formulations make use of photoinitiators with a maximum absorbance within the UV light range. However, UV light can affect the stability of certain drugs, and could present a safety hazard for the operators of 3D pharming machinery [25,26]. In contrast, visible light is a safe energy source to be used by operators through the curing process. The preform tablets utilized to encapsulate the formulation were manufactured through conventional powder compression technique. These were made of microcrystalline cellulose, infused with PEG (35 kDa), and their inner surfaced was brushed with Eudragit E-100, a binder soluble under acidic conditions resulting in fast dissolution of the preform tablet. Naproxen was dispensed into the preform tablets as model compound for the dissolution studies due to its high hydrophobicity. Fast printing times were achieved and the concentration loaded of active pharmaceutical ingredient (API) was significantly enhanced when compared to aqueous formulations.

3.3 MATERIALS AND METHODS

3.3.1 Photocurable Formula Preparation

The reagents PEGDA (250 Da), PEG (200 Da), Eosin Y, Naproxen, and Ibuprofen were obtained from Sigma-Aldrich (St. Louis, MO, USA) and used without further purification. PEGDA constituted the crosslinking agent and main compound of the bioink designed, along PEG 200 which was utilized as a solvent. Formulations with diverse PEGDA weight percentages (W_{PEGDA}) and light exposure times (T_L) were made to manipulate the tensile strength of the gels. Eosin Y at a concentration of 1 mM was added to these formulations as a photo-initiator and 0.05 M mPEG-amine (350 Da, Creative PEG Works, Chapel Hill, NC, USA) was incorporated as a co-

initiator. Naproxen was added at a concentration of 40 mg/mL and the solution was vortexed thoroughly until Eosin Y and Naproxen were completely dissolved.

3.3.2 Gelation and Mechanical Properties

In order to assess the effect of different W_{PEGDA} values on the gel mechanical properties, formulations with 100%, 80%, 60%, 40%, and 20% PEGDA were prepared. 1 mL syringes (BD & Co., Franklin Lakes, NJ, USA), modified by removing their tips, were subsequently loaded with 50 µL of formulation and exposed to visible light (Volpi, V-lux 1000, Auburn, NY, USA) at an intensity of 120 mW/cm^2 to induce gelation. The effect of different T_L values on the tensile strength of tablets was measured by exposing the bioinks for durations of 20 s, 45 s, 1.5 min and 3 min. Moreover, the effect of drug concentration and drug choice in solution was assessed by polymerizing solutions with a W_{PEGDA} of 100%, a T_L of 45 s and diverse concentrations of Naproxen and Ibuprofen. The tensile strength of gels with these two APIs was analyzed.

An Instron (5564 model) was used to measure the failure load of the resulting gels. **Equation 1** was utilized to calculate their tensile strength ($\boldsymbol{\sigma}$), where $\boldsymbol{D}$ is the tablet diameter, $\boldsymbol{H}$ is the thickness, and $\boldsymbol{F}$ represents the failure load [27].

$$\sigma = \frac{2F}{\pi DH} \quad (1)$$

The surface tension ($\boldsymbol{\gamma}$) of the photocurable formulation was measured by **Equation 2** using a tensiometer (Kimble Chase 14818 Tensiometer, Cole-Parmer, Vernon Hills, IL, United States), where $\boldsymbol{h}$ is the distance between menisci of the tube and the capillary, $\boldsymbol{r}$ is the radius of the capillary, $\boldsymbol{\rho}$ is the density of the formulation, and $\boldsymbol{g}$ is the acceleration due to gravity [28]. The density was measured by weighing 1 mL of each formulation in a pre-weighed microcentrifuge tube and dividing the value by the predetermined volume.

$$\gamma = \frac{1}{2} hr\rho g \quad (2)$$

The inverse of Ohnesorge Number, Z value, was calculated to assess the printability of the different formulas engineered. **Equation 3** defines the *Z* value, where $\boldsymbol{a}$ is the radius of the

piezoelectric nozzle printing orifice used to dispense the formulations and $\boldsymbol{\rho}$, $\boldsymbol{\gamma}$, and $\boldsymbol{\eta}$ represent the density, surface tension, and viscosity of the photocurable formula, respectively [29]. The viscosity of the formulations was measured with a rheometer (Discovery HR-2, TA Instruments, New Castle, DE, USA) using a 40 mm 2.016° cone and plate geometry with shear rate ranging from 10 to 100 Hz.

$$Z = \frac{(a\rho\gamma)^{1/2}}{\eta} \tag{3}$$

The swelling ratio (Q_M) of the PEGDA gels was measured by taking the ratio between the swelling mass (M_S) and the dry mass (M_D) of the gel, represented below in **Equation 4 [**30]. Gels were immersed in PBS for 3 days and weighed to obtain their swelling mass. Subsequently, the gels were lyophilized and their dry weight was measured.

$$Q_M = \frac{M_S}{M_D} \tag{4}$$

In-situ photorheology was performed on a rheometer at constant strain of 1% and angular frequency of 10 rad/sec. The visible light source was turned on after 30 s of data collection and the storage modulus (G') of the sample was collected for a period of 10 min. In addition, a flow temperature ramp (25 °C – 50 °C) was performed to measure the viscosity of the photocurable formulas and their susceptibility to temperature, at a constant shear rate of 1 Hz.

To analyze the microarchitecture of the gels, the mesh size (ξ) of the polymerized formulas was calculated (**Equation 5**) [31], where $(\bar{r}_0^2)^{1/2}$ represents the root mean square end-to-end distance of polymer chain and v_S is the polymer volume fraction. **Equation 6** defines v_S, where ρ_s and ρ_w are the density of the PEGDA solution and water, respectively, and $\mathrm{Q_M}$ represents the swelling ratio [31]. **Equation 7** defines $(\bar{r}_0^2)^{1/2}$, where l is the average bond length, C_n is the characteristic ratio of the polymer (typically 4.0 for PEG [30]), M_r is the molecular weight of the repeating unit (44 Da for PEG), and (M_c) is the molecular weight between crosslinks. Finally, **Equation 8** defines (M_c), where V_1 is the molar volume of the solvent (18 cm^3/mol for water [30]), $\bar{v}$ is the specific volume of the polymer (ρ_w/ρ_s), χ_1 is the polymer-solvent interaction parameter

(0.426 for PEG-water [30]), and M_n is the molecular weight of the PEGDA being utilized. In this study, a constant χ_1 was assumed for all ranges of v_S values.

$$\xi = (\bar{r}_0^2)^{1/2} v_s^{-1/3} \tag{5}$$

$$v_S = \frac{\frac{1}{\rho_S}}{\frac{Q_M}{\rho_W} + \frac{1}{\rho_S}} \tag{6}$$

$$(\bar{r}_0^2)^{1/2} = l C_n^{1/2} \sqrt{2 \frac{\overline{M_c}}{M_r}} \tag{7}$$

$$\frac{1}{\overline{M_c}} = \frac{2}{\overline{M_n}} - \frac{\frac{\bar{v}}{V_1}(\ln(1-v_s) + v_s + \chi_1 v_s^2)}{v_s^{-1/3} - \frac{v_s}{2}} \tag{8}$$

3.3.3 Scanning Electron Microscopy (SEM)

Cross-sectional images of the cylindrical tablets were captured with a NOVA 230 NanoSEM scanning electron microscope to further characterize the microstructure of the tablet. The voltage and spot size were set at 3.0 kV and 4.0, respectively, while the pressure mode was set at a low vacuum variable pressure of 50 Pa. Images on cross-sectional areas of 100% and 20% PEGDA gels were capture.

3.3.4 Preform Tablet Fabrication and Characterization

The drug-containing bioinks were directly printed into tablet preforms prepared as previously described [21]. Briefly, the binder microcrystalline cellulose (Avicel® PH-103; FMC Corporation; Philadelphia, PA, USA), and the superdisintegrant croscarmellose sodium (5% (w/w); VIVASOL®; JRS Pharma, Patterson, NY, USA) were pressed into two fitting parts – a 100 µL well and a cap with a locational interference fit – via direct compression technique. A customized press design was used to make the preform tablets, which included two standard B-Type upper punches with tip modifications to produce the positive features of either the cap or the well, and one lower punch designed to sit flush on a hydraulic press stage with a tip that had 0.04-inch radius of curvature and a 0.02-inch blended landing. A standard 0.945 die with a 3/16-inch-deep TSM standard taper and an increased die bore dimension of 0.003 inch at the face of

the die was used during tablet fabrication. The preform tablets (150 mg caps; 300 mg wells) were compressed with 10 kN of force, with a dwell time of 30 s. To prevent absorption of the drug-containing bioink into the preform tablet during printing, the well was infused with PEG (35 kDa) by submerging the tablet in an acetone solution containing 15% (w/w) PEG for 30 min at 55°C. Additionally, the well was brush-coated with Eudagrit® E100 (Evonik, Essen, Germany) (polymethacrylate copolymer) dissolved in acetone at 20% (w/w). The tablet hardness at different locations on the perform tablet was measured using Buehler Vicker Hardness indenter 1600-6305 (Buehler, Lake Bluff, IL, USA) with Vickers indentations up to 500 g load. Surface morphology of the preform tablet was characterized by scanning electron microscopy (NOVA NanoSEM 230, FEI Co., Hillsboro, OR, USA)

3.3.5 Drug Dispensing and Release Kinetics

A MicroFab piezoelectric dispenser (MJ-ABP-01-080, MicroFab, Plano, TX, USA) with an 80 µm diameter nozzle was utilized to test the droplet formation capacity of these formulations and for their subsequent dispense into preform tablets. A microdispensing system (MD-E-3000, Microdrop, Norderstedt, Germany) set at 46 V, with a pulse width of 16 µs and a frequency of 2000 Hz (droplets per second), was used to drive the piezoelectric dispenser. An analog camera (JAI CV-S3300) with a lens (Edmund Optics, Barrington, NJ, USA) and an LED were used to image droplet formation. Formulation with a W_{PEGDA} value of 100% was dispensed into preform tablets through the piezoelectric nozzle for a period of 5 min and exposed to light for 45 s or 20 s at 120 mW/cm^2, to analyze the effect of T_L values on drug release. Additionally, formulation containing 20% PEGDA was pipetted into preform tablets (50 µL) and its drug release kinetics was analyzed to study softer gel precursor solutions that did not meet inkjet printing requirements at room temperature due to higher viscosities. After dispensing and light induced polymerization, a preform cap was attached to finalize the pharmaceutical product. The drug dissolution profile of the formulations was obtained by placing the tablets into Uni-cassettes (Tissue-Tek) and immersing them in a beaker containing 500 mL of dissolution medium, conditioned at 37 °C and

stirred at 60 rpm. The dissolution medium was composed of monobasic potassium phosphate at a concentration of 1.053 mM and a pH of 7.2. Aliquots (1 mL) were taken from the dissolution bath of after 2, 6,10, 12, 18, and 24 h of the dissolution, and the volume taken was replenished with fresh dissolution medium conditioned at 37 °C. Their drug concentration was determined by HPLC (Waters 2690 with a PDA 996 detector) at a wavelength of 330 nm.

3.3.6 2D Spatial Control

To demonstrate spatial control of the formulations upon dispensing and their potential applicability towards PolyJet printing, the dispensing system was attached to a robot (I&J7900-LF, I&J Fisnar Inc., Wayne, NJ, USA). The robot was programmed to dispense formulation in predetermined shapes (square and circle).

3.3.7 Statistical Analysis

Statistical analysis was performed with GraphPad Prism software (GraphPad Software, Inc., San Diego, CA). Statistical significance was assessed using single factor ANOVA test with a Tukey post-test and 95% confidence interval.

3.4 RESULTS AND DISCUSSION

3.4.1 Formulation Characterization

Naproxen, a non-steroidal anti-inflammatory agent [32] and the model drug used in this study, was dissolved in our photocurable formulations at a concentration of 40 mg/mL. This represents a significant solubility increase when compared to aqueous solutions, where the solubility for Naproxen is only 0.0159 mg/mL [33]. To quantify the effect on the mechanical properties of the PEGDA/PEG200 ratio in our formulation, gels with W_{PEGDA} of 20%, 40%, 60%, 80%, and 100% and a T_L of 45 s were manufactured. Gels with lower W_{PEGDA} exhibited a higher opacity when compared to gels with higher W_{PEGDA}, which had a higher transparency resembling the physical appearance of acrylic materials (**Fig. 1**). This characteristic was also observed in gels loaded with Ibuprofen (**Fig. S1**).

The effect of light exposure time was quantified by submitting the formulations to 20 s, 45 s, 1.5 min, and 3 min of visible light an intensity of 120 mW/cm^2. The diameter and thickness of the gels were 4.35 mm and 3.00 mm, respectively, for a 50 µL solution gel. The failure load of the gelled formulations was obtained in order to calculate their tensile strength using **Equation 1**. **Figure 2A** shows the tensile strength values for these formulations under different T_L conditions. The tensile strength of the tablets increased with increasing PEGDA percent and extended light exposure times. Typical tensile strengths of commercially available tablets fall between 1 and 10 MPa [34]. Gels with W_{PEGDA} of 40% or higher showcase desirable tensile strength values at determined T_L values ranging from 20 s to 3 min.

Typically, solutions with viscosities values between 3-20 mPa*s are compatible with piezoelectric nozzles at room temperature [35,36]. Nonetheless, certain piezoelectric nozzles exerting stronger piezo forces can dispense fluids with viscosities of up to 50 mPa*s [37]. A flow temperature ramp was done to analyze the viscosity of our formulations at different temperatures (**Fig. 2B**). Solutions with W_{PEGDA} of 100%, 80%, and 60% fell within the viscosity values ideal for inkjet printing at room temperature, whereas solutions with W_{PEGDA} of 40% and 20% had values higher than 20 mPa*s, requiring minor temperature increases to fall within the printable category. Piezoelectric nozzles with heating capabilities could be utilized to print formulations with lower W_{PEGDA}, since their viscosity decreased significantly by increasing the temperature to 45°C. Higher viscosity values were obtained when loading the bioinks with Ibuprofen at 180 mg/mL, showing the effect on viscosity of higher drug concentrations (**Fig. S2**).

In-situ photo-rheology was performed to assess the gelation kinetics of the precursor solutions, where the storage modulus was recorded over time as the gelation proceeded (**Fig. 2C**). The results show that formulations achieve a higher storage modulus within the first 30 s of light exposure as the W_{PEGDA} increases, having a higher impact on formulations containing 40% PEGDA and above. Similar gelation times were obtained with bioinks carrying Ibuprofen at 180

mg/mL, demonstrating that quick polymerization can be achieved at higher API concentrations (**Fig. S3**).

To assess the effect of drug concentration, gels with different Naproxen concentrations were made and their tensile strength was analyzed (**Fig. 3A**). The gels had a W_{PEGDA} of 100% and a T_L of 45 s. Results show that the mechanical strength of the gels remains constant as the concentration increases up to a maximum of 40 mg/mL, after an initial decay in tensile strength when compared to a gel without drug. However, a decrease in tensile strength was observed as the drug concentration increased when using Ibuprofen, a common analgesic and antipyretic agent [38] (**Fig. 3B**). This behavior is possibly caused by potential disruption of the gel microarchitecture due to higher amounts of API in solution and Ibuprofen's higher hydrodynamic radius, when compared to Naproxen. **Figure 3C** compares the tensile strength of gels containing the same concentration of Naproxen and Ibuprofen. A statistical difference was observed between the gels containing Naproxen and the no drug gel condition, whereas no difference was observed between the Ibuprofen and no drug conditions. This indicated that the mechanical properties of the gels are affected by both, drug choice and its concentration.

To analyze the microstructure of the polymerized gels, SEM analysis was done on the cross-section of cured formulations with W_{PEGDA} of 100% and 20%, with Naproxen. **Figure 4** reveals complete dissolution of the model drug at a concentration of 40 mg/mL, evidenced by the lack of Naproxen crystals within the gel. Furthermore, the SEM images show an increased porosity with decreased W_{PEGDA}, explaining the opacity observed on gels containing higher PEG200 percentages. Similar microarchitectures were observed in gels loaded with Ibuprofen at 180 mg/mL (**Fig. S4**).

The mesh size of the polymer matrix formed by each formulation was analyzed to know what size of molecules could be delivered successfully and its potential effect on drug release kinetics. **Table 1** shows the mesh size obtained for each PEGDA formulation. Higher W_{PEGDA} resulted in smaller mesh size values due to an increased number of crosslinked PEGDA polymer

chains. On the other hand, lower W_{PEGDA} resulted in larger mesh size values, shortening the time for drugs diffusing out through the matrix and yielding a faster drug release. Although drugs could be released through the matrix of the gel, the small mesh size limited the ability for immediate release. Therefore, only sustained release was observed for the formulations developed in this study. Naproxen has a hydrodynamic radius of 0.377 nm [39], allowing it to diffuse through the microarchitecture of the polymerized gel. Slightly smaller mesh sizes were obtained when exposing bioinks with a W_{PEGDA} of 20% and 40% to 3 min of light exposure time, denoting the effect of prolonged polymerization times in the architecture of the gels with low PEGDA percentages (**Table S1**).

3.4.2 Droplet Formation

The inverse of the Ohnesorge number, or Z value, was calculated to define the printability of the formulations engineered (**Equation 3**). This dimensionless number takes in consideration the inertia and surface tension forces of a fluid over its viscosity forces, in order to define its droplet formation capabilities. This parameter also considers the orifice radius of the nozzle being used for inkjet printing. Values ranging from 4 to 14 have been defined as printable substances in the literature, where values above 14 exhibit the formation of satellite droplets and values below 4 present strong viscous forces [29]. The surface tension, viscosity, and density of the formulations was quantified to determine the Z value. In **Figure 2B** we discussed the viscosity of formulations with different W_{PEGDA} and their temperature susceptibility. Fluids with surface tensions falling within the range of 30-70 mN/m are considered printable fluids [35,40]. **Table 2** shows the values obtained for these parameters and the corresponding Z values for each formula at room temperature.

Formulation with a W_{PEGDA} of 100% fell within the printable range, since it achieved a viscosity value below 20 mPa*s. However, we hypothesize that formulations with lower W_{PEGDA} could fall into this category by using piezoelectric nozzles with heating capabilities. The surface tension and densities obtained were adequate for inkjet printing. From this analysis, we conclude

that viscosity was the determining factor in the printability of our formulations, since the other variables had similar values. **Figure 5** shows the droplet formation process for a formula with a W_{PEGDA} of 100% and Naproxen at a concentration of 40 mg/mL. This test was performed with a driver set at 46 V, with a pulse width of 16 µs, and a frequency of 2000 Hz. Similar images were obtained using bioink loaded with 180 mg/mL of Ibuprofen (**Fig. S5**). The formulations sustained a stable printing time of 1 h and a permissible idle time between prints was of 3 min.

3.4.3 Preform Tablet Characterization

Microcrystalline cellulose was chosen as the diluent for the preform tablet because of its good compressibility and compactibility resulting from the powder's ability to undergo plastic deformation and form hydrogen bonds between neighboring hydroxyl groups [41]. These properties are particularly important for the successful formation of the preform tablet's positive features. Additionally, it is broadly compatible with APIs and physiologically inert [42]. To facilitate the rapid disintegration of the preform tablet, croscarmellose sodium was added to the preform tablet at 5% (w/w) [43]. It was previously shown that at least 5 kN compression force was required to produce tablets with adequate mechanical strength and handling properties, and that the addition of the superdisintegrant to the preform tablet did not greatly impact the mechanical properties of the tablet [21]. As such, 10 kN of force were used to fabricate the perform tablets in this study (**Fig. S6**). SEM analysis (**Figure 6A-C**) and the surface hardness profiles of uncoated preform tablets (**Fig. S7**) show low-density regions exist in the periphery and a high-density area exists in the center of the tablet face. It has been previously reported that die wall lubrication can have an impact on the density distribution. Specifically, non-lubricated tablets had a high-density area in the periphery and the material in the center was less dense, while the lubricated die tablet showed an opposite pattern [44]. This is likely due to the low friction coefficient between the walls of the punch and the powder, allowing for powder movement relative to the punch during compression. The custom-made punches used in this study were coated with magnesium

stearate as a lubricant to facilitate the removal of the positive features of the perform tablet from the punch.

The preform tablet's density variation negatively impacted the performance of tablets during printing of the bioink. The increased porosity in the low-density regions of the preform tablet allowed the hydrophobic bioinks to soak into the preform tablet during printing, which not only weakened the preform tablet, but also negates the advantages of using 3D printing for pharmaceutical applications, such as control over drug positioning. To fill the pores in the low-density regions, the preform tablets were first soaked in a high-molecular weight PEG (35 kDa) solution. High-molecular weight PEG was selected because it is immiscible with the low-molecular weight PEGDA in the bioink. Additionally, a thin coating of Eudagrit® E100 was added to the preform tablet well to further inhibit the absorption of the bioink during printing. SEM analysis shows that the polymeric coating fill the pores of the preform tablet's low-density regions (**Figure 6D-E**).

3.4.4 Tablet Dissolution Test

Formulations with a W_{PEGDA} of 100%, a T_L of 45 s or 20 s, and Naproxen at a concentration of 40 mg/mL, were dispensed into blank preform tablets and subsequently exposed to light to induce gelation. After polymerization, the tablets were capped and immersed into 500 mL of dissolution medium, conditioned at 37 °C and stirred at 60 rpm. Aliquots were taken after 2, 6, 10, 12, 18, and 24 h of dissolution and their drug concentration was analyzed through HPLC. The results show that the release profile of drugs can be manipulated by controlling the light exposure time applied to the formulations, where lower T_L values result on faster release kinetics (**Figure 7A**). To assess the release profile of formulations with lower W_{PEGDA}, formulation with 20% W_{PEGDA} was pipetted into preform tablets to study its release kinetics. The release profile obtained indicates that faster release kinetics can be obtained by printing low W_{PEGDA} formulations using piezoelectric nozzles with heating capabilities. **Figure 7B** shows a statistically significant

difference in drug release after 24 h of dissolution when changing T_L from 45 s to 20 s for the same W_{PEGDA} value (100%).

3.4.5 2D Spatial Control

PolyJet is a 3D printing technique where photocurable formulations are dispensed on a tray under constant light exposure, resulting in solid objects with diverse geometries and mechanical properties [45,46]. To show that the 2D deposition of these formulations could be controlled in order to apply them in PolyJet technology, the piezoelectric nozzle was attached to a robot programed to form circle and square geometries. **Figure 8** shows formulation with a W_{PEGDA} of 100% dispensed upon a flat surface and the formation of predetermined geometries. The ability to polymerize these formulations upon light exposure, its droplet formation capability, and the capacity to load hydrophobic drugs, makes the materials designed translatable into PolyJet printing for the 3D pharming of hydrophobic APIs, eliminating the need of a preform tablet as a vessel.

3.5 CONCLUSION

In this study, PEGDA photocurable formulations were engineered towards the 3D pharming of hydrophobic APIs. The formulation containing a PEGDA weight percent of 100% achieved droplet formation and was suitable towards inkjet printing. Formulations having PEGDA percentages of 80%, 60%, 40%, and 20% could be dispensed through piezoelectric nozzles with heating capabilities, since their viscosity falls under acceptable values for inkjet printing at a temperature of 45°C. Drug release analysis of tablets loaded with Naproxen demonstrated that the drug release kinetics can be manipulated by controlling the light exposure time applied to the bioinks and the weight percent of PEGDA utilized, with lower light exposure times and PEGDA percentages resulting in faster release kinetics. Finally, we demonstrate the spatial control of these bioinks through the dispensing process and their applicability towards PolyJet technology due to their droplet formation and gelation capacity. This 3D pharming technique represent an

advancement over conventional powder bed 3D printing and fused deposition modeling, due to its fast processing time and the ability to perform at room temperature, respectively.

3.6 FIGURES

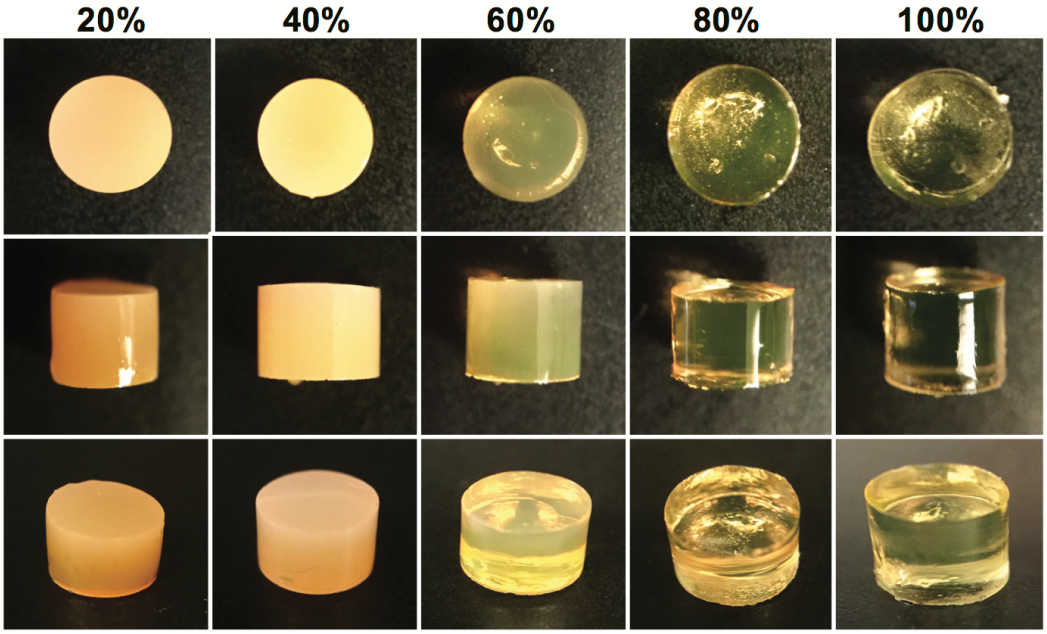

Figure 1. Polymerized PEGDA gels with different W_{PEGDA} values. The bioinks were exposed to a T_L of 1.5 min. It can be observed that the gels have a higher opacity as the W_{PEGDA} decreases, due to a higher concentration of PEG200.

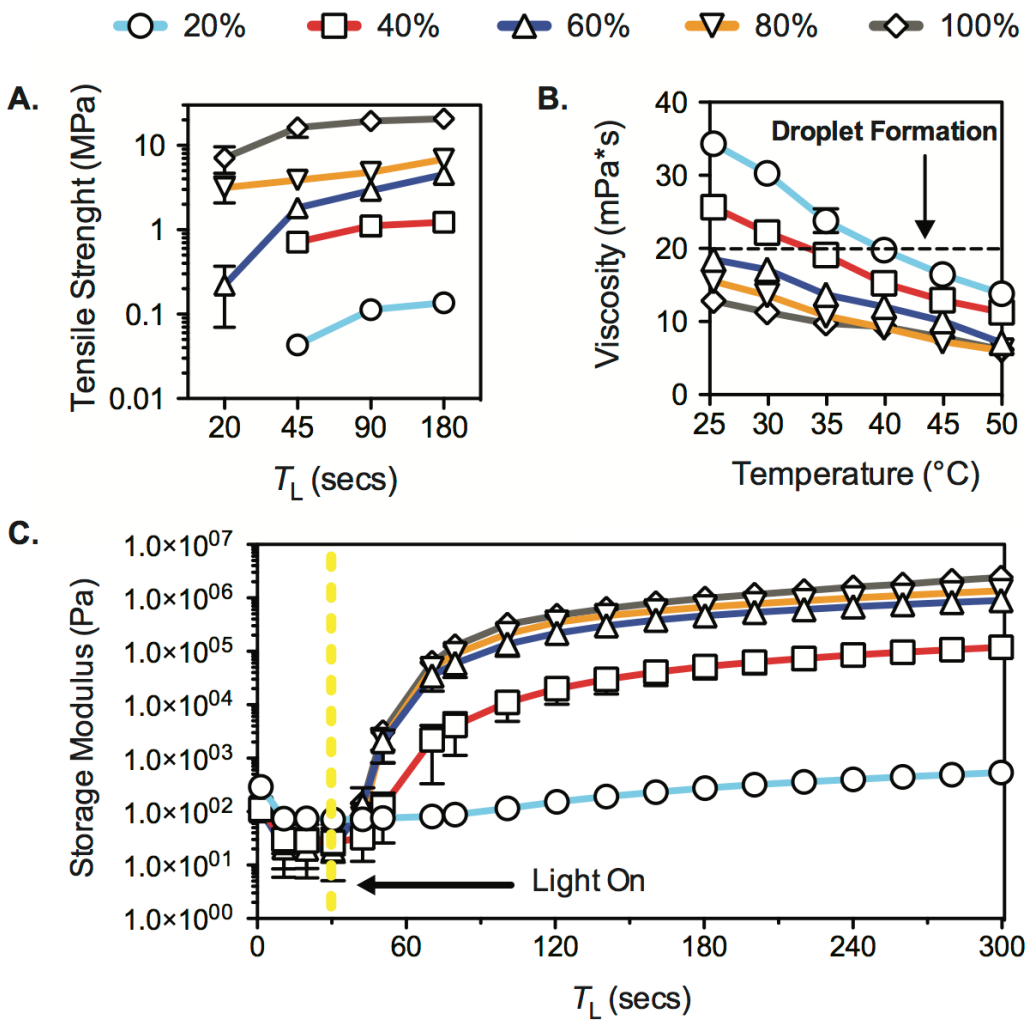

Figure 2. Mechanical properties of polymerized hydrophobic gels. **(A)** Effect of different W_{PEGDA} and T_L values on polymerized gels. **(B)** Effect of increased temperatures on the viscosity of formulations with different W_{PEGDA} values. **(C)** Gelation time of bioinks containing different W_{PEGDA} values. The formulations were exposed to visible light after 30 s of G' data collection.

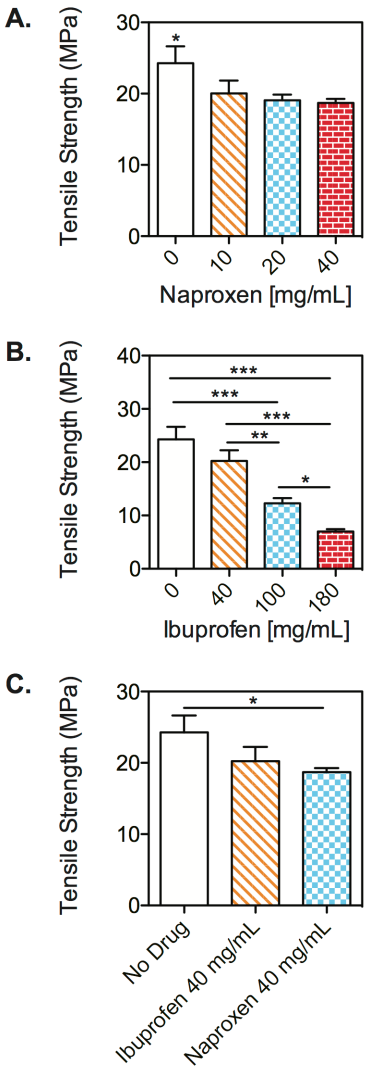

Figure 3. Tensile strength of Naproxen and Ibuprofen loaded gels with a W_{PEGDA} of 100% and a T_L of 45 s. **(A)** Tensile strength of Naproxen tablets with diverse drug concentrations. 40 mg/mL was the maximum solubility achieved for this API in this formulation. **(B)** Tensile strength of Ibuprofen tablets with diverse drug concentrations. 180 mg/mL was the maximum solubility achieved for this API. **(C)** Tensile strength comparison between gels loaded with Naproxen and Ibuprofen at a concentration of 40 mg/mL. The difference observed shows that the mechanical properties of these gels can be impacted by both, the concentration of the drug utilized and the compound chosen as model drug. Asterisks denote statistical significance (* denotes $p < 0.1$; ** denotes $p < 0.01$; *** denotes $p < 0.001$).

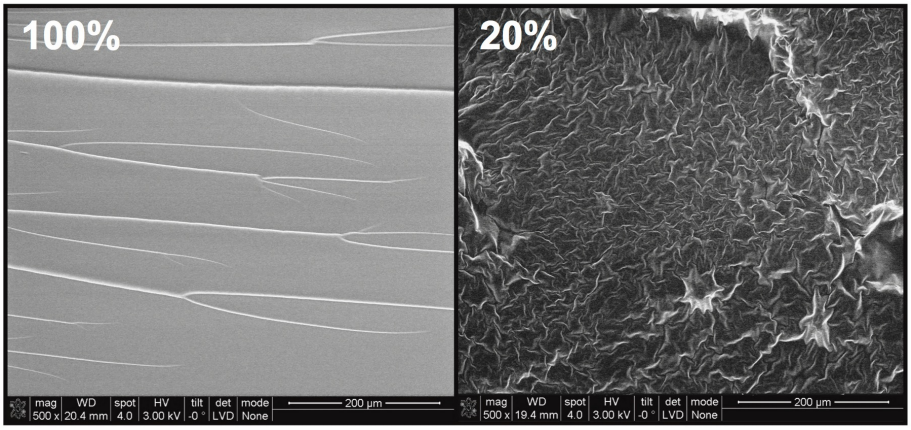

Figure 4. SEM images of polymerized bioinks with W_{PEGDA} of 100% and 20%, exposed to a T_L of 45 s. The images show an increased porosity for the gel with a W_{PEGDA} of 20%. This characteristic explains the increased opacity observed on gels with low PEGDA concentrations.

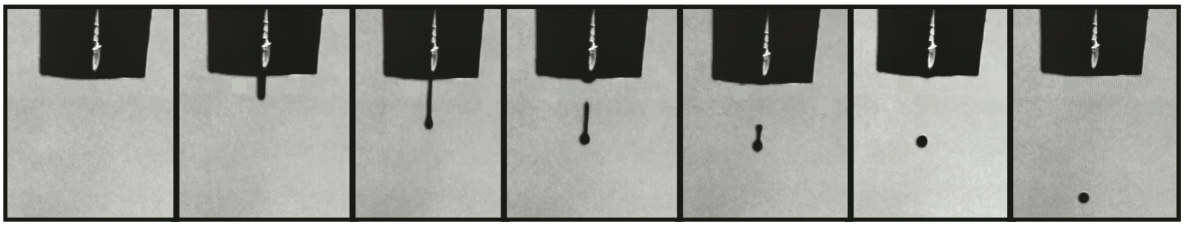

Figure 5. Droplet formation sequence for PEGDA bioink with a W_{PEGDA} of 100% and loaded with Naproxen at a concentration of 40 mg/mL. This formulation had a Z value of 4.47, falling within the printable range (4-14).

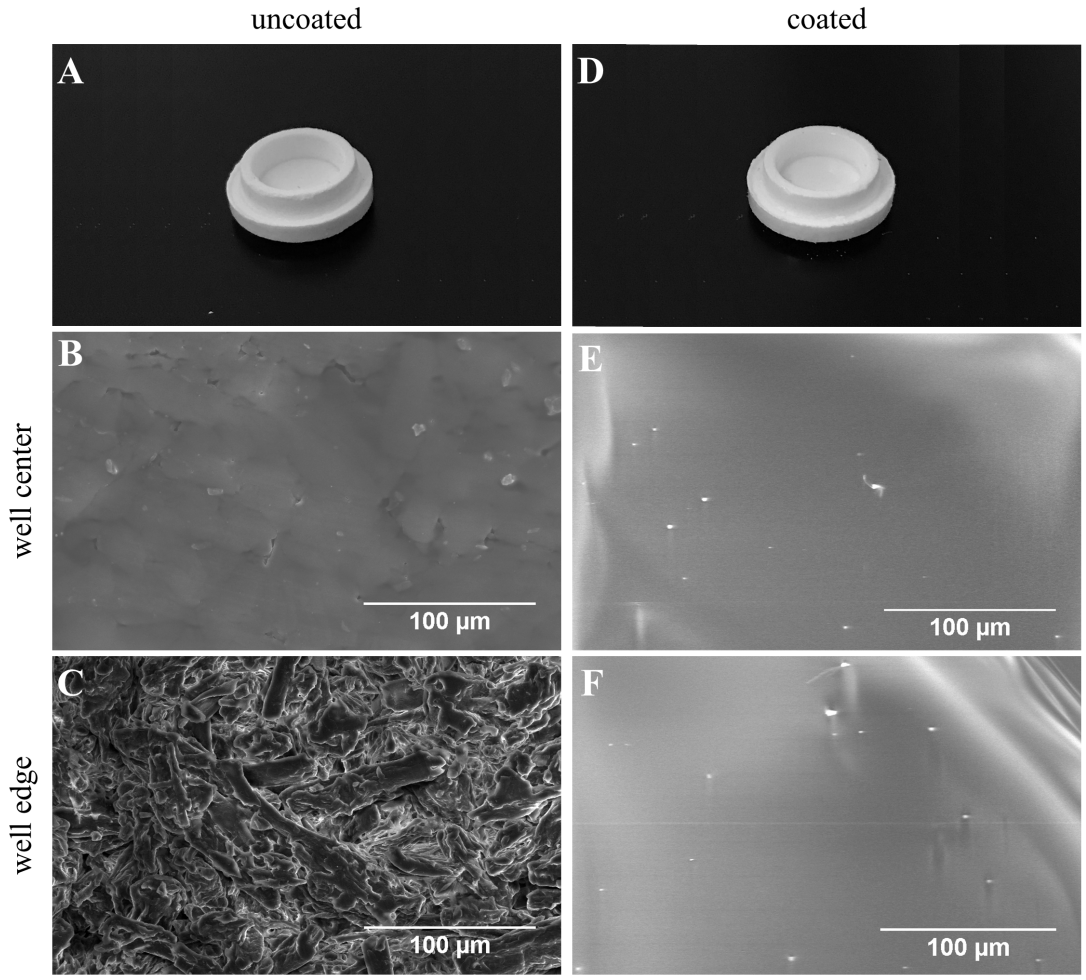

Figure 6. Images of uncoated/coated preform tablets and SEM images of their surface. **(A)** Microcrystalline cellulose uncoated preform tablet made by powder compression. **(B)** Microarchitecture of the uncoated well center section. **(C)** Microarchitecture of the well edge (walls of the well in the preform tablet). A high porosity is observed in this area, causing the leak of bioink in uncoated preform tablets. **(D)** Microcrystalline cellulose E-100 coated preform tablet. **(E)** Well center of the preform tablet coated with E-100. **(F)** Edges of the preform tablet coated with E-100, where a significant decrease in porosity is observed.

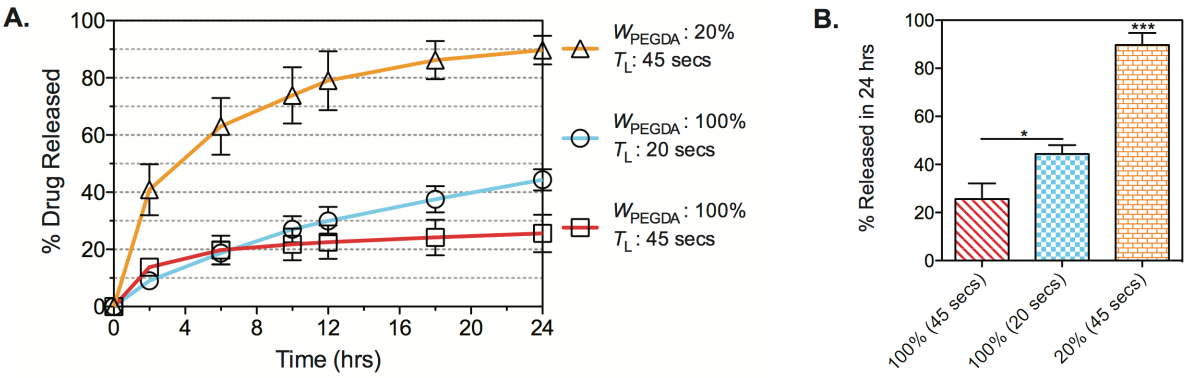

Figure 7. Dissolution test of preform tablets loaded with Naproxen at a concentration of 40 mg/mL. **(A)** Percent of drug release over time. The impact of different W_{PEGDA} and T_L values over drug release is observed, with higher W_{PEGDA} and T_L values resulting in slower drug release kinetics. **(B)** Statistical analysis on percent of drug release after 24 h of dissolution time. (* denotes $p < 0.1$; *** denotes $p < 0.001$).

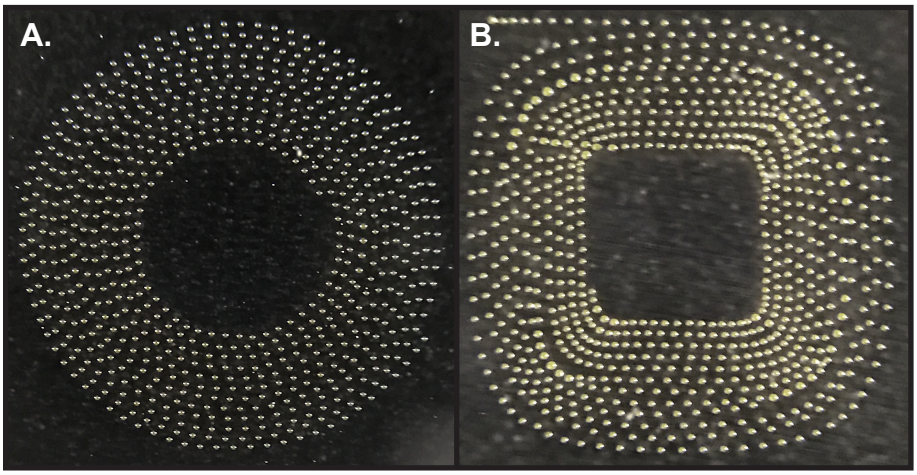

Figure 8. 2D spatial control of the bioinks through the inkjet deposition process. (A) Formation of a circular shape through the dispensing procedure. (B) Control of 2D spatial distribution for the formation of a square.

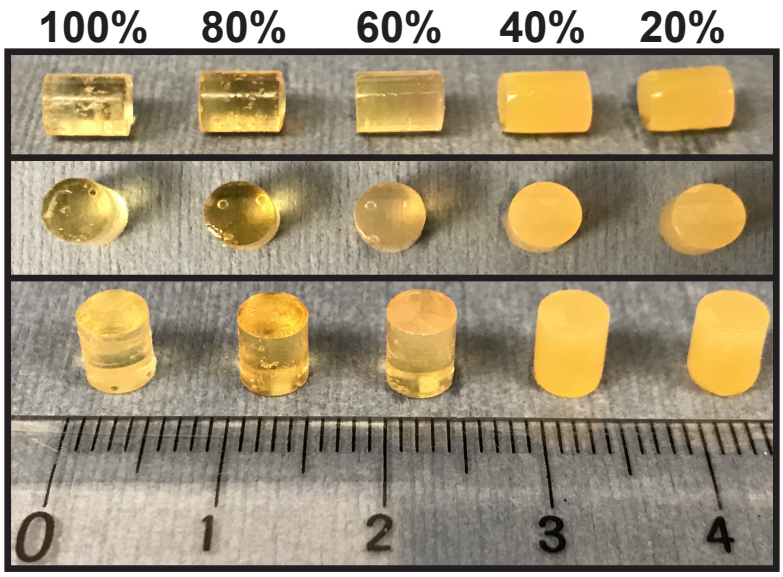

Figure S1. Images of Ibuprofen loaded gels (180 mg/mL) with varying W_{PEGDA} values and a T_L of 3 min. An increased opacity is observed as the W_{PEGDA} is decreased, as seen in **Figure 1.**

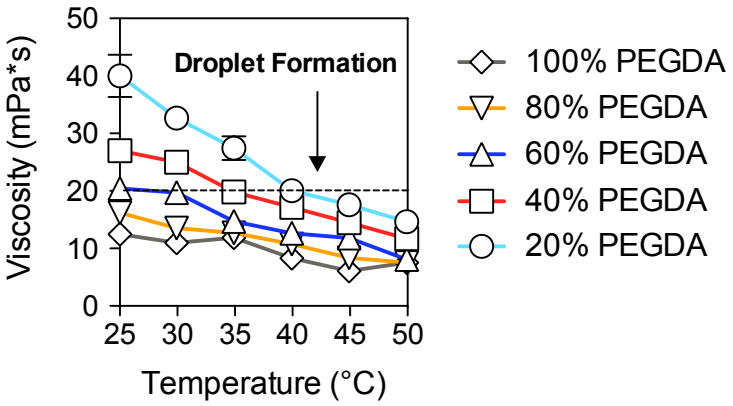

Figure S2. Effect of increased temperatures on the viscosity of Ibuprofen loaded formulations (180 mg/mL) with different W_{PEGDA} values.

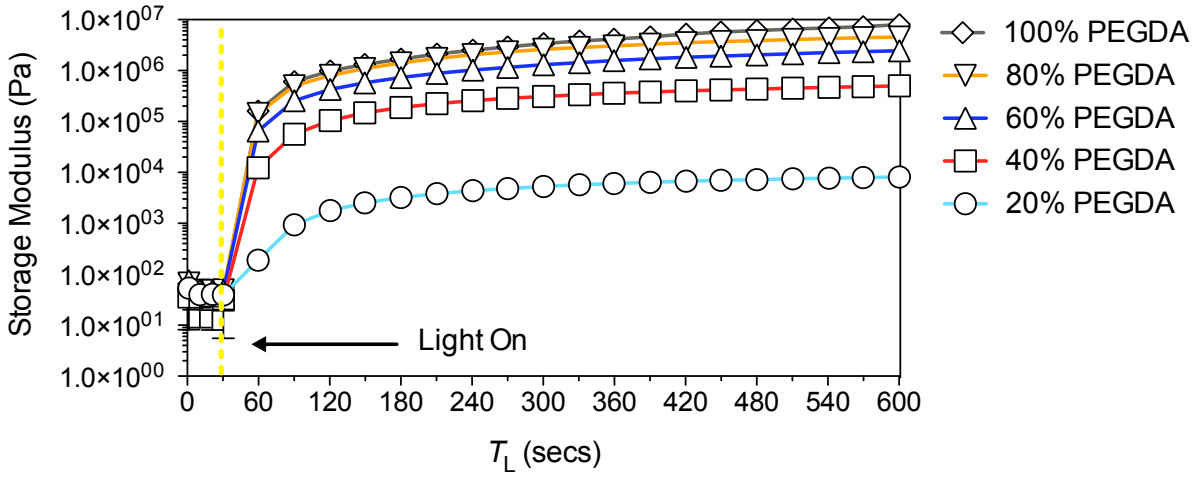

Figure S3. Gelation time of Ibuprofen loaded bioinks (180 mg/mL) containing different W_{PEGDA} values. The formulations were exposed to visible light after 30 s of G' data collection.

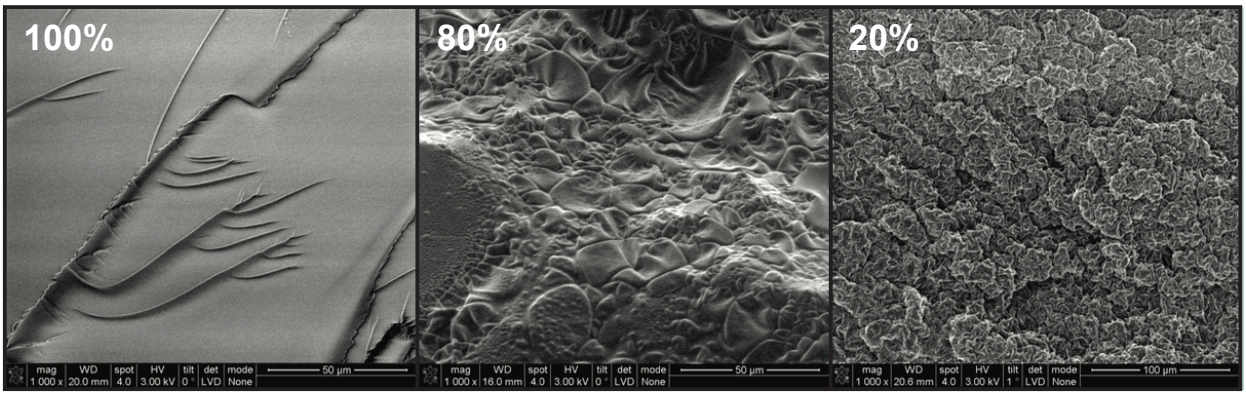

Figure S4. SEM images of polymerized bioinks with W_{PEGDA} values of 100%, 80, and 20%, exposed to a T_L of 3 min. The images show an increased porosity in gels with decreased W_{PEGDA} values. This characteristic explains the increased opacity observed on gels with low PEGDA concentrations in **Figure S1**.

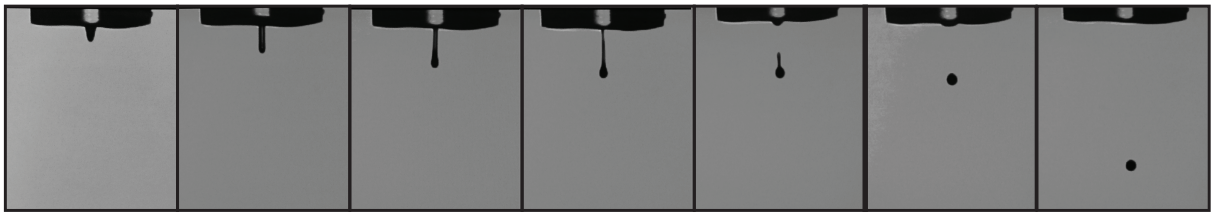

Figure S5. Droplet formation sequence for PEGDA bioink with a W_{PEGDA} of 100% and loaded with Ibuprofen at a concentration of 180 mg/mL.

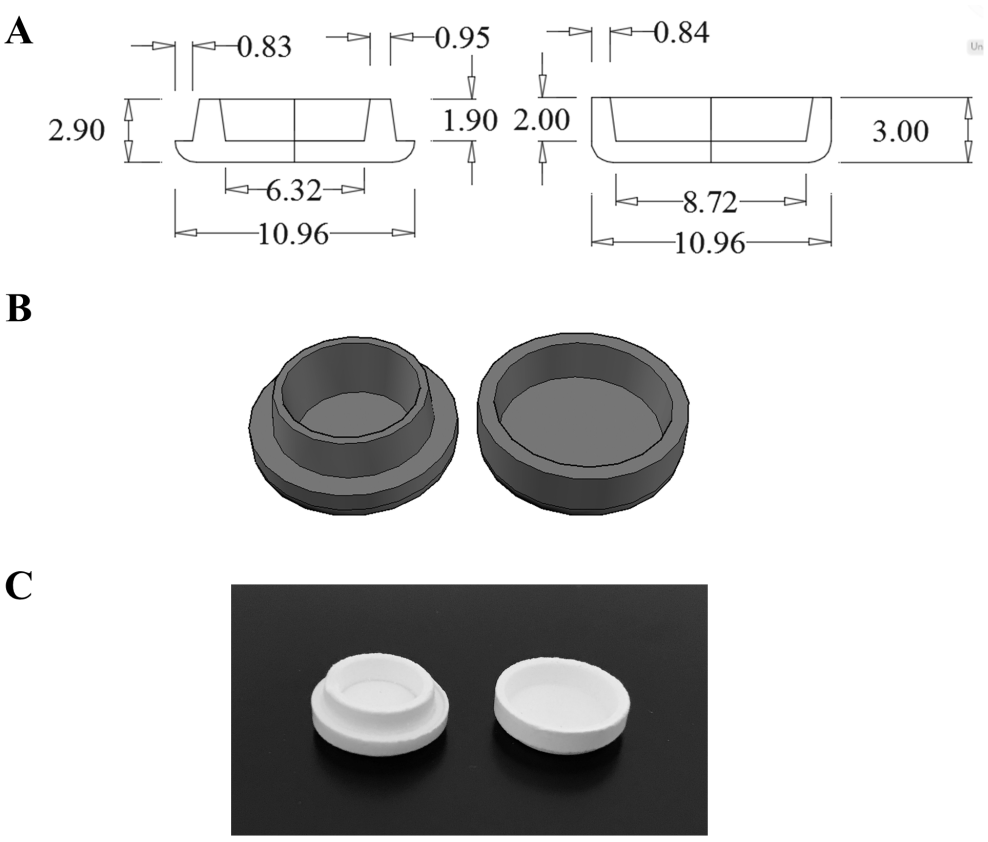

Figure S6. Preform tablet schematics. **(A)** Preform tablet dimensions. **(B)** Preform tablet 3D model. **(C)** Preform tablet fabricated by powder compression.

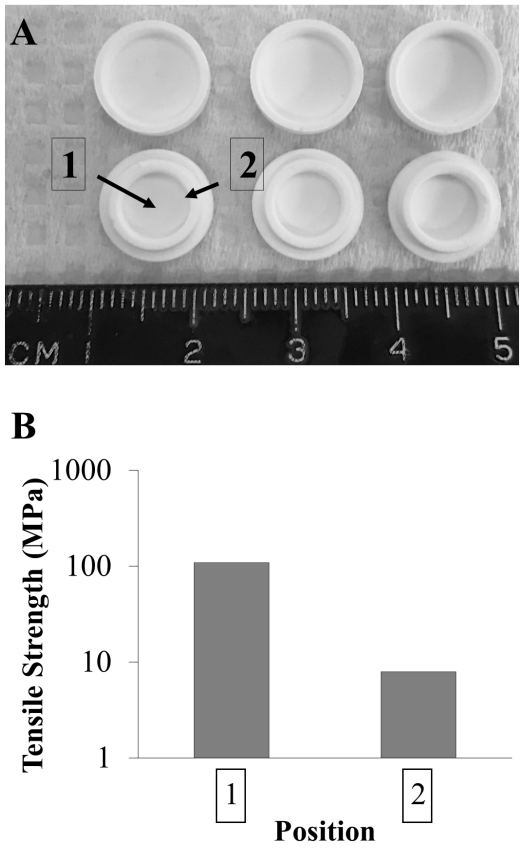

Figure S7. Mechanical properties of different areas within the preform tablet. **(A)** Image demonstrating the two areas tested for tensile strength within the tablet, to assess differences in mechanical properties. **(B)** Tensile strength values of different sections in the preform tablet.

3.7 TABLES

Table 1. Mesh size of polymerized gels with different W_{PEGDA} values and a T_L of 45 s.

W_{PEGDA}	Q_M	v_S	M_c (Da)	$(\bar{r}_0^2)^{1/2}$ (Å)	ξ (Å)
20%	4.17	0.18	122.94	7.09	**12.62**
40%	2.21	0.29	116.14	6.89	**10.42**
60%	1.40	0.39	103.05	6.49	**8.88**
80%	1.16	0.44	94.80	6.23	**8.21**
100%	1.04	0.46	89.15	6.04	**7.80**

Table 2. Droplet formation capacity of Naproxen loaded bioinks.

W_{PEGDA}	r (mm)	ρ (kg/m^3)	γ (mN/m)	η (mPa*s)	Z
100%	0.08	1121.44	36.66	12.84	**4.47**
80%	0.08	1117.78	37.51	15.52	**3.73**
60%	0.08	1123.33	38.46	18.49	**3.18**
40%	0.08	1119.56	39.35	25.7	**2.31**
20%	0.08	1119.44	39.92	34.3	**1.74**

Table S1. Mesh size of polymerized gels with different W_{PEGDA} values and a T_L of 3 min.

W_{PEGDA}	Q_M	v_S	M_c (Da)	$(\bar{r}_0^2)^{1/2}$ (Å)	ξ (Å)
20%	2.9593	0.2334	120.4120	7.0185	11.3996
40%	2.0353	0.3068	114.4700	6.8431	10.1459
60%	1.4976	0.3756	105.5596	6.5714	9.1077
80%	1.2253	0.4237	97.2961	6.3090	8.3998
100%	1.0443	0.4631	89.4085	6.0478	7.8168

3.8 REFERENCES

1. Tutton, R. Personalizing medicine: Futures present and past. *Soc. Sci. Med.* **75,** 1721–1728 (2012).
2. Herxheimer, A. How much drug in the tablet? *Lancet* **337,** 346–348 (1991).
3. Burke, W., Brown Trinidad, S. & Press, N. A. Essential elements of personalized medicine. *Urol. Oncol.* **32,** 193–197 (2014).
4. Bell, S. C. *et al.* A CFTR Potentiator in Patients with Cystic Fibrosis and the G551D Mutation. *N. Engl. J. Med.* **365,** 1663–1672 (2011).
5. Farmer, H., Mccabe, N. & Lord, C. J. Targeting the DNA repair defect in BRCA mutant cells as a therapeutic strategy. *Nature* **434,** 917–921 (2005).
6. Beebe, K. & Kennedy, A. D. Sharpening Precision Medicine by a Thorough Interrogation of Metabolic Individuality. *Comput. Struct. Biotechnol. J.* **14,** 97–105 (2016).
7. Acosta-Vélez, G. F. & Wu, B. M. 3D Pharming : Direct Printing of Personalized Pharmaceutical Tablets Abstract Powder Bed Inkjet 3D Printing. *Polym. Sceiences* **1,** 1–10 (2016).
8. Wu, B. M. *et al.* Solid free-form fabrication of drug delivery devices. *J. Control. Release* **40,** 77–87 (1996).
9. Chia, H. N. & Wu, B. M. Recent advances in 3D printing of biomaterials. *J. Biol. Eng.* **9,** 1–14 (2015).
10. Rowe, C. W. *et al.* Multimechanism oral dosage forms fabricated by three dimensional printing. *J. Control. Release* **66,** 11–17 (2000).
11. Yu, D.-G. *et al.* Novel oral fast-disintegrating drug delivery devices with predefined inner structure fabricated by Three-Dimensional Printing. *J. Pharm. Pharmacol.* **61,** 323–329 (2009).
12. Yu, D. G. *et al.* Tablets With Material Gradients Fabricated by Three-Dimensional Printing. *J. Pharm. Sci.* **96,** 2446--4456 (2007).

13. Sundy, E. & Paul Danckwerts, M. A novel compression-coated doughnut-shaped tablet design for zero-order sustained release. *Eur. J. Pharm. Sci.* **22,** 477–485 (2004).

14. First 3D-printed pill. *Nat. Biotechnol.* **33,** 1014–1014 (2015).

15. Qi, S. & Craig, D. Recent developments in micro- and nanofabrication techniques for the preparation of amorphous pharmaceutical dosage forms. *Adv. Drug Deliv. Rev.* (2016). doi:10.1016/j.addr.2016.01.003

16. Goyanes, A., Robles Martinez, P., Buanz, A., Basit, A. W. & Gaisford, S. Effect of geometry on drug release from 3D printed tablets. *Int. J. Pharm.* (2015). doi:10.1016/j.ijpharm.2015.04.069

17. Wang, J., Goyanes, A., Gaisford, S. & Basit, A. W. Stereolithographic (SLA) 3D Printing of Oral Modified-Release Dosage Forms. *Int. J. Pharm.* (2016). doi:10.1016/j.ijpharm.2016.03.016

18. Melchels, F. P. W., Feijen, J. & Grijpma, D. W. A review on stereolithography and its applications in biomedical engineering. *Biomaterials* **31,** 6121–6130 (2010).

19. Katstra, W. E. *et al.* Oral dosage forms fabricated by Three Dimensional Printing. *J. Control. Release* **66,** 1–9 (2000).

20. Mandrycky, C., Wang, Z., Kim, K. & Kim, D. H. 3D bioprinting for engineering complex tissues. *Biotechnol. Adv.* **34,** 422–434 (2015).

21. Acosta-Vélez, G. F., Linsley, C. S., Craig, M. C. & Wu, B. M. Photocurable Bioink for the Inkjet 3D Pharming of Hydrophilic Drugs. *Bioengineering* **4,** 1–11 (2017).

22. Savjani, K. T., Gajjar, A. K. & Savjani, J. K. Drug Solubility: Importance and Enhancement Techniques. *Int. Sch. Res. Netw.* **2012,** (2012).

23. Shih, H. & Lin, C. C. Visible-light-mediated thiol-ene hydrogelation using eosin-Y as the only photoinitiator. *Macromol. Rapid Commun.* **34,** 269–273 (2013).

24. Majek, M., Filace, F. & von Wangelin, A. J. On the mechanism of photocatalytic reactions with eosin Y. *Beilstein J. Org. Chem.* **10,** 981–9 (2014).

25. Pilaniya, K.; Chandrawanshi, H.K.; Pilaniya, U.; Manchandani, P.; Jain, P.; Singh, N. Recent trends in the impurity profile of pharmaceuticals. *J. Adv. Pharm. Technol. Res.* **1**, 302–310 (2010).

26. Tønnesen, H. H. Photoreactivity of drugs. *Sol. Radiat. Hum. Heal.* 102–113 (2008).

27. United States Pharmacopoeia Convention. <1217> Tablet breaking force. *United States Pharmacopoeia Natl. Formul. (USP 37 - NF 32)* 1146 (2014).

28. Cole-Parmer Instrument Company. Available online: https://pim-resources.coleparmer.com/instruction manual/surface-tension-apparatus-instruction-manual.pdf (accessed on 12 January 2017).

29. Jang, D. *et al.* Influence of Fluid Physical Properties on Ink-Jet Printability. *Langmuir* **25,** 2629–2635 (2009).

30. Zustiak, S. P. & Leach, J. B. Hydrolytically Degradable Poly (Ethylene Glycol) Hydrogel Scaffolds with Tunable Degradation and Mechanical Properties. *Biomacromolecules* **11,** 1348–1357 (2010).

31. Lin, C. & Metters, A. T. Hydrogels in controlled release formulations : Network design and mathematical modeling. *Adv. Drug Deliv. Rev.* **58,** 1379–1408 (2006).

32. Desager, J. P., Vanderbist, M. & Harvengt, C. Naproxen Plasma Levels in Volunteers After Single-Dose Administration by Oral and Rectal Routes. *J. Clin. Pharmacol.* 189–193 (1976).

33. Antonić, J. & Heath, E. Determination of NSAIDs in river sediment samples. *Anal. Bioanal. Chem.* **387,** 1337–1342 (2007).

34. Juban, A., Nouguier-Lehon, C., Briancon, S., Hoc, T. & Puel, F. Predictive model for tensile strength of pharmaceutical tablets based on local hardness measurements. *Int. J. Pharm.* **490,** 438–445 (2015).

35. Yun, Y. H., Kim, J. D., Lee, B. K., Cho, Y. W. & Lee, H. Y. Polymer inkjet printing: Construction of three-dimensional structures at micro-scale by repeated lamination.

Macromol. Res. **17,** 197–202 (2009).

36. De Gans, B. J. & Schubert, U. S. Inkjet printing of polymer micro-arrays and libraries: Instrumentation, requirements, and perspectives. *Macromol. Rapid Commun.* **24,** 659–666 (2003).

37. Delrot, P., Modestino, M. A., Gallaire, F., Psaltis, D. & Moser, C. Inkjet Printing of Viscous Monodisperse Microdroplets by Laser-Induced Flow Focusing. *Phys. Rev. Appl.* **6,** 1–8 (2016).

38. Bushra, R. & Aslam, N. An overview of clinical pharmacology of Ibuprofen. *Oman Med. J.* **25,** 155–161 (2010).

39. Bešter-Rogač, M. Nonsteroidal Anti-Inflammatory Drugs Ion Mobility: A Conductometric Study of Salicylate, Naproxen, Diclofenac and Ibuprofen Dilute Aqueous Solutions. *Acta Chim. Slov.* **56,** 70–77 (2009).

40. Ngamna, O. *et al.* Inkjet printable polyaniline nanoformulations. *Langmuir* **23,** 8569–8574 (2007).

41. Bi, Y. X.; Sunada, H.; Yonezawa, Y.; Danjo, K. Evaluation of Rapidly Disintegrating Tablets Prepared by a Direct Compression Method. *Drug Development and Industrial Pharmacy*, **25** (5), 571-581 (1999).

42. Thoorens, G., Krier, F., Leclercq, B., Carlin, B. & Evrard, B. Microcrystalline cellulose , a direct compression binder in a quality by design environment — A review. *Int. J. Pharm.* **473,** 64–72 (2014).

43. Raymond C R, Paul J S, M. E. Q. Handbook Pharmaceutical Excipients,Sixth Edition. *London Pharm. Press* (2009).

44. Sinka, I. C., Cunningham, J. C. & Zavaliangos, A. Analysis of Tablet Compaction. II. Finite Element Analysis of Density Distributions in Convex Tablets. *J. Pharm. Sci.* **93,** 2040–2053 (2004).

45. Ibrahim, D. *et al.* Dimensional error of selective laser sintering , three-dimensional printing

and PolyJet models in the reproduction of mandibular anatomy. *J. Cranio-Maxillofacial Surg.* **37,** 167–173 (2009).

46. Ionita, C. N. *et al.* Challenges and limitations of patient-specific vascular phantom fabrication using 3D Polyjet printing. *Proc SPIE Int Soc Opt Eng.* **9038,** (2014).

CHAPTER FOUR: USE OF PHOTOCURABLE BIOINKS FOR THE 3D PHARMING OF COMBINATION THERAPIES

4.1 ABSTRACT

Combination therapies are under development for the treatment of a variety of conditions in an effort to decrease the drug dosage administered to patients and reduce potential side effects. 3D Pharming, the direct printing of pharmaceutical tablets, is an attractive strategy for their manufacture since it allows for the rapid production of solid dosage forms containing multiple active pharmaceutical ingredients and personalized dosages. This study reports on the design and characterization of a polypill fabricated through the combination of inkjet printing and powder bed 3D printing technologies for the treatment of hypertension. The drugs Lisinopril and Spironolactone were loaded into a hydrophilic hyaluronic acid photocurable bioink and a hydrophobic poly(ethylene glycol) photocurable bioink, respectively. The bioinks were dispensed through a piezoelectric nozzle onto a blank preform tablet, composed of two attachable compartments fabricated through powder bed 3D printing. Subsequently, the bioinks were polymerized, the preform tablet parts were assembled, and a drug release analysis of the tablet was performed resulting in a dual sustained release of the loaded compounds. The study confirms the potential of inkjet printing, in conjunction with powder bed 3D printing, for the production of combination therapy oral dosage forms involving both, hydrophilic and hydrophobic drugs.

4.2 INTRODUCTION

Personalized medicine is becoming a reality, due in part to technological advances related to additive manufacturing. For instance, most hearing aids are now custom-made to fit each user's ear canal [1], and Invisalign™ aligners and retainers are created from a process that uses 3D printing [2]. Additionally, a one-of-a-kind bioresorbable tracheal splint fabricated using laser-based 3D printing was successfully used to treat an infant with tracheobronchomalacia [3]. Recently, interest in the application of 3D printing as a way to manufacture pharmaceutical tablets – known as 3D Pharming [4] – has been rapidly growing since it can create personalized

pharmaceutical products as well as products with increased complexity, and allow for on-demand manufacturing [5,6]. Furthermore, it intends to provide oral dosages containing multiple active pharmaceutical ingredients, potentially enhancing the compliance of patients taking multiple drugs on a daily basis [7].

The capacity to locate multiple drugs within a single oral dosage form opens the door for the development of combination therapies through 3D Pharming. Currently, combination therapies are being developed for a variety of medical conditions, such as hypertension, type 2 diabetes, and cancer [8–13]. It has been demonstrated that combining multiple active ingredients towards the treatment of a given condition can result in treatments with lower dosages and fewer side effects [14–17]. 3D Pharming technologies emerge as a feasible option towards the manufacture of pharmaceutical combination therapies, allowing an enhanced dosage control of these treatments resulting in a therapy tailored to the patient. Techniques, such as fused deposition modeling [18] and extrusion printing at room temperature [19,20], have been implemented towards the manufacture of pharmaceutical tablets with multiple active ingredients.

In previous research we engineered a hyaluronic acid based photocurable bioink for the inkjet 3D Pharming of hydrophilic compounds [21]. Additionally, we engineered a poly(ethylene glycol) diacrylate based bioink capable of loading hydrophobic drugs, previously discussed in Chapter 3. In this chapter, we demonstrate the use of such bioinks towards the manufacture of a combination therapy for the treatment of hypertension. The active pharmaceutical ingredients (APIs) Lisinopril and Spironolactone were chosen as model drugs for this combination therapy. Lisinopril, an angiotensin-converting enzyme inhibitor (ACEI) for the treatment of hypertension [22,23], was chosen due to its hydrophilicity. Spironolactone, a potassium-sparing diuretic for the treatment of hypertension and congestive heart failure [24], was chosen as a hydrophobic drug model. The formulated bioinks were dispensed through a piezoelectric nozzle at room temperature into a blank preform tablet featuring two compartments, one for each formulation. The preform tablet parts were manufactured through powder bed 3D printing, using calcium

sulfate as excipient. Once the drugs were dispensed, they were exposed to light to induce photopolymerization of the bioinks, and the preform tablet parts were assembled to finalize the pharmaceutical product. A sustained drug release profile was achieved for both APIs in this oral dosage form. This 3D pharming method allows for the fabrication of oral compound therapies at room temperature, with quick manufacturing times, and controlled dosages.

4.3 MATERIALS AND METHODS

4.3.1 Hydrophilic Photocurable Bioink Preparation

Hyaluronic Acid Norbornene (HANB) was synthesized as previously described [21]. Briefly, hyaluronic acid (60 kDa·MW) (Genzyme Corporation, Cambridge, MA, USA) was modified with hydrazide groups through a reaction with adipic acid dihydrazide (ADH) in the presence of 1-ethyl-3-(dimethylaminopropyl) carbodiimide hydrochloride (EDC). The product was dialyzed for 3 days against DI water (Fisherbrand regenerated cellulose, MWCO 12,000–14,000 Da, Houston, TX, USA), frozen, and lyophilized. On a second reaction, the HA functionalized with hydrazide groups (HA-ADH) was reacted cis-5-norbornene-*endo*-2,3-dicarboxylic anhydride (Sigma-Aldrich, St. Louis, MO, USA), resulting in norbornene functionalized HA (HANB). The product was dialyzed against DI water for 3 days, filtered, lyophilized, and stored at −20 °C. HANB was characterized by proton nuclear magnetic resonance spectroscopy (^{1}H NMR) on a Bruker AV300 broad band FT NMR Spectrometer (Billerica, MA, USA). The degree of modification obtained was ~ 50%.

Following its synthesis, HANB was dissolved in PBS and mixed with poly(ethylene glycol) dithiol (1500 Da, PEGDT) at a crosslinking ratio (ratio of thiol groups to norbornene groups, r_{ratio}) of 0.6. HANB was added at a weight percent (W_{HANB}) of 3%. Eosin Y was added as a photoinitiator and poly(ethylene glycol) (PEG200) was added to optimize the viscosity of the formulation. Each of these two components constituted 10% v/v of the bioink. Lisinopril dihydrate (Fisher Scientific, Pittsburgh, PA, USA) was added at a concentration of 40 mg/mL. All chemicals were purchased from Sigma-Aldrich unless otherwise stated.

4.3.2 *Hydrophobic Photocurable Bioink Preparation*

The hydrophobic bioink was formulated as described in Chapter 3, section 3.3.1, with minor modifications. Briefly, the bioink was composed of 30% poly(ethylene glycol) diacrylate (PEGDA, 250 Da), 50% PEG200, and 20% ethanol. Eosin Y (1.0 mM) and mPEG-amine (0.05 M) (350 Da, Creative PEG Works, Chapel Hill, NC, USA) were added as photoinitiator and co-initiator, respectively. Spironolactone was added at a concentration of 20 mg/mL. All chemicals were purchased from Sigma-Aldrich unless otherwise stated.

4.3.3 Bioinks Gelation and Mechanical Properties

The tensile strength of polymerized gels was analyzed to characterize the mechanical properties of the bioinks. 1 mL syringes (BD & Co., Franklin Lakes, NJ, USA), modified by eliminating their tips, were loaded with 50 µL of bioink. Gels were formed with hydrophilic and hydrophobic bioinks by exposing them to visible light at an intensity of 120 mW/cm^2 for a period of 2 min and 1 min, respectively. Additionally, the tensile strength of gels with varied drug concentrations was measured to analyze the impact of drug load on the mechanical properties of the polymerized bioinks. An Instron (5564 model) was used to measure the failure load of the gels fabricated. The tensile strength ($\boldsymbol{\sigma}$) was calculated through **Equation 1**, where $\boldsymbol{D}$ is the gel diameter, $\boldsymbol{H}$ is the thickness, and $\boldsymbol{F}$ represents the failure load [25].

$$\sigma = \frac{2F}{\pi DH} \tag{1}$$

The inverse of the Ohnesorge number (*Z* value) of the bioinks was calculated to assess the printability of these solutions through inkjet printing piezoelectric nozzles. **Equation 2** defines the *Z* value, where $\boldsymbol{a}$ is the radius of the piezoelectric nozzle printing orifice and $\boldsymbol{\rho}$, $\boldsymbol{\gamma}$, and $\boldsymbol{\eta}$ represent the density, surface tension, and viscosity of the photocurable formula, respectively [26].

$$Z = \frac{(a\rho\gamma)^{1/2}}{\eta} \tag{2}$$

The surface tension was measured with a tensiometer (Kimble Chase 14818 Tensiometer, Cole-Parmer, Vernon Hills, IL, United States) and calculated by using **Equation 3,** where $\boldsymbol{h}$ is the distance between menisci of the formulation in the test tube and the one in the capillary tube, $\boldsymbol{r}$ is the radius of the capillary, $\boldsymbol{\rho}$ is the density of the formulation, and $\boldsymbol{g}$ is the acceleration due to gravity [27]. 1 mL of each bioink was weighted and the mass obtained was divided by the pre-determined volume to calculate the density. The viscosity of the bioinks was measured with a rhemoter (Discovery HR-2, TA Instruments, New Castle, DE, USA). A cone and plate geometry (using a 40 mm 2.016°) was utilized for the experiment, with a shear rate ranging from 10 to 100 Hz.

$$\gamma = \frac{1}{2} hr\rho g \tag{3}$$

4.3.4 Scanning Electron Microscopy (SEM)

The microarchitecture of the gels was observed with a NOVA 230 NanoSEM scanning electron microscope. Images of lyophilized hydrophilic gels were taken, as well as cross-sectional images of hydrophobic gels.

4.3.5 Preform Tablet Fabrication and Characterization

The drug-containing bioinks were directly printed into tablet preforms that were fabricated by 3D printing (ProJet 660; 3D Systems, Inc.; Rock Hill, SC, USA). The printing materials consisted of calcium sulfate hemihydrate powder (VisiJet PXL Core; 3D Systems, Inc.; Rock Hill, SC, USA), and a liquid inkjet binder comprised of deionized water containing 5% ethanol and 0.25% Tween 80. The polypill preform tablet was designed with two separate chambers that could each hold up to 250 µL of ink and be assembled into a single tablet. The assembled dimensions were kept below the 22 mm maximum tablet size recommended by the Food and Drug Administration (FDA) [28]. Additionally, each chamber was independently modified to prevent absorption of the respective drug-containing bioink into the preform tablet during printing, as previously reported [21]. Briefly, the chamber holding the hydrophobic formulation was infused

with PEG (35 kDa) by submerging the tablet in an acetone solution containing 15% (w/w) PEG for 30 min at 55°C. Next, the well was brush-coated with Eudagrit® E100 (Evonik, Essen, Germany) (polymethacrylate copolymer) dissolved in acetone at 20% (w/w). The chamber holding the hydrophilic formulation was infused with Eudagrit® E100 dissolved in acetone at 10% (w/w). Surface morphology of the preform tablet was characterized by scanning electron microscopy (NOVA NanoSEM 230, FEI Co., Hillsboro, OR, USA).

4.3.6 Drug Release Kinetics

A piezoelectric dispenser with a nozzle diameter of 80 μm (MJ-ABP-01-080, MicroFab, Plano, TX, USA) was used to assess the droplet formation capability of the engineered bioinks. This dispenser was controlled with a microdispensing system (MD-E-3000, Microdrop, Norderstedt, Germany). The dispensing parameters used were 46 V, a 16 μm pulse width, and a frequency of 2000 Hz. The droplet formation process was captured with an analog camera (JAI CV-S3300), equipped with a lens (Edmund Optics, Barrington, NJ, USA). An LED light was connected to the microdispensing system, in order to control its strobe delay.

Lisinopril loaded hydrophilic bioink was dispensed in the bottom part of the polypill (250 μL) and exposed to visible light (120 mW/cm^2) for 2 min, to induce gelation of the hydrogel precursor solution. Spironolactone loaded hydrophobic bioink was dispensed into the upper piece of the polypill (125 μL) and exposed to light for 1 min. Following the gelation of the bioinks, the pieces of the polypill were assembled to finalize the pharmaceutical product.

The tablets were placed into Uni-cassettes (Tissue-Tek) and immersed into beakers containing 500 mL of dissolution medium (monobasic potassium phosphate 1.053mM, pH of 2.5), conditioned at 37 °C and stirred at 60 rpm. Aliquots of 1 mL were taken after 0.5, 2, 4, 6, 8, 12, 18, and 24 h. The volume removed was replenished with fresh dissolution medium conditioned at 37 °C. The drug concentration in each aliquot was measured with an HPLC (Waters 2690 with a

PDA 996 detector). The wavelength used to detect the APIs were 220 nm and 240 nm for Lisinopril and Spironolactone, respectively.

4.3.7 Statistical Analysis

Statistical analysis was performed with GraphPad Prism software (GraphPad Software, Inc., San Diego, CA). Statistical significance was assessed using single factor ANOVA test with a Tukey post-test and 95% confidence interval.

4.4 RESULTS AND DISCUSSION

4.4.1 Bioinks Characterization

Hyaluronic acid is a natural glycosaminoglycan found in connective, neural, and epithelial tissue [29,30]. The biocompatibility of hyaluronic acid hydrogels has been assessed in tissue engineering studies, where diverse cell types have been cultured in hydrogels for the formation of tissues and the study of biological processes [31–33]. Moreover, hyaluronic acid photocurable formulations can polymerize under quick gelation times (**Fig. S1**). Lisinopril was dissolved in a hyaluronic acid based hydrophilic bioink at a concentration of 40 mg/mL. The Lisinopril formulation was dispensed into a modified syringe (50 µL) and exposed to visible light at an intensity of 120 mW/cm^2 for 2 min (**Fig. 1**). The storage modulus of the resulting hydrogel was quantified to assess the mechanical properties of the polymerized bioink, due to its viscoelastic property. Additionally, hydrogels with different drug concentrations (20 and 10 mg/mL) were polymerized to study the effect of drug load on the mechanical properties of this hydrophilic material (**Fig. 2A**). The results indicate that this hydrophilic material has a low storage modulus due to its elevated water content and the low W_{HANB} (3%) utilized for its fabrication. The elevated water content of the hydrogel allows for the effective diffusion of the hydrophilic API out of the oral dosage form, given the dissolution of the preform tablet designed to disintegrate under acidic conditions similar to the ones found in the stomach. The hydrogels had an average G' of 1003.86 Pa. **Figure 2A** indicates that drug load has no influence in the mechanical properties of the hydrogel, where larger drug concentrations had no impact over the G' of the gels. This result is consonant with the G' data

shown in Chapter 2 (**Fig. 2E**), where Ropinirole loaded at a concentration of 40 mg/mL had no impact on the mechanical properties of the gel, compared to hydrogels with no drug. However, a decrease in G' was noticed on hydrogels loaded with Ropinirole at a concentration of 80 mg/mL. It can be stated that the G' remains stable for this Lisinopril formulation at concentrations between 0 and 40 mg/mL, the maximum Lisinopril concentration achievable in the hyaluronic acid solution.

Spironolactone was chosen as the second model drug in this study due to its high hydrophobicity. The model drug was dissolved in a PEG based bioink specifically engineered for hydrophobic drugs, at a concentration of 20 mg/mL. 50 µL of formulation were pipetted into a modified syringe, the solution was exposed to light for 1 min (**Fig. 1**), and the tensile strength of the resulting gel was measured (**Fig. 2B**). Results show an average tensile strength for this material of 176.66 kPa. The typical tensile strength of pharmaceutical tablets is within the range of 1 and 10 MPa [34]. The G' obtained for this gel is below this range and therefore, this material should be always used in combination with a preform tablet that provides support and physical stability to the oral dosage form. Furthermore, the effect of drug concentration on the mechanical properties of the gel was studied by measuring the tensile strength of gels containing 100, 80, 40, and 20 mg/mL. **Figure 2B** shows that drug concentration had no impact on the tensile strength of the material. This contrast with results shown in Chapter 3 (**Fig. 3**), where a decrease in tensile strength was observed with increasing Naproxen and Ibuprofen concentrations. This divergence is due to the lower W_{PEGDA} value used in this formulation (30%). These results indicate that softer materials conformed of photo-polymerized bioinks, such as the hyaluronic acid hydrogel, tend to have a steady mechanical stability when exposed to increasing drug concentrations. Stronger gels can experience significant differences in mechanical properties (**Fig S2**).

SEM imaging was performed on both gels to observe the microarchitecture of the polymerized structures. **Figure 3** shows a porous microarchitecture in both gels, allowing for the effective release of the dissolved API within them. The wrinkles observed in the hydrophilic gel (**Fig. 3A**) are a consequence of the lyophilized/dehydrated nature of the sample tested.

4.4.2 Droplet Formation

To study the droplet formation ability of these bioinks, the inverse of the Ohnesorge number, denominated as Z value, was calculated (**Equation 3**). This dimensionless number considers the inertia and surface tension forces of a fluid over its viscosity forces to define its droplet formation ability. The orifice radius of the nozzle used for the inkjet printing of the fluid is also a factor taken into consideration within this number. Z values between 4 and 14 are considered printable fluids [26]. Values above 14 typically exhibit the formation of satellite droplets, whereas values below 4 present strong viscous forces. The viscosity, surface tension, and density of the bioinks was quantified, in order to determine their Z value. **Table 1** shows the results obtained for these parameters at room temperature and the Z value for the two bioinks utilized in this study. The hydrophilic bioink experienced a higher viscosity value (9.83 cP), resulting in a lower Z value than the hydrophobic formulation. The later one had lower viscosity and surface tension parameters (4.88 cP and 31.41 mN/m, respectively), resulting in a higher Z value of 10.52. However, both formulations fell within the defined range for printable fluids as depicted in **Figure 4** and **Figure 5**, where the droplet formation sequence of these bioinks can be observed.

4.4.3 Preform Tablet Characterization

Calcium sulfate hemihydrate is clinically used in the preparation of plaster of Paris, which is used for casts that immobilize fractures, and is not used in tablet formulations [35]. Calcium sulfate dihydrate, however, has been commonly used in pharmaceutical applications [36], and the dihydrate is formed when hemihydrate is mixed with water [37]. In this study, water was used as the liquid binder during the fabrication of the perform tablets via 3D printing (**Fig. 6**). Upon contact with the powder, water causes the dissolution of the calcium sulfate hemihydrate and recrystallization of the dihydrate form [38]. SEM analysis (**Fig. 7A**) shows that pores exist within the uncoated preform tablet wall. These pores negatively impacted the performance of tablets during printing of the bioink. Specifically, the porosity in the preform tablet allowed both the

hydrophilic and hydrophobic bioinks to soak into the preform tablet during printing, which not only weakened the preform tablet, but also negates the advantages of using 3D printing for pharmaceutical applications, such as control over drug positioning (pictures not shown). To fill the pores, two different coatings were used depending on the ink being used for printing. For the hydrophilic bioink, the preform tablets were soaked in Eudagrit® E100 (**Fig. 7B**). For the hydrophobic bioink, the preform tablets were first soaked in a high-molecular weight PEG (35 kDa) solution. High-molecular weight PEG was selected because it is immiscible with the low-molecular weight PEGDA in the bioink (**Fig. 7C**). Additionally, a thin coating of Eudagrit® E100 was added to the preform tablet well to further inhibit the absorption of the bioink during printing. SEM analysis shows that the polymeric coating fills the pores of the preform tablet (**Fig. 7D**).

4.4.4 Polypill Dissolution Test

The hyaluronic acid based hydrophilic bioink was loaded with Lisinopril at a concentration of 40 mg/mL. 250 µL of this formulation were dispensed into the bottom compartment of the preform tablet and further exposed to visible light for 2 min, to induce gelation of the photocurable bioink. Likewise, the PEG based hydrophobic bioink was loaded with Spironolactone at a concentration of 20 mg/mL. 125 µL of this formulation were loaded into the top compartment of the preform tablet and exposed to visible light for a period of 1 min (**Fig. 8**). Once the bioinks were polymerized, the two compartments were attached and the small cap was placed to seal the top compartment, completing the oral dosage form. The tablet was immersed in a beaker containing 500 mL of dissolution medium, conditioned at 37 °C and stirred at 60 rpm. Aliquots were taken after 0.5, 2, 4, 6, 8, 12, 18, and 24 h of dissolution and their drug concentration was assessed through HPLC analysis. The results obtained show a dual sustained release of Lisinopril and Spironolactone in a period of 24 h (**Fig. 9**). The preform tablet dissolved almost in its entirety with the exception of the lower part of the top compartment, exposing completely the gels to the dissolution medium (**Fig S3**). Lisinopril experienced faster drug release kinetics, when compared to Spironolactone. This result can be explained by the differences within the microarchitecture

and composition of the gels. The hydrophilic formula has over 90% of water content, facilitating the diffusion of Lisinopril, a hydrophilic compound, into the dissolution medium. Moreover, the hydrogel has a W_{HANB} of only 3%, allowing small molecules to easily diffuse through the polymerize matrix. The hydrophobic formulation has a higher polymeric content (W_{PEGDA} = 30%) resulting in a mesh size of ~ 11 Å, based on data shown in Chapter 3 (**Table 1**). Naproxen and Ibuprofen have a hydrodynamic radius of 3.77 Å and 6.80 Å [39], respectively, and molecular weights of 230.26 Da and 206.29 Da. It can be hypothesized that the hydrodynamic radius of Spironolactone is close to the mesh size of the polymerized hydrophobic gel (11 Å), since it has a significantly higher molecular weight than the model drugs used in Chapter 3, Naproxen and Ibuprofen. This characteristic would explain the slower release profile observed with Spironolactone, due to an impaired diffusion of the molecule through the gel matrix. The use of a higher PEGDA molecular weight for the fabrication of the gel could result in larger mesh sizes and consequently, enhanced drug release kinetics.

The dual release of these APIs for the treatment of hypertension demonstrates the use of inkjet printing for the fabrication of combination therapies. Moreover, it shows that the therapy could contain both, hydrophilic and hydrophobic compounds. This technology would be especially applicable towards drugs that achieve their pharmacological effect at low dosages and could be targeted towards the development of oral dosage forms for children, who require small dosages not always commercially available. Moreover, children experience drastic changes in metabolism that affect the dosage needed to achieve a given target pharmacological effect.

4.5 CONCLUSION

In this study, a combination therapy oral dosage form for the treatment of hypertension was designed. The polypill featured the use of a hyaluronic acid photocurable hydrophilic bioink and a PEG photocurable hydrophobic bioink, loaded with Lisinopril and Spironolactone, respectively. A preform tablet with two compartments able to hold these bioinks was designed and manufactured through powder bed 3D printing. The formulations were dispensed through a

piezoelectric nozzle designed for inkjet printing and subsequently polymerized through exposure to visible light. The preform parts were assembled and a dissolution study was carried out, where a dual sustained release of the drugs Lisinopril and Spironolactone was observed over a period of 24 h. This study shows the capacity of photocurable formulations towards the manufacture of compound therapy oral dosage forms incorporating hydrophilic and hydrophobic APIs, with a special application towards drugs that achieve their pharmacological effect at low dosages.

4.6 FIGURES

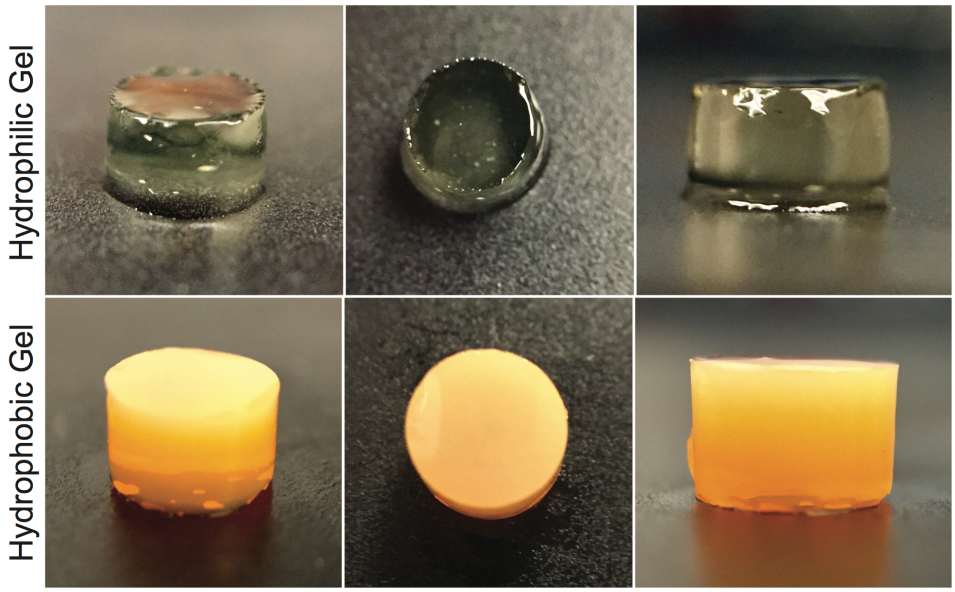

Figure 1. The upper row shows images of the polymerized hyaluronic acid based bioink, loaded with Lisinopril at a concentration of 40 mg/mL. This bioink has a W_{HANB} value of 3% and a T_L of 2 min. The bottom images show polymerized PEGDA gels with a W_{PEGDA} value of 30%, a W_{EtOH} value of 20%, and a T_L of 1.0 min. It can be observed that the hydrophobic gel has a high opacity due to a high concentration of PEG200 (50%).

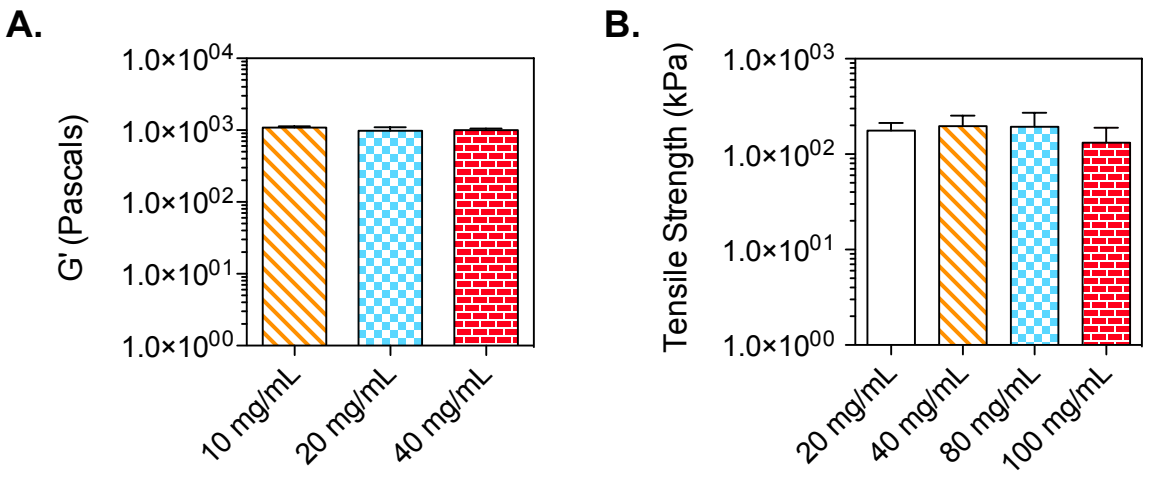

Figure 2. Tensile strength of Lisinopril and Spironolactone gels. **(A)** Tensile strength of Lisinopril tablets with diverse drug concentrations. 40 mg/mL was the maximum solubility achieved for this API in this bioink formulation. No statistical difference was observed between samples with varying Lisinopril concentrations. **(B)** Tensile strength of Spironolactone tablets with diverse drug concentrations. 100 mg/mL was the maximum solubility achieved for this API. No statistical difference was observed between samples with varying concentrations.

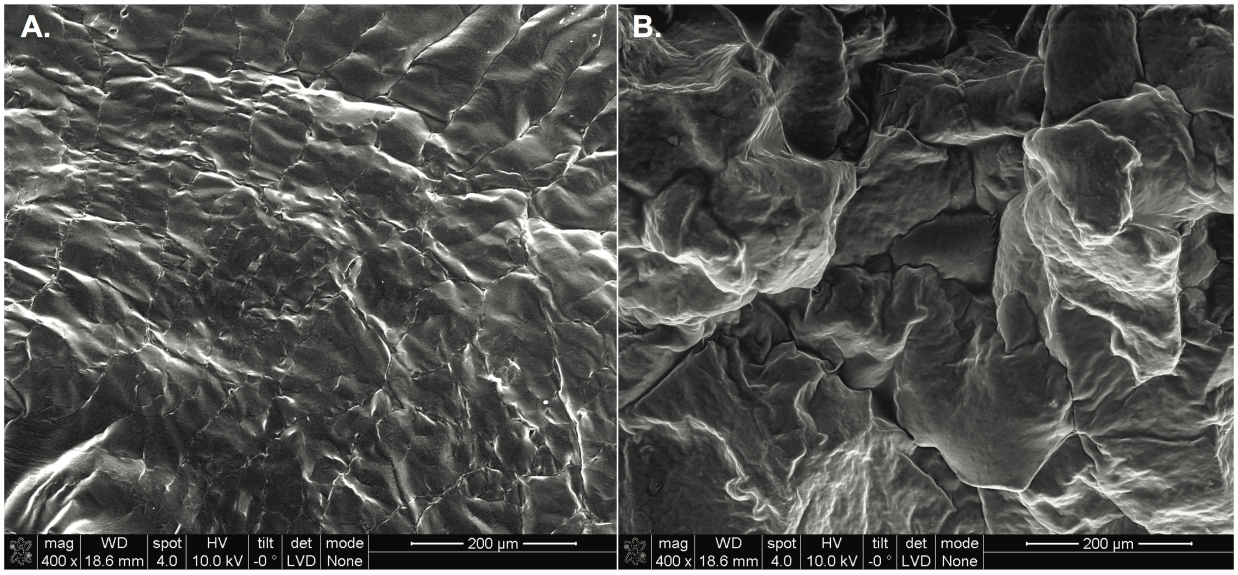

Figure 3. Cross-sectional SEM images of polymerized bioinks loaded with Lisinopril and Spironolactone. **(A)** Lyophilized Lisinopril loaded hydrogel (40 mg/mL) with a W_{HANB} of 3% and an r_{ratio} of 0.6. This bioink was exposed to a T_L of 2 min. **(B)** Polymerized hydrophobic ink loaded with Spironolactone (20 mg/mL). This formulation contained a W_{PEGDA} of 20% and a T_L of 1 min.

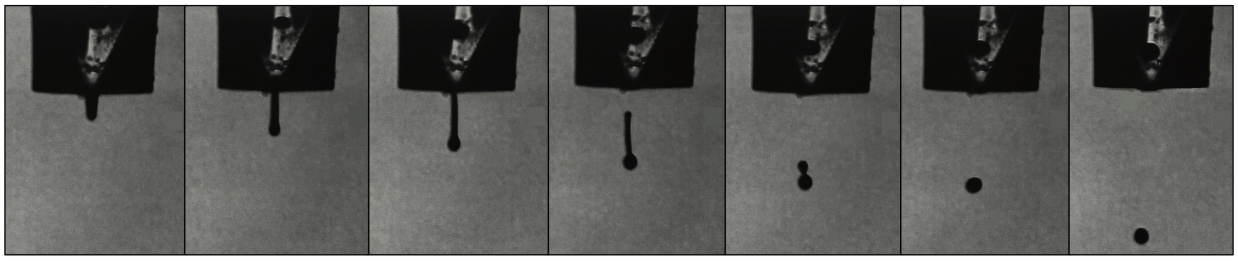

Figure 4. Droplet formation sequence for hyaluronic acid based bioink with a W_{PEGDA} of 3%, an r_{ratio} of 0.6, and loaded with Lisinopril at a concentration of 40 mg/mL. This formulation had a Z value of 6.99, falling within the printable range (4-14).

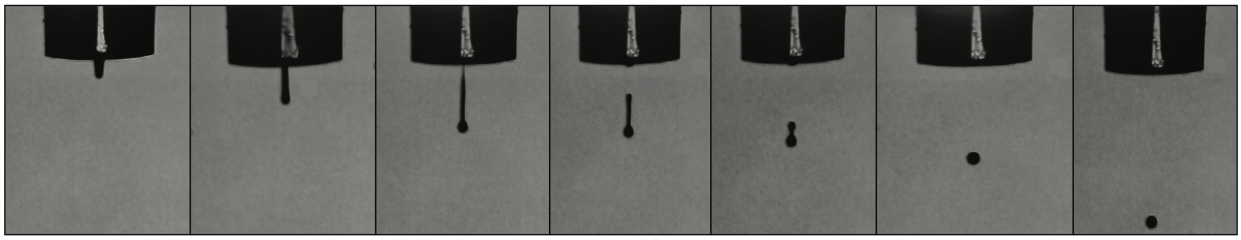

Figure 5. Droplet formation sequence for PEGDA based bioink with a W_{PEGDA} of 30%, and loaded with Spironolactone at a concentration of 20 mg/mL. This formulation had a Z value of 10.52, falling within the printable range (4-14).

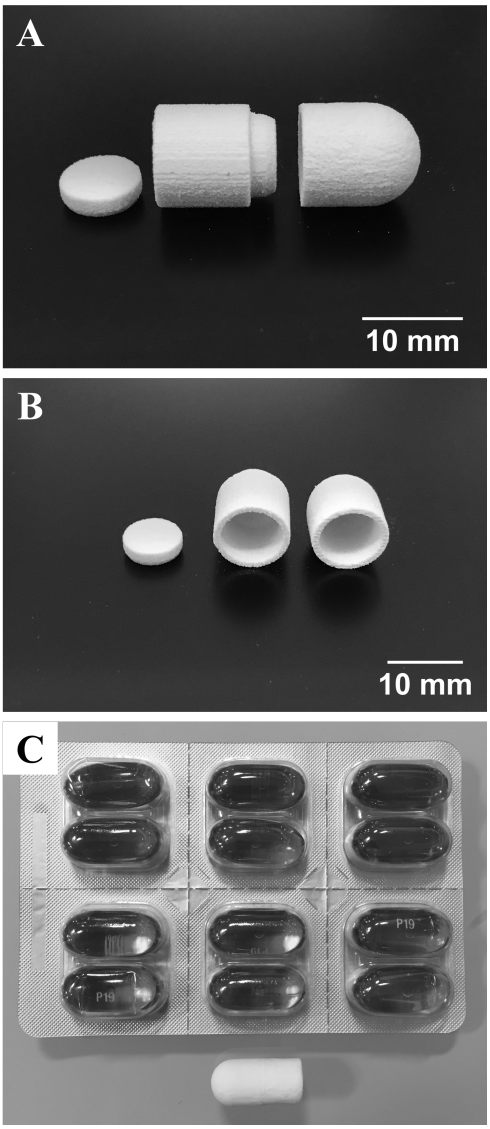

Figure 6. Multiple compartments fabricated preform tablet. **(A)** Side view of the 3 pieces constituting the preform tablet. From left to right, top cap, top compartment, and bottom compartment. These pieces were manufactured by powder bed 3D printing using as binder DI water with 5% ethanol and 0.25% Tween 80. The powder utilized for their construction was calcium sulfate. Each of the two wells have a 250 µL capacity. **(B)** Front view of the preform tablet fabricated. **(C)** Comparison between the assembled version of the preform tablet and commercially available gel capsules.

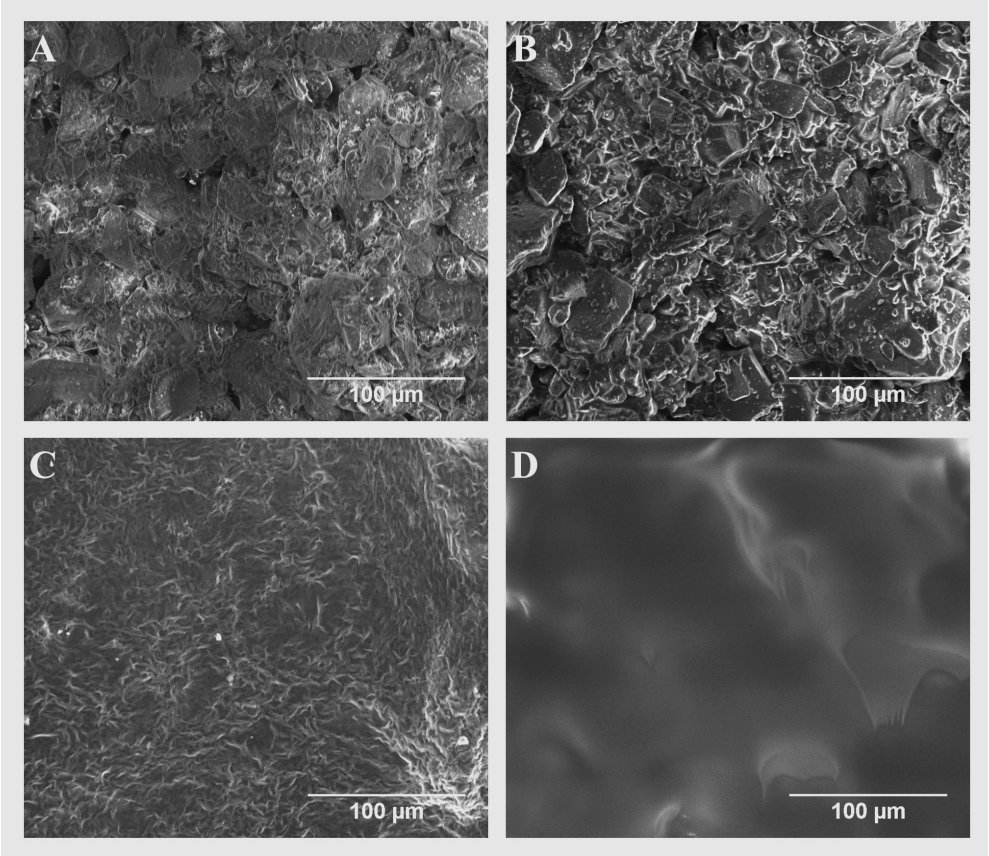

Figure 7. SEM imaging of the untreated and coated preform tablet surfaces. **(A)** Surface of untreated preform tablet. **(B)** Bottom compartment infused with a 10% E-100 in acetone solution. **(C)** Top compartment infused with a 15% PEG (35 kDa) in acetone solution. **(D)** Inner section of the top compartment preform tablet, brushed with a 20% E-100 in acetone solution.

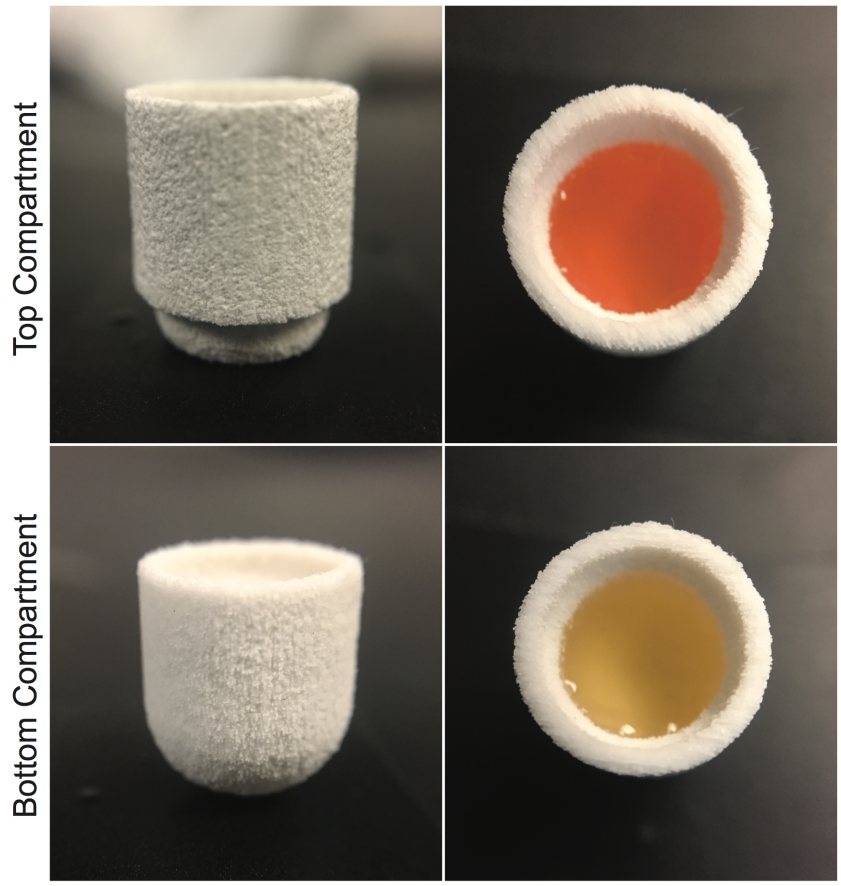

Figure 8. Multiple compartments preform tablet loaded with hydrophilic (bottom) and hydrophobic (top) bioinks.

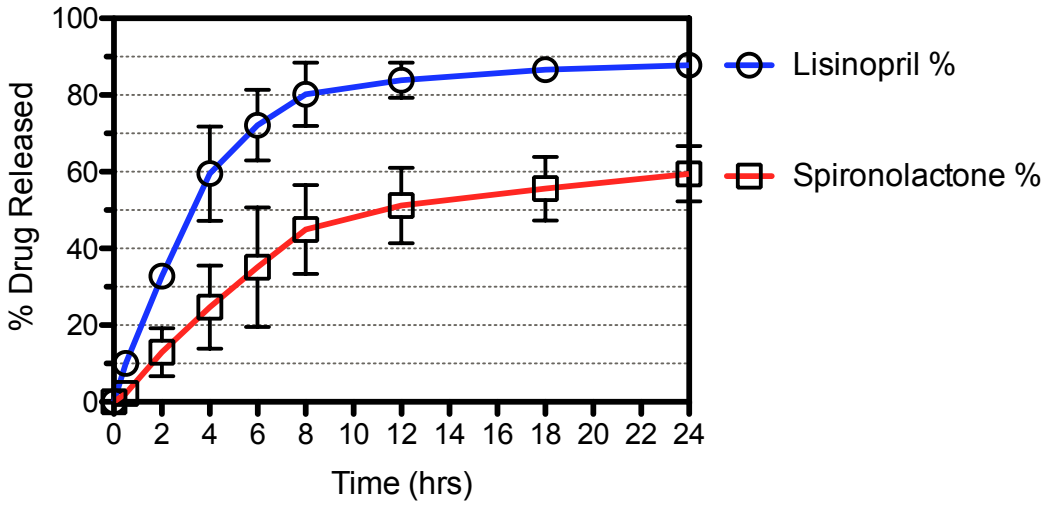

Figure 9. Dissolution test of polypill. A sustained release profile was achieved for both APIs. Around 90% of the Lisinopril loaded was release in a period of 24 h, releasing most of the drug within the first 8 h. Above 60% of the Spironolactone loaded was released in a period of 24 h.

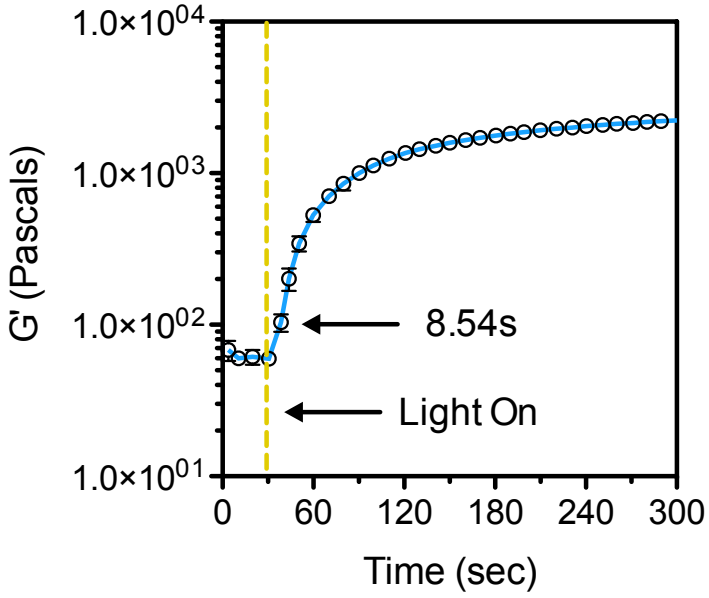

Figure S1. Gelation kinetics obtained through in-situ photorheology of the hydrophilic bioink. The gelation kinetics were assessed through in-situ photorheology in a rheometer, at a constant strain of 1% and an angular frequency of 10 rad/sec. In this test, the storage modulus (G') of the bioinks was measured for 30 s without light exposure. Immediately after this time, a visible light source was turned on and the G' was measured for another 270 s. Results show that the formulation achieves a G' higher than 100 Pa in 8.54 s.

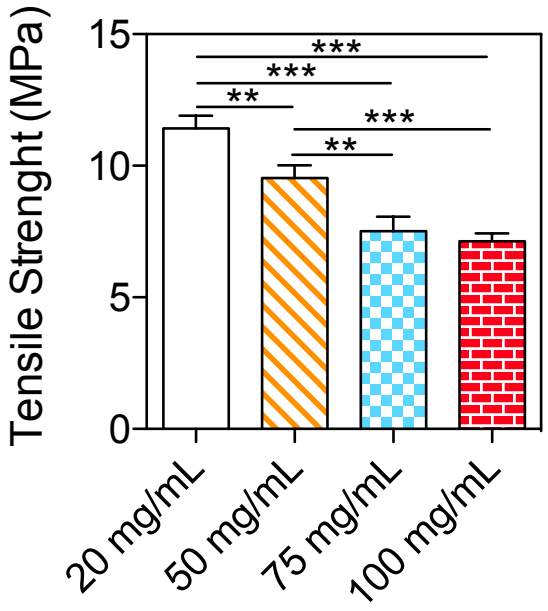

Figure S2. Tensile Strength of PEGDA based (W_{PEGDA} = 100%) gels loaded with varying concentrations of Spironolactone. These gels were exposed to light for a period of 3 min. We can see that light exposure time has a direct effect on tensile strength, since significant differences were observed under these conditions, diverging from results shown in Figure 2B.

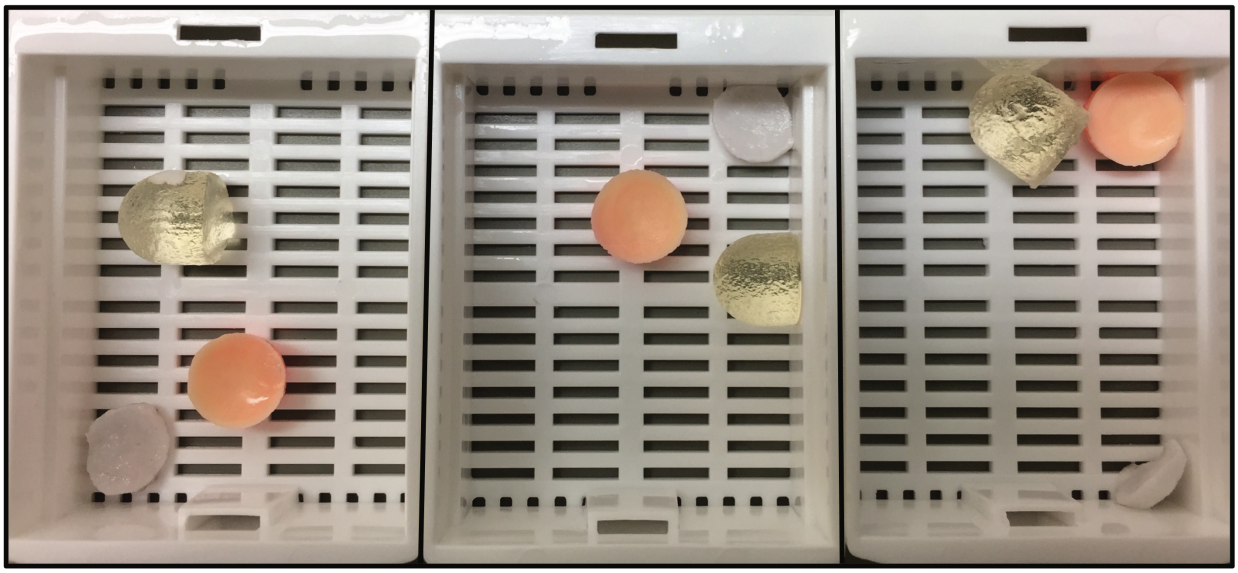

Figure S3. Exposed gels after 24 h of dissolution time. It can be observed that most of the preform tablet is dissolved after the dissolution process.

4.7 TABLES

Table 1. Physical properties and Z value of formulated bioinks.

Bioink	r (mm)	P (kg/m^3)	γ (mN/m)	η (mPa*s)	Z
Hydrophilic	0.08	1022.27	57.76	9.83	**6.99**
Hydrophobic	0.08	1048.00	31.41	4.88	**10.52**

4.8 REFERENCES

1. Banks, J. Adding value in additive manufacturing: Researchers in the United Kingdom and Europe look to 3D printing for customization. *IEEE Pulse* **4,** 22–26 (2013).
2. Kaye, R., Goldstein, T., Zeltsman, D., Grande, D. A. & Smith, L. P. Three dimensional printing: A review on the utility within medicine and otolaryngology. *Int. J. Pediatr. Otorhinolaryngol.* **89,** 145–148 (2016).
3. Zopf, D. A., Hollister, S. J., Nelson, M. E., Ohye, R. G. & Green, G. E. Bioresorbable Airway Splint Created with a Three-Dimensional Printer. *N. Engl. J. Med.* **368,** 2043–2045 (2013).
4. Acosta-Vélez, G. F. & Wu, B. M. 3D Pharming : Direct Printing of Personalized Pharmaceutical Tablets Abstract Powder Bed Inkjet 3D Printing. *Polym. Sceiences* **1,** 1–10 (2016).
5. Norman, J., Madurawe, R. D., Moore, C. M. V, Khan, M. A. & Khairuzzaman, A. A new chapter in pharmaceutical manufacturing: 3D-printed drug products. *Adv. Drug Deliv. Rev.* **108,** 39–50 (2017).
6. Boudriau, S. *et al.* Randomized Comparative Bioavailability of a Novel Three-Dimensional Printed Fast-Melt Formulation of Levetiracetam Following the Administration of a Single 1000-mg Dose to Healthy Human Volunteers Under Fasting and Fed Conditions. *Drugs R D* **16,** 229–238 (2016).
7. Preis, M. & Öblom, H. 3D-Printed Drugs for Children — Are We Ready Yet? *AAPS PharmSciTech* (2017). doi:10.1208/s12249-016-0704-y
8. Chow, C. K. *et al.* Quarter-dose quadruple combination therapy for initial treatment of hypertension: placebo-controlled, crossover, randomised trial and systematic review. *Lancet* **389,** 1035–1042 (2017).
9. Weichselbaum, R. R., Liang, H., Deng, L. & Fu, Y.-X. Radiotherapy and immunotherapy: a beneficial liaison? *Nat. Rev. Clin. Oncol.* (2017). doi:10.1038/nrclinonc.2016.211

10. Gradman, A. H., Basile, J. N., Carter, B. L. & Bakris, G. L. Combination therapy in hypertension. *J. Am. Soc. Hypertens.* **4,** 42–50 (2016).

11. Cahn, A. & Cefalu, W. T. Clinical considerations for use of initial combination therapy in type 2 diabetes. *Diabetes Care* **39,** S137–S145 (2016).

12. Melero, I. *et al.* Evolving synergistic combinations of targeted immunotherapies to combat cancer. *Nat. Rev. Cancer* **15,** 457–72 (2015).

13. Cicero, A. F. Combination Therapy with Olmesartan/Hydrochlorothiazide to Improve Blood Pressure Control. *J. Clin. Exp. Cardiolog.* **6,** (2015).

14. Sun, W., Sanderson, P. E. & Zheng, W. Drug combination therapy increases successful drug repositioning. *Drug Discov. Today* **21,** 1189–1195 (2016).

15. Terrie, Y. C. Monitoring combination drug therapy. *Pharm. Times* **76,** 1–6 (2010).

16. Follath, F. Challenging the dogma of high target doses in the treatment of heart failure: Is more always better? *Arch. Cardiovasc. Dis.* **102,** 785–789 (2009).

17. Farr, M. & Bacon, P. A. How and when should combination therapy be used? The role of an anchor drug. *Rheumatol. (United Kingdom)* **34,** 100–103 (1995).

18. Goyanes, A. *et al.* 3D printing of medicines: Engineering novel oral devices with unique design and drug release characteristics. *Mol. Pharm.* 4077–4084 (2015). doi:10.1021/acs.molpharmaceut.5b00510

19. Khaled, S. A., Burley, J. C., Alexander, M. R., Yang, J. & Roberts, C. J. 3D printing of five-in-one dose combination polypill with defined immediate and sustained release profiles. *J. Control. Release* **217,** 308–314 (2015).

20. Khaled, S. a., Burley, J. C., Alexander, M. R., Yang, J. & Roberts, C. J. 3D printing of tablets containing multiple drugs with defined release profiles. *Int. J. Pharm.* (2015). doi:10.1016/j.ijpharm.2015.07.067

21. Acosta-Vélez, G. F., Linsley, C. S., Craig, M. C. & Wu, B. M. Photocurable Bioink for the Inkjet 3D Pharming of Hydrophilic Drugs. *Bioengineering* **4,** 1–11 (2017).

22. Trachtman, H. *et al.* Pharmacokinetics, pharmacodynamics, and safety of lisinopril in pediatric kidney transplant patients: Implications for starting dose selection. *Clin. Pharmacol. Ther.* **98,** 25–33 (2015).

23. Snauwaert, E., Vande Walle, J. & De Bruyne, P. Therapeutic efficacy and safety of ACE inhibitors in the hypertensive paediatric population: a review. *Arch. Dis. Child.* **102,** 63–71 (2017).

24. Larik, F. A. *et al.* Synthetic approaches towards the multi target drug spironolactone and its potent analogues/derivatives. *Steroids* **118,** 76–92 (2017).

25. United States Pharmacopoeia Convention. <1217> Tablet breaking force. *United States Pharmacopoeia Natl. Formul. (USP 37 - NF 32)* 1146 (2014).

26. Jang, D. *et al.* Influence of Fluid Physical Properties on Ink-Jet Printability. *Langmuir* **25,** 2629–2635 (2009).

27. Cole-Parmer Instrument Company. Available online: https://pim-resources.coleparmer.com/instruction manual/surface-tension-apparatus-instruction-manual.pdf (accessed on 12 January 2017).

28. Department of Health and Human Services, Food and Drug Administration, C. for D. E. and R. (CDER). Size , Shape , and Other Physical Attributes of Generic Tablets and Capsules. Guidance for Industry. (2015).

29. Fraser, J. R., Laurent, T. C. & Laurent, U. B. Hyaluronan: its nature, distribution, functions and turnover. *J. Intern. Med.* **242,** 27–33 (1997).

30. Allison, D. D. & Grande-Allen, K. J. Review. Hyaluronan: A Powerful Tissue Engineering Tool. *Tissue Eng. Part A* **12,** 2131–2140 (2006).

31. Highley, C. B., Prestwich, G. D. & Burdick, J. A. Recent advances in hyaluronic acid hydrogels for biomedical applications. *Curr. Opin. Biotechnol.* **40,** 35–40 (2016).

32. Owen, S. C., Fisher, S. a., Tam, R. Y., Nimmo, C. M. & Shoichet, M. S. Hyaluronic acid click hydrogels emulate the extracellular matrix. *Langmuir* **29,** 7393–7400 (2013).

33. Kim, I. L., Mauck, R. L. & Burdick, J. A. Hydrogel design for cartilage tissue engineering: A case study with hyaluronic acid. *Biomaterials* **32,** 8771–8782 (2011).

34. Juban, A., Nouguier-Lehon, C., Briancon, S., Hoc, T. & Puel, F. Predictive model for tensile strength of pharmaceutical tablets based on local hardness measurements. *Int. J. Pharm.* **490,** 438–445 (2015).

35. Raymond C R, Paul J S, M. E. Q. Handbook Pharmaceutical Excipients,Sixth Edition. *London Pharm. Press* (2009).

36. Williams, R. O., Reynolds, T. D., Cabelka, T. D., Sykora, M. a & Mahaguna, V. Investigation of excipient type and level on drug release from controlled release tablets containing HPMC. *Pharm. Dev. Technol.* **7,** 181–193 (2002).

37. Thomas, M. V. & Puleo, D. A. Calcium sulfate: Properties and clinical applications. *J. Biomed. Mater. Res. - Part B Appl. Biomater.* **88,** 597–610 (2009).

38. Singh, N. B. & Middendorf, B. Calcium sulphate hemihydrate hydration leading to gypsum crystallization. *Prog. Cryst. Growth Charact. Mater.* **53,** 57–77 (2007).

39. Bešter-Rogač, M. Nonsteroidal Anti-Inflammatory Drugs Ion Mobility: A Conductometric Study of Salicylate, Naproxen, Diclofenac and Ibuprofen Dilute Aqueous Solutions. *Acta Chim. Slov.* **56,** 70–77 (2009).

CHAPTER FIVE: CONCLUSIONS AND FUTURE DIRECTIONS

The objective of this project was to develop a technology for the manufacture of pharmaceutical tablets with fast fabrication times and at room temperature, in order to address some of the limitations experienced in the most common technologies utilized towards 3D Pharming, powder bed 3D printing and fused deposition modeling. To achieve this goal, a set of two photocurable bioinks, constituted by the biocompatible polymers hyaluronic acid and poly(ethylene glycol), were engineered. These bioinks work in conjunction with fabricated blank preform tablets, made by traditional powder compression or by powder bed 3D printing, that serve as a scaffold to the bioinks dispensed. Chapter 2 demonstrates de engineering of a hyaluronic acid based hydrophilic bioink with quick gelation times and immediate drug release profiles. Chapter 3 shows the engineering of a PEG based hydrophobic bioink capable of producing a sustained release of the drug loaded and with tunable mechanical properties and release profiles. Chapter 4 demonstrates the use of the engineered bioinks to fabricate a combination therapy with two highly recognized drugs towards the treatment of hypertension. The combination of drugs with hydrophilic and hydrophobic properties was shown, expanding the use of inkjet printing towards the dispense of multiple APIs at fast printing speeds and at room temperature. These studies present a new 3D Pharming technology that allows for the manufacture of oral dosage forms at room temperature, with controlled dosages, quick printing times, tunable release profiles, and the combination of multiple drugs.

Limitations of this technology include the potential incompatibility of drugs containing thiol or reactive alkene groups within their chemical structure. Moreover, the maximum amount of drug loaded in the preform tablet is defined by the highest solubility achieved of the compound to be delivered within the engineered bioink. Future work includes the development of strategies to enhance the portfolio of APIs compatible with this technology and an enhanced control of drug release kinetics, as discussed in the following section.

5.1 FUTURE DIRECTIONS

The materials developed could be utilized with PolyJet technology, a 3D printing technique that uses inkjet printing to dispense photocurable materials onto a stage under the presence of a constant light source [1,2]. This allows for the material to be cured as it falls onto the stage, resulting in a 3D structure. Applying such technology with the photocurable formulations designed would allow for the manufacture of dosage forms without the need of a preform tablet. For this to be a possibility, the bioink has to have the capacity to achieve strong mechanical properties, such as the ones reached by some of the hydrophobic formulations created.

In addition to the materials engineered, additional work is needed towards the development of new materials that intrinsically allow for the extended release of hydrophilic drugs without the need of preform tablets to control drug release profiles. A hydrophilic biocompatible material capable of reaching strong mechanical properties could result into sustained release profiles. The formulation of a hyaluronic acid bioink with a high W_{HANB} percent would result in a strong hydrogel with potentially an extended release profile of the drug to be discharged. Piezoelectric nozzles with temperature control capacity might be needed to manipulate the viscosity of these solutions involving higher polymer concentrations.

Further work is needed to achieve immediate release of hydrophobic drugs. The engineering of biocompatible photocurable emulsions are an attractive strategy to achieve this goal. Cured water-in-oil emulsions would result into highly porous scaffolds once exposed to an aqueous environment [3]. This increased porosity would significantly enhance the drug release kinetics of hydrophobic drugs.

The development of polymers capable of undergoing gelation under other mechanism excluding light initiation as a catalyst is an appealing option, in order to expand the portfolio of drug compatible with these 3D Pharming scheme. Materials that polymerize through the formation of ionic bonds are an alternative worth of exploration towards this end. An example of such a material is sodium alginate and its polymerization in the presence of calcium [4,5].

5.2 CHALLENGES FOR THE TRANSITION OF 3D PHARMING INTO PHARMACIES

An important goal of 3D Pharming is its implementation at pharmacies, hospitals, and point of care centers towards the advancement of personalized medicine. However, this technology faces multiple challenges due mainly to FDA regulations limiting the creation of personalized tablets at will with diverse dosages and drug combinations, and the technology improvements needed in order to effectively implement 3D Pharming at pharmacies. The following are some key barriers for the adoption of 3D printers at pharmacies and point of care locations:

- Under FDA regulation, each dosage formulation of a drug (100mg, 20mg, etc.) requires a new set of clinical trials to prove the efficacy of that dosage. This would directly inhibit the use of 3D printers for dosage control, since each tablet printed at a dosage not clinically tested previously would require a new clinical trial, forbidding the dispense of such tablets. Changes in FDA regulations are required in order to allow for the manufacture of dosage personalized tablets *in-situ* at a pharmacy or point of care facility.
- Technology to define what dosage accurately works better for a given individual needs to be developed. Efforts are being done on pharmacogenomics, creating data bases that match drugs to specific traits in the genome of individuals, assuring the efficacy of active ingredients for a given person in terms of drug choice. However, in terms drug dosage further work needs to be done to better identify the dosage that would result in the best therapeutic effect for any given patient.
- Printing speed is certainly critical for the use of such technology at a point-of-care facility or pharmacy, specially for locations with high patient populations. Likewise, drug compatibility with 3D pharming techniques (prevention of drug degradation through the process) and the capacity to achieve high dosages in order to provide a larger 3D pharmed drug portfolio to the patients are critical aspects that need to be addressed.

- This technology would require a re-training of individuals working at pharmacies, in order to operate 3D pharming machinery and the quality control aspects of the novel technology.
- Another important aspect is the design of a storage system for the different new formulation reagents, since pre-manufactured bottles of tablets for the APIs that qualify initially for 3D pharming manufacture will no longer be part of the drug dispensing system. The active ingredients and excipients needed for 3D Pharming (bioinks, powders, thermoplastic materials, pure APIs, etc.) would potentially require different storage mechanisms to ensure their stability and extended shelf life.
- There are several 3D Pharming techniques developed but the manufacture of high dosage tablets, at high speeds, room temperature, and with the potential combination of multiple APIs remains a hurdle for the available techniques. Technology improvements are needed in order to allow a larger quantity of drugs to be dispensed through 3D Pharming technologies with a high fabrication efficiency.
- Other hurdles include:
    - The creation of GMP facilities in each pharmacy holding a 3D printer for the manufacture of tablets, to guarantee a good pharmaceutical product.
    - The development of quality controls to make sure the dosage being loaded is accurate.
    - The development of a system to test a small sample of the tablets manufactured at the pharmacy and confirm that it has the correct dosage and drug choice, before it is dispensed to the patient.

Patients consuming drugs that achieve their pharmacological effect at low dosages would benefit initially from this technology, since the technology already exist to manufacture and dispense tablets with low dosages of APIs. Moreover, patients taking multiple drugs on a daily

basis would benefit from the potential manufacture of a customized tablet that combines all the needed drugs into one tablet. This would probably increase the compliance of the patients taking their medications, due to a lower tablet burden. Additionally, an application that would not require changes in regulations is the use of 3D pharming during the clinical trials phase of drug candidates, since during this time changes on the drug dosage are constantly required, in order to determine the correct dosage needed for a given API.

Risks of the technology would be potential machinery malfunctions or the lack of in-stock tablets within pharmacies ready to be dispensed in the event of a crisis, where large quantities of product would be needed in a short period of time. Good quality control mechanisms need to be implemented to assure that the equipment is working properly and that errors can be detected accurately. Finally, a back-up system for the mass production of some high demand drug products needs to be in place, in case of an emergency.

5.3 REFERENCES

1. Ibrahim, D. *et al.* Dimensional error of selective laser sintering , three-dimensional printing and PolyJet models in the reproduction of mandibular anatomy. *J. Cranio-Maxillofacial Surg.* **37,** 167–173 (2009).
2. Ionita, C. N. *et al.* Challenges and limitations of patient-specific vascular phantom fabrication using 3D Polyjet printing. *Proc SPIE Int Soc Opt Eng.* **9038,** (2014).
3. Sears, N. A., Dhavalikar, P. S. & Cosgriff-Hernandez, E. M. Emulsion Inks for 3D Printing of High Porosity Materials. *Macromol. Rapid Commun.* **37,** 1369–1374 (2016).
4. Song, S. J. *et al.* Sodium Alginate Hydrogel-Based Bioprinting Using a Novel Multinozzle Bioprinting System. *Artif. Organs* **35,** 1132–1136 (2011).
5. Lin, C. & Metters, A. T. Hydrogels in controlled release formulations : Network design and mathematical modeling. *Adv. Drug Deliv. Rev.* **58,** 1379–1408 (2006).